A Perturbation Model for Normal and Sickle Cell Blood Microcirculation

by
Yonatan Tekleab

B.S. Aeronautics and Astronautics
Massachusetts Institute of Technology, 2006

Submitted to the Department of Aeronautics and Astronautics in partial fulfillment of the requirements for the degree of

Master of Science in Aeronautics and Astronautics

at the

MASSACHUSETTS INSTITUTE OF TECHNOLOGY

June 2011

Author: _____
Department of Aeronautics and Astronautics
May 19, 2011

Certified by: _____
Wesley L. Harris
Professor of Aeronautics and Astronautics
and Associate Provost for Faculty Equity
Thesis Supervisor

Accepted by: _____
Eytan H. Modiano
Associate Professor of Aeronautics and Astronautics
Chair, Graduate Program Committee

A Perturbation Model for Normal and Sickle Cell Blood Microcirculation

by
Yonatan Tekleab

Submitted to the Department of Aeronautics and Astronautics on
May 19, 2011, in partial fulfillment of the requirements for the
degree of Master of Science in Aeronautics and Astronautics

Abstract

Sickle cell disease is a genetic disorder that alters red blood cells such that their hemoglobin cannot effectively bind and release oxygen. This causes issues that affect how the cell operates in the smallest vessels of the body. In the past, computational models have been used to study the microcirculation to gain a better understanding of blood disorders such as sickle cell disease. A fast, time efficient computational model has been developed to analyze perturbations in the microcirculation caused by sickle cell disease. The model uses a finite difference, Crank-Nicholson scheme for the flow and oxygen computation, while using the level set computational method to advect the red blood cell membrane on a staggered grid. A number of initial and boundary conditions were tested in the model. The simulation data shows several important parameters to be significant in the perturbation of the blood flow and oxygen concentration profiles. Specifically, the Hill coefficient, arterial oxygen partial pressure, oxygen partial pressure at 50% hemoglobin saturation, and cell membrane stiffness are significant factors.

Thesis Supervisor: Wesley L. Harris
Title: Professor of Aeronautics and Astronautics
Associate Provost for Faculty Equity

Acknowledgements

First, I would like to thank my residential, academic, and thesis advisor, Professor Wesley L. Harris, for allowing me the opportunity to work on such a significant project. For the past eight years, Professor Harris has been a mentor and source of great support in my academic and professional career as well as in my personal life.

I also want to thank Professors Jean-Christophe Nave and Benjamin Seibold of the Department of Mathematics. Professors Nave and Seibold assisted greatly in the development of my computational model.

Also, I want to thank the entire Department of Aeronautics and Astronautics at MIT. The students, faculty and staff have been wonderful and I truly appreciate working alongside the wonderful people of Course XVI at MIT.

I would also like to thank those who have supported me throughout my graduate studies. My friends and family have been a tremendous source of encouragement, providing me with the motivation to push forward and focus at the most difficult times. I give many thanks to my parents, Elsa Teklemariam and Tekleab Tsegay who have always urged me to strive for excellence. Finally, I would like to thank my girlfriend Yamicia Connor, who has always been an invaluable foundation of support, especially over the past year. Her dedication to her work inspires me every day. Thank you.

The help and encouragement of everyone listed above is sincerely appreciated.

Table of Contents

List of Figures

List of Tables

Symbols

x, y	spatial coordinates
t	time
$\underline{v}$	two dimensional velocity vector
ρ	plasma density
p	plasma pressure
μ	plasma viscosity
u, v	x & y velocity components
V_{avg}	average RBC velocity
D_{cap}	diameter of capillary
R_k	capillary centerline to end of tissue length
R_w	capillary centerline to capillary wall length
Re	Reynolds number for plasma flow
c	oxygen concentration
D_{ox}	oxygen diffusion constant
D^{Hb}	diffusivity of hemoglobin
D^{Mb}	diffusivity of myoglobin
R	oxygen generation/consumption
R^{Hb}	oxygen generation inside the RBC by hemoglobin
R^{Mb}	oxygen consumption inside the tissue by myoglobin
R^{plasma}	oxygen generation/consumption in plasma
M	metabolic oxygen consumption in tissue
$[Hb_4O_8]$	concentration of oxyhemoglobin
$[Hb_4]$	concentration of deoxyhemoglobin
$[MbO_2]$	concentration of oxymyoglobin
$[Mb]$	concentration of deoxymyoglobin
$[Hb_4]_{tot}$	concentration of total hemoglobin
$[Mb]_{tot}$	concentration of total myoglobin
k_{-1}^{Hb}	hemoglobin dissociation rate constant
k_{-1}^{Mb}	myoglobin dissociation rate constant
k_{+1}^{Hb}	hemoglobin association rate constant
k_{+1}^{Mb}	myoglobin association rate constant
K_{eq}^{Hb}	hemoglobin equilibrium constant
K_{eq}^{Mb}	myoglobin equilibrium constant
$c_{50\%}^{Hb}$	oxygen concentration at 50% hemoglobin saturation
$c_{50\%}^{Mb}$	oxygen concentration at 50% myoglobin saturation
$p_{50\%}^{Hb}$	oxygen partial pressure at 50% hemoglobin

$p_{50\%}^{Mb}$	oxygen partial pressure at 50% myoglobin
S^{Hb}	hemoglobin saturation
S^{Mb}	myoglobin saturation
$\boldsymbol{n}$	Hill coefficient
U, V	x & y velocity components in computational domain
P	pressure in computational domain
h	discrete spatial grid length
ϕ	level set function
F	magnitude of velocity
$\hat{n}$	velocity unit vector
Ω	level set domain
a	pressure jump across membrane
J	jump matrix, containing all pressure jump values
p_{O_2}	partial pressure of oxygen
σ	red blood cell membrane stress
κ	red blood cell membrane curvature
k_{RBC}	red blood cell membrane stiffness
i, j	reference spatial indices
n	reference timestep
α	Henry's Law constant
j	stiffness index
a	semi-major axis
b	semi-minor axis

1 Introduction

Sickle cell disease is a genetic blood disorder which degrades the oxygen carrying capacity of a Red Blood Cell (RBC). Sickle cell disease affects the entire body because reduced oxygen in the blood leads to lower oxygen in vital tissues and organs throughout the body, leading to hypoxia and acute pain. Individuals with sickle cell disease are expected to live only into their mid 40s. **[1]** Not only is the life expectancy shortened, but the quality of life is also extremely diminished. Affected individuals must be careful so as not to cause the onset of a crisis, which involves extremely painful acute pain, usually in the extremities. This generally involves avoiding rigorous physical activity, staying well hydrated, maintaining a healthy diet, and avoiding low-oxygen atmospheres (aircrafts, high elevations, etc.).

1.1 Genetics and Pathophysiology of Sickle Cell

Sickle cell disease is caused by a hereditary mutation in a gene causing altered hemoglobin proteins in the erythrocytes. As blood is pumped from the heart through the lungs, oxygen molecules bind to the hemoglobin creating a complex called oxyhemoglobin. The oxygen breaks its bond with the hemoglobin and diffuses through the RBC membrane to the tissue, providing the body with oxygen. The unbound hemoglobin molecules are then referred to as deoxyhemoglobin. A

healthy adult erythrocyte contains the *hemoglobin A* (HbA) protein within its cytoplasm; however a sickle RBC contains sickle hemoglobin, the *hemoglobin S* (HbS) protein. An HbA molecule contains two α-chains and two β-chains as shown in Figure 1.1. The genetic mutation in HbS causes a change in the β-chains, replacing a hydrophilic amino acid with a hydrophobic amino acid, thus changing the binding affinity between hemoglobin molecules. The increased binding affinity between HbS molecules results in anemia, or decreased binding of oxygen molecules. Under conditions of low oxygen concentration, there is a far greater probability of the HbS molecules bonding to each other.

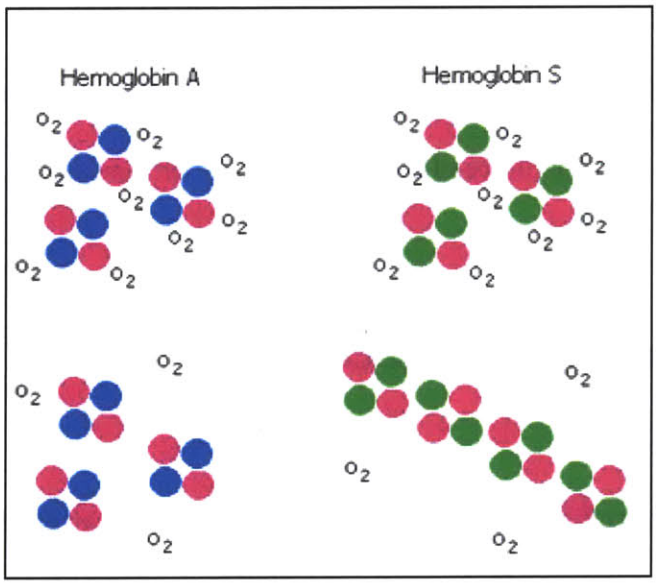

Oxyhemoglobin under high [O_2]

Deoxyhemoglobin under low [O_2]

Figure 1.1 – Oxyhemoglobin and Deoxyhemoglobin A & S [2]
The Pink circles represent hemoglobin α-chains; the blue and green represent the HbA and HbS β-chains respectively. The HbS protein molecules polymerize under low oxygen conditions, forming long chains.
(Source: http://www.bio.davidson.edu/people/midorcas/animalphysiology/websites/2005/Eppolito/)

Sickle cell primarily affects populations from tropical and subtropical regions that are heavily stricken by malaria. Highest concentrations of sickle cell are found in Africa, the Mediterranean, India, and the Middle East. In the United States, nearly 85% of all sickle cell cases presented are found in people of African descent. **[2]** Figure 1.2 shows a comparison between malaria stricken regions and areas of high concentrations of sickle cell disease in Africa. This correlation is due to the fact that individuals with sickle cell disease are resistant to Plasmodium falciparum, the parasite that causes malaria. Typically, malaria is acquired when a mosquito carrying the parasite bites a human. The parasite travels through the bloodstream to the liver, infecting erythrocytes and liver cells (hepatocytes). Healthy RBCs have a lifespan of 90 to 120 days, whereas a sickle cell only lives 10 to 20 days. In a healthy erythrocyte, the parasite will typically survive long enough to reproduce; however, in a sickle erythrocyte the cell will die before the parasite undergoes reproduction. **[3]**

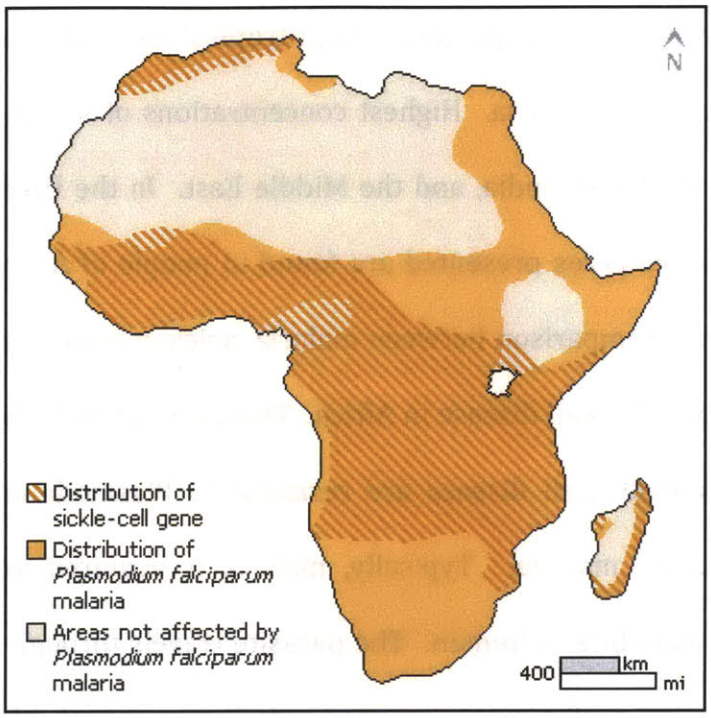

Figure 1.2 – Distribution of Sickle Cell gene and Malaria parasite
(source: http://images.encarta.msn.com)

Sickle cell is an evolutionary advantage in humans to protect from malaria. Humans have two sets of all genes; therefore there are two sickle cell genes. Individuals with one HbS gene, and one HbA gene, are said to be carriers of the sickle cell trait. A fraction of their erythrocytes will be sickle, but not enough to result in anemia or other sickle cell disease symptoms, but enough such that the malaria parasite cannot reproduce effectively enough to thrive. An individual having two HbS genes will have all sickle erythrocytes and suffer from the disease. Therefore an individual with only one HbS gene has an advantage because they are both resistant to malaria, and they do not exhibit the disease symptoms.

1.2 Blood Flow Dynamics

In the human body, blood is pumped from the lungs to the rest of the body, moving from the large arteries, to smaller arteries, then finally into the smallest capillaries. In the larger arteries, both healthy and sickle erythrocytes are free to flow in groups without altering their natural shapes. The internal diameter of a capillary is roughly 8μm; whereas the erythrocyte diameter at rest is about 10μm. The erythrocytes must flow single-file and squeeze into a "bullet-like" shape as they pass through these narrow passages. **[4]**

For individuals with sickle hemoglobin, this process is slightly different. Throughout this process, the sickle cells are releasing oxygen and the hemoglobin molecules are beginning to polymerize, forming branching chains. Over time, the erythrocytes will continue to diffuse oxygen and the hemoglobin will continue to polymerize, forming longer and longer fibers until they begin to affect the shape of the cell. The membrane begins to stiffen and take the shape of the fibers. Figure 1.3 and Figure 1.4 show the HbS polymerization and the sickle erythrocyte shape.

The sickle erythrocytes have stiff membranes and are not flexible enough to flow smoothly within the capillaries. They can become stuck in the capillary causing a vaso-occlusion. The occlusion prevents the flow of blood and thus oxygen to the tissue downstream, causing ischemia, pain and restricted oxygen to tissue. In some cases a sufficient number of vessels are occluded, causing organ damage or even

failure. This phenomenon is known as a vaso-occlusive crisis. Vaso-occlusive crises are extremely painful and unpredictable events. This unpredictability makes it very difficult to manage.

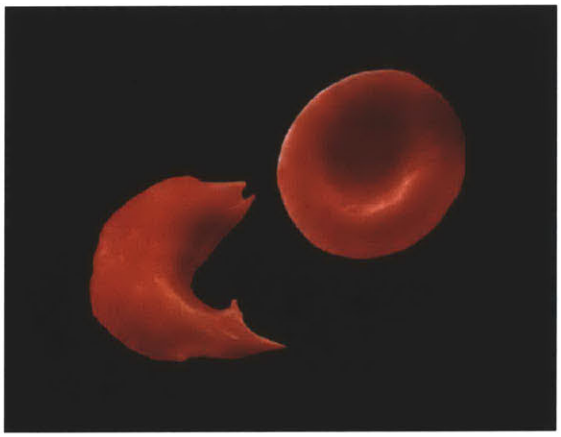

Figure 1.3 – Normal vs. Sickle RBC
The sickle cell takes the shape of the polymerized hemoglobin.

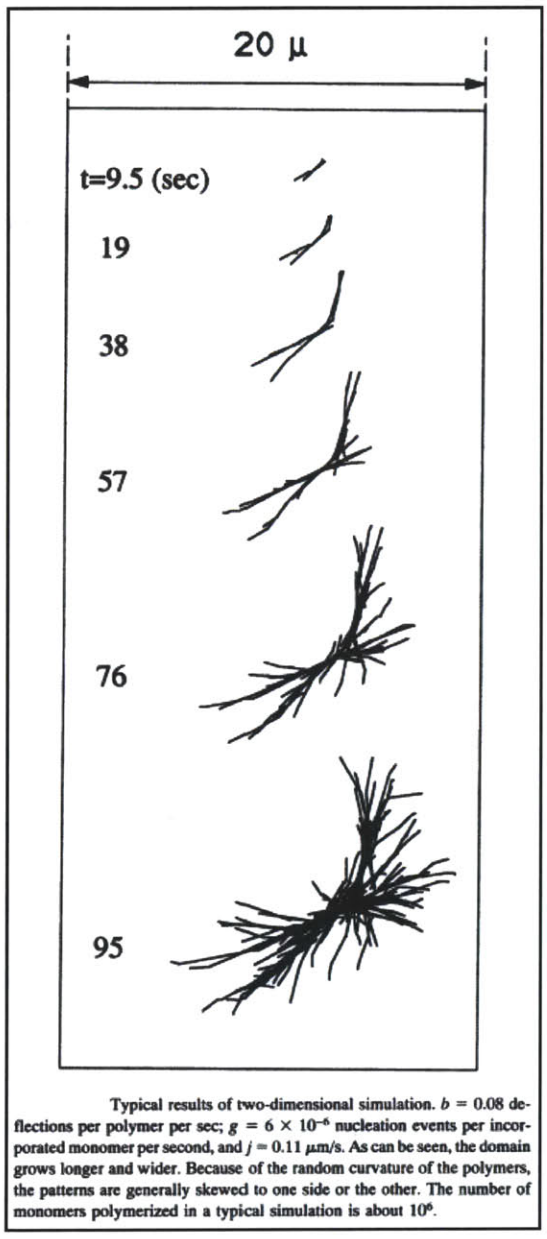

Typical results of two-dimensional simulation. $b = 0.08$ deflections per polymer per sec; $g = 6 \times 10^{-6}$ nucleation events per incorporated monomer per second, and $j = 0.11$ μm/s. As can be seen, the domain grows longer and wider. Because of the random curvature of the polymers, the patterns are generally skewed to one side or the other. The number of monomers polymerized in a typical simulation is about 10^6.

Figure 1.4 – HbS Polymerization
This model illustrates the polymerization of HbS over time. **[5]**

1.1 Current Treatment

At the moment, there is no cure for sickle cell disease. Affected individuals must live with this illness for their entire life. There are treatments that aim to treat the symptoms of the disease and prevent the onset of crises; however, none of these treatments are completely effective in all sickle cell patients.

Drug therapies include anti-sickling drugs such as Hemoxin and Hydroxyurea. These drugs prevent the erythrocytes from sickling by triggering the production of fetal hemoglobin (HbF). **[6]** Fetal hemoglobin is produced by the body during the prenatal and infancy period, but is stopped around 18 to 24 weeks after birth. **[7]** HbF does not polymerize and will not cause the blood cell to sickle. Unfortunately, the long-term effects of these drugs are unclear. Sickle cell crises are typically treated symptomatically. Patients are treated with pure oxygen to stop hypoxia and opioids to manage the pain. Blood transfusions can also be carried out to resupply the body with healthy HbA carrying erythrocytes.

There are some promising remedies that are undergoing testing. Bone marrow transplants have been shown to be effective among children. It is believed that healthy transplanted bone marrow can produce healthy erythrocytes; however, the complications from a bone marrow transplant can be life-threatening.

1.2 Previous Blood Flow Models

A properly functioning blood microcirculation system is critical to the health of humans. There exist several macro-level models of the fluid dynamics of the blood microcirculation system. These models have provided useful information and an improved understanding of the blood microcirculation system. However, these models do not include some analytical details corresponding to a critical microscopic description of the physical, dynamical, and chemical diffusion, which are necessary to predict the behavior of some diseases such as sickle cell anemia. These models are based on empirical results combined with simplified physical descriptions that often neglect the microscopic complexity of blood cell structure and oxygen transport through the blood cell membrane into the surrounding tissue. Specific numerical methods and empirical results have advanced sufficiently to the point where more realistic models of the blood microcirculation systems may be developed.

The Le Floch-Harris **[8]** model is a novel methodology, developed to address sickle cell disease, based on highly descriptive mathematical models for blood flow in the capillaries. The investigations focus on the coupling between oxygen delivery and red blood cell dynamics, which is crucial to understanding sickle cell crises and is unique to this blood disease. The model entails an extensive study of blood dynamics through simulations of red cells deforming within the capillary vessels,

and relies on the use of a system of equations describing oxygen transfer, blood plasma dynamics and red cell membrane deformation mechanics.

The Le Floch-Harris model aims to achieve an improved understanding of the complex interaction and interdependence of blood plasma dynamics, red blood cell membrane deformation, and oxygen transport from the red blood cells to the surrounding tissue. A physically plausible model of this complex interaction and interdependent state of the blood microcirculation constitutes the first product of the proposed coupled, multi-scale numerical simulation. The results/models are expected to lead to the development of new research strategies for sickle cell disease. The Le Floch-Harris simulation models could be used not only to assess current researched remedies, but also to spur innovative research initiatives, based on the study of the physical properties coupled in sickle cell disease.

The Le Floch-Harris model uses a 5-layer model which incorporates the following 5 domains: RBC cytoplasm, blood plasma, endothelium (capillary wall), the interstitium (space between the capillary vessel and the surrounding tissue). **[8]** Le Floch's model assumes constant radius, circular cross section along the length of the capillary. This assumption allows the approximation of the flow as being a 3-D, axially symmetric flow. The erythrocytes are assumed to be symmetric about the centerline.

1.3 Mathematical Model

The primary objective this research is to create a simplified mathematical model of the healthy and sickle microcirculation in the capillary and surrounding tissue. This model would serve as a proof of concept for a simplistic model that can demonstrate similar results to more complex models such as the Le Floch-Harris model. The results will be compared to those of more complex models to either validate or refute it. If indeed, our model is shown to have merit, it can then serve as a first order approximation for more complicated models, saving time and providing some indication of the specific ranges of parameters that might lead to crisis within individuals with sickle cell disease.

We will begin with the following set of governing fluid dynamics equations for our system: (1) the continuity equation, (2) Navier-Stokes equation, and (3) Fick's Law of mass diffusion, which we will refer to as the oxygen diffusion equation.

$$\nabla \cdot \underline{v} = 0 \ , \tag{1.1}$$

$$\rho\left(\frac{\partial \underline{v}}{\partial t} + \underline{v} \cdot \nabla \underline{v}\right) = -\nabla p + \mu \nabla^2 \underline{v} \ , \tag{1.2}$$

$$\frac{\partial c}{\partial t} + \nabla \cdot \left(c\underline{v} - D_{ox} \nabla c\right) = R(c) \ , \tag{1.3}$$

Our unknown field quantities are $\underline{v}$, the velocity vector field, c, the oxygen concentration field, and p, the pressure field. R represents the oxygen

generation/consumption function which is a function of oxygen concentration and will be explained later.

The flow of the blood within the capillary is completely characterized by these governing equations and is constrained by the boundary and initial conditions of the flow. A no-slip/no-flux condition will be used for the plasma at the capillary wall while periodic boundary conditions are used at the inlet and outlet. The oxygen concentration will use Neumann boundary conditions at the tissue boundaries. The initial conditions will be constant field values everywhere for the oxygen concentration and velocity field. These initial and boundary conditions will be discussed in further detail in chapter 2.

Our flow equations represent a flow in two dimensions, using a Cartesian coordinate system. For simplicity, we will approximate the three dimensional axial capillary flow and oxygen diffusion as a two dimensional flow between two long, parallel, flat plates. The healthy microcirculation flow will represent a *mean*, baseline flow. Perturbations in the flow parameters and cell membrane characteristics will be introduced to model the sickle nature of the RBC and plasma flow.

We seek to show that the simplified, two dimensional system of equations will produce results comparable to results determined computationally from the set of nonlinear partial differential equations. From our solutions, we will be able to

characterize and identify the physiological parameters that can be modified, changing the flow dynamics to produce more favorable outcomes in the blood flow.

There will be some degree of uncertainty due to the nonlinearities in the governing equations. If we can show that these nonlinearities produce small or negligible results for the physiological parameters within the boundaries of the human tolerance, we will have proved that a simpler, less computationally expensive method can yield similar results. If however, we cannot show that the effects of the nonlinear terms are small, we will be able to show that the nonlinear terms play a large role in the physics of the blood flow, meaning that even small perturbations may have large, resounding effects. This may open up the discussion of the involvement of chaos in fluid dynamics during the onset of crisis.

2 Microcirculation Model

2.1 Physical System

The general hemodynamics of the microcirculation includes the arterioles, capillaries, and venules. Our particular area of interest is within the smallest blood vessels of the circulatory system, the capillaries. As oxygen rich erythrocytes enter the capillaries from the arterioles, oxygen molecules are unbound from the oxyhemoglobin complexes. The hemoglobin molecules continue to release oxygen as the erythrocyte traverses axially along the capillary and into the venules. In the sickle case, the erythrocyte membrane stiffness will increase as the hemoglobin saturation decreases due to the hemoglobin polymerization phenomenon.

The heart comprises four chambers surrounded by cardiac smooth muscle. The cardiac muscle contracts around these chambers to pump blood into the lungs and throughout the body. Oxygen rich blood is carried from the left ventricle of the heart, downstream into the smaller vessels to deliver oxygen and other nutrients to tissue throughout the body. The periodic contraction of the left ventricle causes the blood pressure to vary in time creating pulsating oscillations. These oscillations can be seen in Figure 2.1.

The blood leaves the left ventricle, entering the aorta, the largest artery in the body. From the aorta, the blood travels into smaller arteries, which then branch into

several arterioles and eventually millions of capillaries. **[9]** Although a capillary has a much smaller cross section than the aorta, the total cross sectional area of all capillaries is orders of magnitude larger, thereby reducing the flow velocity and greatly dampening the oscillations in pressure.

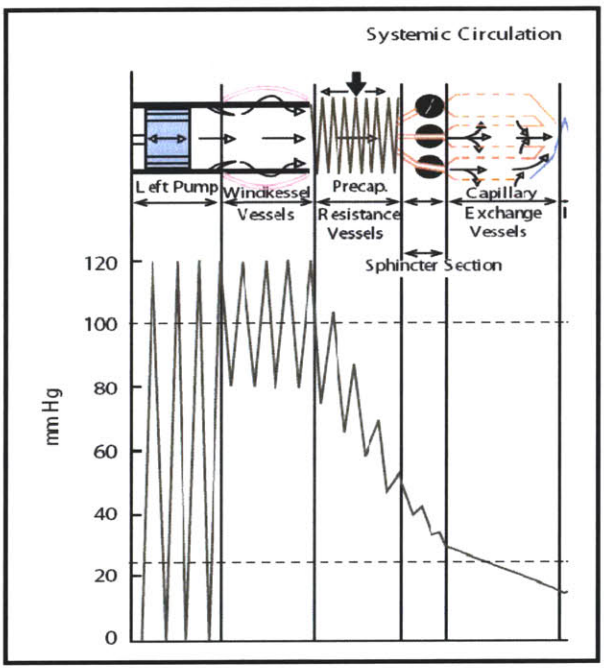

Figure 2.1 – Systemic Circulation Pressure
Pressure oscillations are dampened out by the time the blood reaches the capillaries. **[10]**

The plasma flow is driven by the beating of the heart. In the capillary, the flow pressure drops about 20mmHg (2666 Pa) across an average length of 8mm. This yields a pressure gradient in the capillary of, $\frac{dp}{dx} = 3.33 \times 10^5 \frac{Pa}{m}$. **[10]** This calculated value is consistent with the Le Floch-Harris model $\frac{dp}{dx}$ value of $3.33 \times 10^5 \frac{Pa}{m}$. **[9]**.

In addition to erythrocytes, the blood also contains many other components. In addition to oxygen delivery, the circulatory system serves as the delivery pathway for the leukocytes and platelets. The relative amount of erythrocytes in blood is defined by the hematocrit. The hematocrit is a ratio of red cell volume to total blood volume. In healthy adult humans, the hematocrit is roughly 0.45 which means that about 45% of blood is RBC by volume. About 55% of blood volume is plasma. **[11]** Therefore, blood volume of leukocytes and platelets is less than 1%. By this rationale, we will assume that our capillary flow model contains only plasma and erythrocytes.

To accurately capture the dynamics of the oxygen diffusion and plasma flow, it is critical that we appropriately model the physical system by defining the boundary conditions at every interface. The capillary flow model must comprise the contents within the capillary as well as the capillary wall itself in addition to the surrounding tissue. The plasma and RBCs do not cross through the capillary walls; however the oxygen molecules will diffuse into the surrounding tissue.

First we determine the specific regions or "layers" in our model. In the Vadapalli, Goldman, and Popel **[12]** 5-layer model, the interstitium and vascular wall are accounted for in addition to the RBC cytoplasm, blood plasma, and tissue. The relative thicknesses of each of the regions are shown in Table 2.1. As illustrated in

Figure 2.2 and Table 2.1, the interstitium and vascular wall layers are very thin in comparison to the other regions.

Table 2.1 – Relative Thickness of Regions

Region	Thickness [m]	% Thickness
Plasma	3.5E-6	17.5%
Endothelium	0.30E-6	1.5%
Interstitium	0.35E-6	1.7%
Tissue	15.9E-6	79.3%

The oxygen consumption rates in the smallest regions, the endothelium and interstitium, are small in comparison to that of the tissue. Due to small size and low oxygen consumption rates, these two regions will be neglected in our calculations. We will instead use a 3-layer representation for our model.

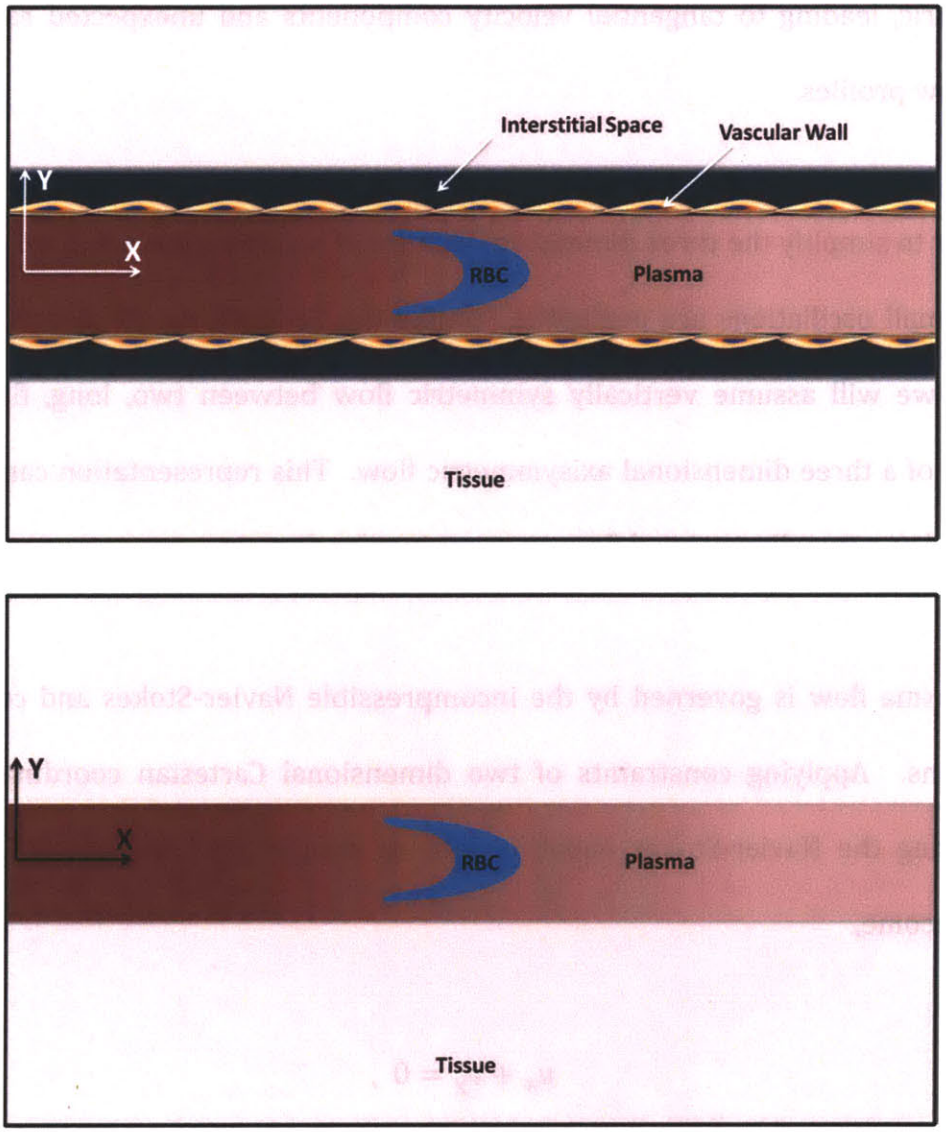

Figure 2.2 – 5-Layer and 3-Layer Models
In addition to the RBC, plasma and tissue, the 5-layer model also incorporates the interstitial space and the vascular wall, which are both very thin.

In reality, the blood flow in the capillary is not absolutely axially symmetric. Small oscillations in the flow due to fluctuations in the flow speed, pressure variations, and changes in the capillary wall radius or curvature can cause the flow to be non-

symmetric, leading to tangential velocity components and unexpected radial and axial flow profiles.

In order to simplify the three dimensional nature of our system, we will assume that these small oscillations are negligible. Unlike the Le Floch or the Krogh cylinder model, we will assume vertically symmetric flow between two, long, flat plates instead of a three dimensional axisymmetric flow. This representation can then be modeled as a two dimensional flow on a rectangular domain.

The plasma flow is governed by the incompressible Navier-Stokes and continuity equations. Applying constraints of two dimensional Cartesian coordinates, and separating the Navier-Stokes equation into its components, equations (1.1) and (1.2) become,

$$u_x + v_y = 0 \ , \tag{2.1}$$

$$\rho(u_t + uu_x + vu_y) = -p_x + \mu(u_{xx} + u_{yy}) \ , \tag{2.2}$$

$$\rho(v_t + uv_x + vv_y) = -p_y + \mu(v_{xx} + v_{yy}) \ , \tag{2.3}$$

The plasma flow boundary conditions applied are no-slip/no-flux at the capillary wall, and periodicity at the entrance and exit of the channel.

$$\underline{v}_{wall} = 0 \ , \tag{2.4}$$

$$\underline{v}_{entrance} = \underline{v}_{exit} \ , \tag{2.5}$$

The RBC serves as the oxygen delivery vehicle for the body, delivering fresh oxygen from the lungs throughout the body via the circulatory system. At the level of the capillary, the oxygen diffuses through the RBC membrane, through the plasma and into the tissue. At the same time, the tissue is consuming the oxygen by binding the oxygen molecules to the myoglobin complexes, thereby reducing the concentration of oxygen in the tissue. Therefore, we can model the moving RBC as an oxygen source and the tissue as an oxygen sink.

Within the RBC cytoplasm there are several organelles, however our only interest is in the hemoglobin protein because it makes up 97% of the entire RBC dry content **[9]** and it directly influences the oxygen production rate. Therefore, we will only model the hemoglobin within the RBC and assume it is evenly distributed throughout the cytoplasm. Similarly, the myoglobin is considered to be evenly distributed throughout the tissue. Furthermore, we will assume that oxygen can diffuse freely from the RBC cytoplasm through the cell membrane and into the tissue.

The plasma and RBC are in motion while oxygen is diffusing through the layers; however we assume there is no moving fluid in the tissue. Our oxygen transport must have an advection term to account for the fluid flow in the capillary.

Simplifying equation (1.3) by applying 2D Cartesian coordinates, and the constraint of continuity, we obtain equation (2.6).

(2.6)

(2.7)

The oxygen generation/consumption function, , represents the rate at which oxygen is produced, therefore it can be calculated as the oxygen concentration time derivative, — . must be calculated at each layer of our model. These can rates can be derived from the chemical kinetics of the oxygen-hemoglobin and oxygen-myoglobin association reactions.

$$Hb_4 + 4O_2 \underset{k_{-1}^{Hb}}{\overset{k_{-1}^{Hb}}{\rightleftharpoons}} Hb_4O_8, \tag{2.8}$$

—— ——— (2.9)

$$Mb + O_2 \underset{k_{-1}^{Mb}}{\overset{k_{-1}^{Mb}}{\rightleftharpoons}} MbO_2, \tag{2.10}$$

—— ——— (2.11)

, also written as , is the oxygen concentration field. and are forward rate reaction constants, while and are the kinetic dissociation rate

constants, or the kinetic reaction rate constants for the reverse reactions. K_{eq}^{Hb} and K_{eq}^{Mb} are the equilibrium constants. Using these equations, R^{Hb} and R^{Mb} can be derived.

$$R^{Hb} = \frac{\partial c}{\partial t}\Big|_{chem}^{Hb} = 4k_{-1}^{Hb}[Hb_4O_8] - 4k_{+1}^{Hb}[Hb_4]c^4 \ , \tag{2.12}$$

$$R^{Mb} = \frac{\partial c}{\partial t}\Big|_{chem}^{Mb} = k_{-1}^{Mb}[MbO_2] - k_{+1}^{Mb}[Mb]c \ , \tag{2.13}$$

As mentioned in chapter 1, the hemoglobin protein is a tetramer containing two α-chains and two β-chains, each of which includes an oxygen-binding heme group. This allows each hemoglobin protein to bind four oxygen molecules. Conversely, each myoglobin protein contains only one heme group, limiting it to binding only one oxygen molecule.

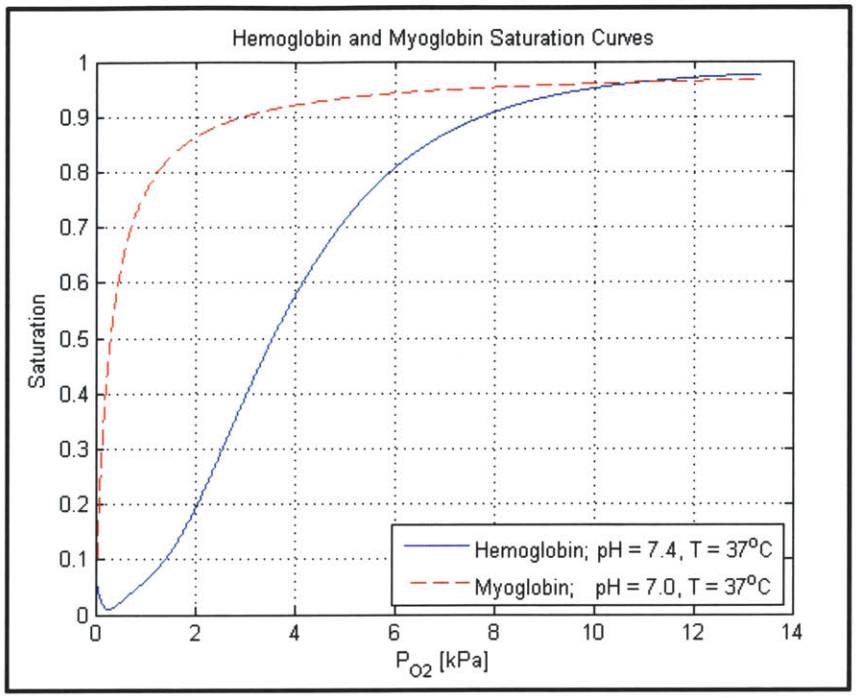

Figure 2.3 – Hemoglobin and Myoglobin Saturation Curves
The cooperative binding properties of hemoglobin lead to a stronger affinity for oxygen than that of myoglobin. The Hemoglobin curve is accurate above 1kPa.

At 50% saturation, equations (2.9) and (2.11) become

$$\left(c_{50\%}^{Hb}\right)^4 = \left(K_{eq}^{Hb}\right)^{-1} = \frac{k_{-1}^{Hb}}{k_{+1}^{Hb}}\,, \tag{2.14}$$

$$c_{50\%}^{Mb} = \left(K_{eq}^{Mb}\right)^{-1} = \frac{k_{-1}^{Mb}}{k_{+1}^{Mb}}\,, \tag{2.15}$$

Saturation is defined as,

$$S^{Hb} = \frac{[Hb_4O_8]}{[Hb_4]_{tot}}\,, \tag{2.16}$$

$$S^{Mb} = \frac{[MbO_2]}{[Mb]_{tot}}, \tag{2.17}$$

In the cell cytoplasm, $R = R^{Hb}$. Free oxygen is produced as the oxyhemoglobin complex unbinds, releasing oxygen; therefore, R^{Hb} is a function of the local hemoglobin saturation. In the plasma, oxygen is neither consumed nor produced and the function is zero in this region. In the tissue, R depends on the rate at which oxygen is consumed by binding to the myoglobin, R^{Mb}, in addition the constant consumption rate of the tissue, M, due to general metabolic activities.

$$R^{Hb} = \left.\frac{\partial c}{\partial t}\right|_{chem}^{Hb} = k_{-1}^{Hb}[Hb]\left(S^{Hb} - (1 - S^{Hb})\left(\frac{c}{c_{50\%}^{Hb}}\right)^{n}\right), \tag{2.18}$$

$$R^{plasma} = \left.\frac{\partial c}{\partial t}\right|_{chem}^{plasma} = 0, \tag{2.19}$$

$$R^{Mb} = \left.\frac{\partial c}{\partial t}\right|_{chem}^{Mb} = k_{-1}^{Mb}[Mb]\left(S^{Mb} - (1 - S^{Mb})\left(\frac{c}{c_{50\%}^{Mb}}\right)\right), \tag{2.20}$$

$[Hb]$ and $[Mb]$ are the concentration of hemoglobin subunits inside the RBC and the concentration of myoglobin in the tissue respectively. $\boldsymbol{n}$ is the Hill coefficient, which is an empirically found value. Finally, R is then given by the sum of values in each region from equation (2.7),

$$R = k_{-1}^{Hb}[Hb]\left(S^{Hb} - (1 - S^{Hb})\left(\frac{c}{c_{50\%}^{Hb}}\right)^{n}\right) + k_{-1}^{Mb}[Mb]\left(S^{Mb} - (1 - S^{Mb})\left(\frac{c}{c_{50\%}^{Mb}}\right)\right) + M \ , \tag{2.21}$$

Each of the quantities in equation (2.21) are known constants in each region with the exception of the oxygen concentration, which we are solving for, and the hemoglobin and myoglobin saturation values, which are functions of oxygen concentration. By the principle of conservation, the total number of hemoglobin proteins and myoglobin proteins in the system do not change.

To calculate the hemoglobin and myoglobin saturation values, we use a similar diffusion analysis. Looking at the diffusion of the saturation of hemoglobin and myoglobin, we obtain equations similar to equation (2.6).

$$S_t^{Hb} + uS_x^{Hb} + vS_y^{Hb} - D^{Hb}\left(S_{xx}^{Hb} + S_{yy}^{Hb}\right) = -\frac{R^{Hb}}{[Hb]} \ , \tag{2.22}$$

$$S_t^{Mb} + uS_x^{Mb} + vS_y^{Mb} - D^{Mb}\left(S_{xx}^{Mb} + S_{yy}^{Mb}\right) = -\frac{R^{Mb}}{[Mb]} \ , \tag{2.23}$$

Substituting equations (2.18) and (2.20), we get

$$S_t^{Hb} + uS_x^{Hb} + vS_y^{Hb} - D^{Hb}\left(S_{xx}^{Hb} + S_{yy}^{Hb}\right) = -k_{-1}^{Hb}\left(S^{Hb} - (1 - S^{Hb})\left(\frac{c}{c_{50\%}^{Hb}}\right)^{n}\right), \quad (2.24)$$

$$S_t^{Mb} + uS_x^{Mb} + vS_y^{Mb} - D^{Mb}\left(S_{xx}^{Mb} + S_{yy}^{Mb}\right) = -k_{-1}^{Mb}\left(S^{Mb} - (1 - S^{Mb})\left(\frac{c}{c_{50\%}^{Mb}}\right)\right), \quad (2.25)$$

Using equations (2.6), (2.21), (2.24), and (2.25), we can completely define the oxygen concentration and rate of oxygen diffusion everywhere in the system.

2.2 Computational Model

The computational model for the capillary flow was constructed using Matlab® software. The blood plasma flow and oxygen concentration calculations are solved using a finite difference method on a static, staggered, Marker-and-Cell (MAC) grid. The finite difference scheme used to solve the blood plasma flow conditions is based on a Navier-Stokes solver **[13]** developed by Benjamin Seibold of the Mathematics Department at MIT. The plasma and RBC membrane interactions are implemented using the level set method. **[14]**

Table 2.2 – Plasma Flow Parameters

Parameter	Value
ρ	$1025 \frac{kg}{m^3}$
V_{avg}	$10^{-3} \frac{m}{s}$
D_{cap}	$8 \times 10^{-6} m$
μ	$1.5 \times 10^{-3} Pa \cdot s$
$Re = \frac{\rho V_{avg} D_{cap}}{\mu}$	5.47×10^{-3}

A Cartesian coordinate system is used because the physical system is approximated as a 2D plasma flow on a rectangular surface, as shown in Figure 2.2. The RBC is modeled as an elastic membrane with a bending stiffness k_{RBC}. The properties of the blood flow and RBC membrane are listed in Table 2.2.

2.2.1 Blood Plasma Flow

The compactness and efficiency of Seibold's method results from the fixed geometry and static discritization of the grid in time. Therefore, the system matrices are the same at each time step and need to be computed only once. **[13]**

The blood plasma follows the 2D incompressible Navier-Stokes equations, (2.2) and (2.3), and is constrained by the incompressible 2D mass continuity, equation (2.1). The dimensionless, scalar component versions of these equations are shown below.

$$u_x + v_y = 0 \ , \tag{2.26}$$

$$u_t = -(u^2)_x - (uv)_y + \frac{1}{Re}(u_{xx} + u_{yy}) - p_x \ , \tag{2.27}$$

$$v_t = -(uv)_x - (v^2)_y + \frac{1}{Re}(v_{xx} + v_{yy}) - p_y \ , \tag{2.28}$$

The time step updates for velocity components U^n and V^n will be computed in a series of steps, by incorporating each term in the Navier-Stokes equations. First, we will incorporate the nonlinear advective terms from equation (2.27), $[-(u^2)_x - (uv)_y]$, and equation (2.28), $[-(uv)_x - (v^2)_y]$. The first updated values of velocity will be denoted as U^* and V^*. These values are solved explicitly using an upwinding scheme as shown in equations (2.29) and (2.30).

$$\frac{U^* - U^n}{\Delta t} = -((U^n)^2)_x - (U^n V^n)_y \ , \tag{2.29}$$

$$\frac{V^* - V^n}{\Delta t} = -(U^n V^n)_x - ((V^n)^2)_y \ , \tag{2.30}$$

Next we update velocity by incorporating the viscosity terms, $\left[\frac{1}{Re}(u_{xx} + u_{yy})\right]$ and $\left[\frac{1}{Re}(v_{xx} + v_{yy})\right]$, implicitly.

$$\frac{U^{**} - U^{*}}{\Delta t} = \frac{1}{Re}\left(U_{xx}^{**} + U_{yy}^{**}\right) , \tag{2.31}$$

$$\frac{V^{**} - V^{*}}{\Delta t} = \frac{1}{Re}\left(V_{xx}^{**} + V_{yy}^{**}\right) , \tag{2.32}$$

Finally, we can update the velocity by including the pressure terms, $[-p_x]$ and $[-p_y]$, implicitly.

$$\frac{U^{n+1} - U^{**}}{\Delta t} = -(P^{n+1})_x , \tag{2.33}$$

$$\frac{V^{n+1} - V^{**}}{\Delta t} = -(P^{n+1})_y , \tag{2.34}$$

Equations (2.33) and (2.34) can be rewritten in vector form as,

$$\frac{\underline{U}^{n+1} - \underline{U}^{**}}{\Delta t} = -\nabla P^{n+1} , \tag{2.35}$$

The pressure is found by computing the divergence of both sides, which eliminates the $\underline{U}^{n+1}$ term due to the continuity constraint, and you are left with

$$-\frac{\nabla \cdot \underline{U}^{**}}{\Delta t} = -\Delta P^{n+1} , \tag{2.36}$$

Applying the inverse Laplacian operator to equation (2.36) then gives the pressure at the new time step (P^{n+1}). Finally, we can take the gradient of the pressure field to obtain the velocities.

$$\underline{G}^{n+1} = -\nabla \mathrm{P}^{\mathrm{n+1}} \ , \tag{2.37}$$

$$\underline{U}^{n+1} = \underline{U}^{**} + \Delta t \underline{G}^{n+1} \ , \tag{2.38}$$

As mentioned previously, the efficiency of these calculations is in large part due to having calculated the system matrices only once before marching through the finite difference scheme. The system matrices for our system are essentially inverse Laplacian operators. These system matrices are implemented using the Crank-Nicolson scheme, which is second-order accurate in time and space.

2.2.1.1 Spatial and Time Discritization

The advection term calculation above uses a centered difference scheme, which is second order accurate as opposed to a forward or backward difference scheme. Despite the higher order of accuracy, using a centered difference scheme can create oscillations due to the coupling of the variables because they are all calculated at the same points. To eliminate this phenomenon, we use a staggered grid. **[13]**

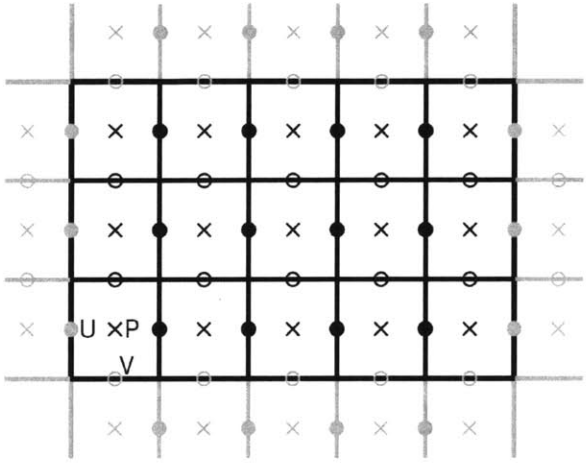

Figure 2.4 – Staggered MAC Grid
Interior cells are shown in black and boundary cells are shown in gray. Crosses denote cell centers where fluid pressure and other quantities are calculated. The circles denote the cell borders where velocity components are calculated (U-velocity in filled circles and V-velocity in unfilled circles)

Consider a rectangular domain, which is discretized into rectangular elements on a staggered grid. In this grid, the velocities are defined on the boundaries and the pressures are defined in the centers of the cell as shown in Figure 2.4.

For our solution to converge with stability, we must satisfy the Courant–Friedrichs–Lewy (CFL) condition. The limiting time step will be for the explicit upwind calculation of the advection terms. The diffusion terms are calculated using a second-order accurate, Crank-Nicolson scheme which is unconditionally stable. **[15]** Therefore, to ensure overall stability, the following conditions must hold true.

CFL condition for advective term:

$$u_{max}\frac{\Delta t}{\Delta x} + v_{max}\frac{\Delta t}{\Delta x} \leq 1 \ , \tag{2.39}$$

The horizontal and vertical grid sizes are the same; $\Delta x = \Delta y = h$, therefore,

$$(u_{max} + v_{max})\frac{\Delta t}{h} \leq 1 \ , \tag{2.40}$$

$$\Delta t \leq \frac{h}{(u_{max} + v_{max})} \ , \tag{2.41}$$

We desire a time step as large as possible to reduce computational time for the simulation, but small enough to ensure stability. Equation (2.41) shows that the maximum time step is related to the grid spacing and maximum speed of the flow within the capillary, which changes in time. Instead of choosing a new time step at each iteration, we can choose a time step small enough such that it always satisfy the CFL condition.

Since we are using non-dimensional equations for our model, all quantities are relative and the actual values are meaningless before they are dimensionalized. By design, we can set the initial velocity at all points within the flow to unity, and the maximum velocity should not exceed this value by much more. Test cases of the model with very small time steps have shown that the maximum velocity does not

exceed three. For total certainty, we will use the value of four for the maximum velocity.

Next, we must calculate the grid size. All of our equations have been non-dimensionalized using the capillary diameter as a reference length. Therefore the diameter of the capillary will be set to unity and all other values will be proportional. The length of our channel will be set to be a multiple of the diameter.

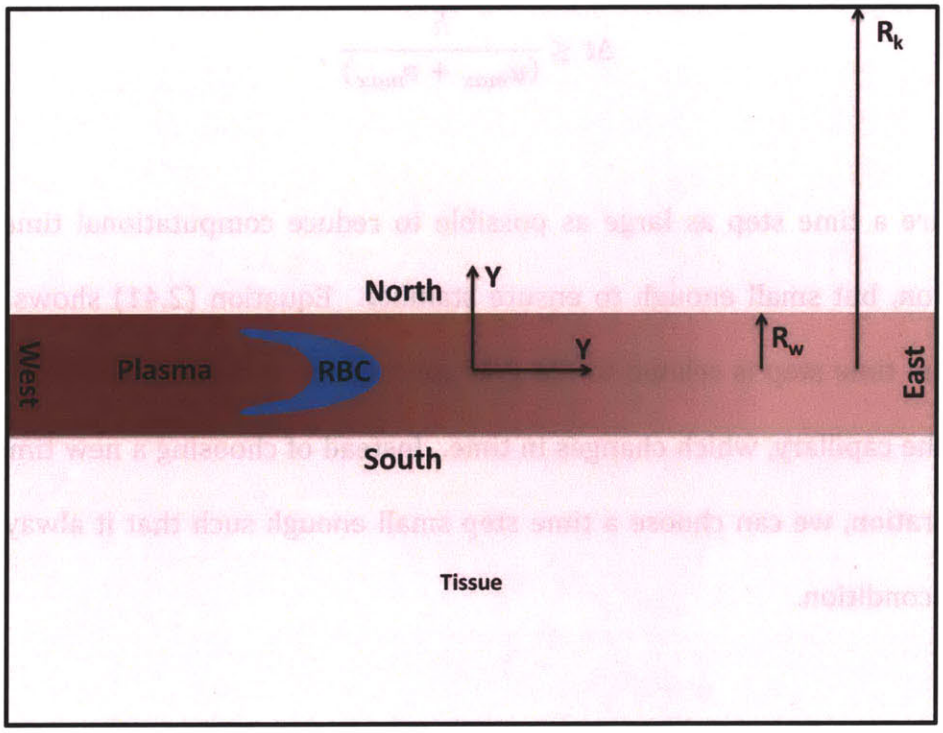

Figure 2.5 – Computational domain in 3-Layer Model
Coordinate axes at the center of the computational domain

Based on computational time and accuracy, the optimal grid step size is determined to be . Using equation (2.41) and the values determined for grid step size

and maximum velocity, the time step is calculated, $\Delta t = 0.0050$. Test simulations however, show much smoother results for a lower time step of $\Delta t = 0.0025$, therefore we will be using this value.

For our flow calculations, it is important that we can calculate velocities, pressures, and their derivatives at the same points. We can find these values at neighboring locations by averaging or by finding first or second differences for the derivatives.

2.2.1.2 Flow Boundaries

The flow is bounded by two other regions. The first, on the north and south boundaries, is the capillary wall. At the capillary wall, the plasma velocity is zero because we impose a no slip / no flux condition. The east and west border of the computational domain are set to be periodic. The flow velocities and pressure gradient are also periodic such that the flow properties are continuous on the east and west boundaries of the capillary channel.

$$\underline{v}_N = \underline{v}_S = 0 \ , \tag{2.42}$$

$$\underline{v}_E = \underline{v}_W \ , \tag{2.43}$$

The second boundary is the RBC membrane. The flow properties for this boundary and inside the RBC will be discussed in the next section.

2.2.2 RBC Membrane

The level set method is used to dictate the advection of the RBC membrane. A function $\phi(x,y)$ is produced in the mesh space such that $\phi(x,y) = 0$ defines the boundary between the cell and the plasma. The domain inside the boundary, Ω^-, is defined by $\phi(x,y) < 0$, and the domain outside the boundary, Ω^+, is defined by $\phi(x,y) > 0$. Our zero level set function is initially approximated as an ellipse with the semi-major axis along the diameter of the capillary and the semi-minor axis along the axis of the capillary.

The rate at which the level set function propagates depends on the flow speed. This propagation will follow the convection equation:

$$\phi_t + \underline{v} \cdot \nabla\phi = 0 \ , \tag{2.44}$$

By definition, the gradient of the level set function is parallel to the velocity vector. Therefore, we can rewrite our velocity vector as the product of the magnitude of the velocity, F, and unit vector in the direction of the level set function, $\frac{\nabla\phi}{|\nabla\phi|}$. Substituting these quantities into equation (2.44) yields the level set function.

$$\phi_t + F|\nabla\phi| = 0 \ , \tag{2.45}$$

In order to determine F, the propagation rate, we can use the dot product of the velocity and gradient of the level set:

$$\underline{v} \cdot \nabla\phi = F\hat{n} \cdot \nabla\phi \ , \tag{2.46}$$

$$\langle u, v \rangle \cdot \langle \phi_x, \phi_y \rangle = F \frac{\nabla\phi}{|\nabla\phi|} \cdot \nabla\phi \ , \tag{2.47}$$

$$u\phi_x + v\phi_y = F|\nabla\phi| \ , \tag{2.48}$$

$$u\phi_x + v\phi_y = F \frac{\phi_x^2 + \phi_y^2}{\sqrt{\phi_x^2 + \phi_y^2}} \ , \tag{2.49}$$

$$F = \frac{u\phi_x + v\phi_y}{\sqrt{\phi_x^2 + \phi_y^2}} \ , \tag{2.50}$$

The propagation rate, F, is calculated at each iteration, and as shown in equation (2.50), F is dependent on the plasma flow velocity. For greater accuracy, the level set function is moved onto a finer mesh and propagated on this grid at a proportionally smaller time step. It is then returned to the original, coarser mesh. This allows us to have a more accurate advection scheme while saving time by running the rest of the simulation at such a coarser mesh.

The fluid both inside and outside the RBC are governed by the Navier-Stokes equations, however, the RBC membrane acts on the fluid as an additional body force. Unlike the capillary wall, the RBC membrane does not have a no-slip condition. In our computational model, the flow is discontinuous at the boundary due to the

reactionary body force of the membrane acting on the cytoplasm. These membrane stresses on the fluid can be expressed as a jump in pressure across the fluid; therefore, they can be incorporated into the Navier-Stokes calculations of the plasma flow. This pressure jump must be accounted for when calculating the pressure of a fluid element that accesses a pressure of a neighboring cell that is on the opposite side of the membrane.

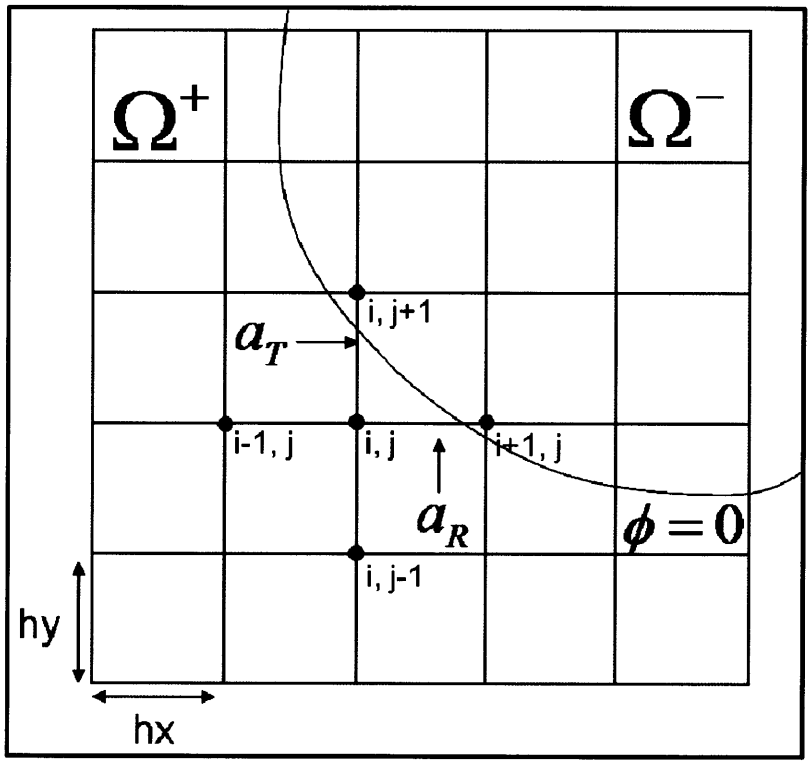

Figure 2.6 – Jump condition at RBC boundary
Jump conditions and are shown on a 5-point stencil. Jump conditions are applied for points on the stencil that lie in a different domain than the center point.

Figure 2.6 illustrates an example of a point (i,j) which has two points in its stencil on the opposite side of the level set boundary. The stencil for the 2nd difference of the pressure would be written as

$$\frac{1}{(h_x)^2}(p_{i-1,j} - 2p_{i,j} + p_{i+1,j}) + \frac{1}{(h_y)^2}(p_{i-1,j} - 2p_{i,j} + p_{i+1,j}) = f_{i,j} + \frac{a_R}{(h_x)^2} + \frac{a_T}{(h_y)^2}, \quad (2.51)$$

The a_R and a_T terms account for the pressure jump, across the boundary for the right-hand $(i+1,j)$ and top $(i,j+1)$ points respectively, caused by the stress applied on the fluid by the RBC membrane. Notice that there are no additional terms for the left-hand $(i-1,j)$ or bottom $(i,j-1)$ points because there are on the same side of the boundary as the center point (i,j) on the stencil.

RBC membrane stiffness is a uniform value across the membrane, but varies for healthy and sickle erythrocytes. We use a value of $k_{RBC} = 1.9 \times 10^{-5} \frac{N}{m}$ for healthy erythrocytes. **[16]** In sickle erythrocytes, the membrane stiffness is dependent on local oxygen concentration. As the oxygen diffuses out of the cell, the oxyhemoglobin complexes are unbound, producing free oxygen and consequently, change their molecular conformation, leaving them vulnerable to polymerization in the sickle case. Although my model does not directly simulate the polymerization of

HbS and its affect on the RBC shape, this model does capture the increase in cell membrane rigidity for the oxygen-reduced sickle RBC.

Berger and King propose an inverse exponential relationship between stiffness and oxygen concentration.

$$\frac{k_{RBC}}{(k_{RBC})_0} = \left(\frac{c}{c_0}\right)^{-j} = \left(\frac{p_{O_2}}{(p_{O_2})_0}\right)^{-j}, \tag{2.52}$$

In equation (2.52), $(k_{RBC})_0$ represents the stiffness of a normal cell; c_0 and $(p_{O_2})_0$ represent the oxygen concentration and oxygen partial pressure when the cell is fully oxygenated at the arterial end of the capillary. The stiffness index, j, is a positive constant. Berger and King use data from an experiment conducted by Usami et. al., to justify the stiffness index value. Figure 2.7 shows the non-dimensional resistance, which we refer to as $\frac{k_{RBC}}{(k_{RBC})_0}$, plotted against the oxygen partial pressure in both linear and log-log axes. Based on these plots, it appears that a stiffness index of $j = 2$ is reasonable. Based on the slope from the best-fit line on the logarithmic plot, it appears that a stiffness index of $j = 2$ is reasonable value.

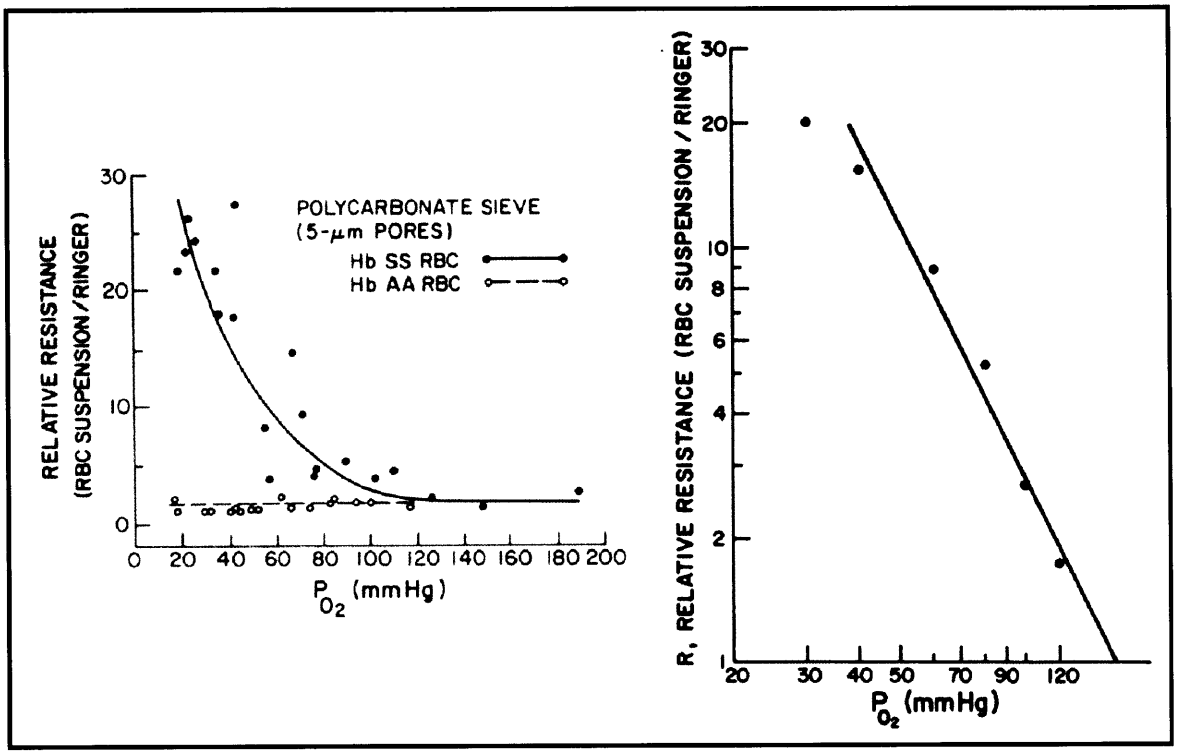

Figure 2.7 – RBC Membrane Stiffness vs. O_2 Partial Pressure [18]

Membrane stiffness for healthy and sickle RBCs are plotted on linear and log-log plots. The plots indicate an exponential relationship between membrane stiffness and O_2 partial pressure for sickle RBCs, and no change in membrane stiffness for healthy RBCs.

This value, however, serves as an upper bound for the stiffness index because in the experiment, the sickle blood was "allowed sufficient time to equilibrate with the oxygen tension" **[17]**. Therefore, the stiffness index will vary in the range

The membrane stress is calculated as the product of the membrane stiffness and the curvature of the membrane.

$$\sigma = k_{RBC}\kappa \ , \tag{2.53}$$

where the curvature, κ, is calculated from the level set function,

$$\kappa = \frac{\phi_{xx}\phi_y^2 - 2\phi_x\phi_y\phi_{xy} + \phi_{yy}\phi_x^2}{\left(\phi_x^2 + \phi_y^2\right)^{\frac{3}{2}}} \ , \tag{2.54}$$

This is another simplification in our model. Creating a stress function that is directly proportional to curvature assumes that at rest, the membrane would take the shape of a circle, the shape that would minimize overall stress on the object. However in reality, at rest, the RBC has a bi-concave shape. As the fluid within and exterior to the cell moves, it will deform the RBC, causing different stress levels on the cell membrane.

This could have some impact on the results of this simulation, by creating the appearance of higher stress values at the points of greatest curvature. Additionally, this model might slightly decrease the apparent surface area of the RBC, which could impact the velocity profiles. This would not impact the oxygen diffusion however, because the diffusion calculations are dependent on the volume of the RBC, not the surface area, which is controlled to remain unchanging with each time step.

The membrane stress at each point adjacent to the membrane is calculated to account for the total pressure jump. These values are summed into a matrix, J, which is then added to the pressure term when P^{n+1} is calculated.

2.2.3 Oxygen Diffusion

The oxygen diffusion is incorporated into our computational model, allowing us to observe the oxygen concentration throughout the system as the RBC traverses the capillary. The oxygen diffusion component must model the oxygen-hemoglobin interaction, oxygen diffusion throughout the RBC, plasma, and tissue, the oxygen-myoglobin interaction (binding of free oxygen), and the consumption of free oxygen.

Like the fluid pressure, the oxygen concentration will be calculated at the cell centers in our computational grid. Therefore, all saturation values, flow velocities and oxygen concentration derivatives must be averaged or differenced to provide values at the cell centers as well. Equation (2.6) is rewritten in the computational domain as

$$\frac{C^{n+1} - C^n}{\Delta t} + U^n C_x^n + V^n C_x^n - D_{ox}\left(C_{xx}^n + C_{yy}^n\right) = R(C^n) \ , \qquad (2.55)$$

The first spatial derivative of the oxygen concentration is calculated using an explicit centered difference scheme. The second spatial derivatives are derived using an implicit Crank-Nicolson scheme. The oxygen concentration update can then be calculated as,

$$C^{n+1} = C^n + \Delta t\big[R(C^n) - U^n C_x^n - V^n C_y^n + D_{ox}\left(C_{xx}^n + C_{yy}^n\right)\big] , \tag{2.56}$$

S^{Hb} and S^{Mb} updates are calculated in a similar fashion. Equations (2.24) and (2.25) in the computational domain are written as,

$$\frac{{S^{Hb}}^{n+1} - {S^{Hb}}^n}{\Delta t} + U^n {S_x^{Hb}}^n + V^n {S_y^{Hb}}^n - D^{Hb}\left({S_{xx}^{Hb}}^n + {S_{yy}^{Hb}}^n\right) = -k_{-1}^{Hb}\left({S^{Hb}}^n - \left(1 - {S^{Hb}}^n\right)\left(\frac{C^n}{C_{50\%}^{Hb}}\right)^{\boldsymbol{n}}\right) , \tag{2.57}$$

$$\frac{{S^{Mb}}^{n+1} - {S^{Mb}}^n}{\Delta t} + U^n {S_x^{Mb}}^n + V^n {S_y^{Mb}}^n - D^{Mb}\left({S_{xx}^{Mb}}^n + {S_{yy}^{Mb}}^n\right) = -k_{-1}^{Mb}\left({S^{Mb}}^n - \left(1 - {S^{Mb}}^n\right)\left(\frac{C^n}{C_{50\%}^{Mb}}\right)\right) , \tag{2.58}$$

R contains no derivatives and is calculated explicitly according to equation (2.21). In the computational domain, it is rewritten as,

$$R^n = k_{-1}^{Hb}[Hb]\left(S^{Hb^n} - \left(1 - S^{Hb^n}\right)\left(\frac{C^n}{c_{50\%}^{Hb}}\right)^n\right) + k_{-1}^{Mb}[Mb]\left(S^{Mb^n} - \left(1 - S^{Mb^n}\right)\left(\frac{C^n}{c_{50\%}^{Mb}}\right)\right) + M \ , \tag{2.59}$$

Table 2.3 lists all of the oxygen diffusion constants used in this model for the normal blood and their values in comparison with those of the Le Floch-Harris model. Most parameter values are nearly identical with the exception of the Hill coefficient and the oxygen concentration at 50% hemoglobin and myoglobin saturation.

Table 2.3 – Oxygen Diffusion Parameters for normal blood
Tekleab-Harris model vs. Le Floch-Harris model

Constant	Symbol	Value	
		Tekleab-Harris Model	Le Floch-Harris Model
O_2 diffusion constant	D_{ox}	$2.40 \times 10^{-9} \frac{m^2}{s}$	$2.41 \times 10^{-9} \frac{m^2}{s}$
Diffusivity of Hemoglobin	D^{Hb}	$1.40 \times 10^{-11} \frac{m^2}{s}$	$1.38 \times 10^{-11} \frac{m^2}{s}$
Diffusivity of Myoglobin	D^{Mb}	$6.10 \times 10^{-11} \frac{m^2}{s}$	$6.10 \times 10^{-11} \frac{m^2}{s}$
Hb dissociation rate constant	k_{-1}^{Hb}	$44 s^{-1}$	$44 s^{-1}$
Mb dissociation rate constant	k_{-1}^{Mb}	$15.6 s^{-1}$	N/A
Hb concentration in RBC	$[Hb]$	$21.099 \frac{mol}{m^3}$	$21.099 \frac{mol}{m^3}$
Mb concentration in tissue	$[Mb]$	$0.4 \frac{mol}{m^3}$	$0.4 \frac{mol}{m^3}$
O_2 concentration at 50% Hb saturation	$c_{50\%}^{Hb}$	$3.430 \times 10^{-2} \frac{mol}{m^3}$	$4.412 \times 10^{-2} \frac{mol}{m^3}$
O_2 concentration at 50% Hb saturation	$c_{50\%}^{Mb}$	$3.271 \times 10^{-3} \frac{mol}{m^3}$	$7.981 \times 10^{-3} \frac{mol}{m^3}$
O_2 consumption rate in tissue	M	$-6.1321 \times 10^{-3} \frac{mol}{m^3 - s}$	$-6.1321 \times 10^{-3} \frac{mol}{m^3 - s}$

Henry's law constant	α	$1.029 \times 10^{-5} \frac{mol}{m^3 - Pa}$	$1.130 \times 10^{-5} \frac{mol}{m^3 - Pa}$
Hill coefficient **[19]**	$\boldsymbol{n}$	2.7	2.2

To simulate the sickle blood, we modify four parameters. The diagram in Figure 2.8 shows the relative values of these four parameters between the normal and sickle cases.

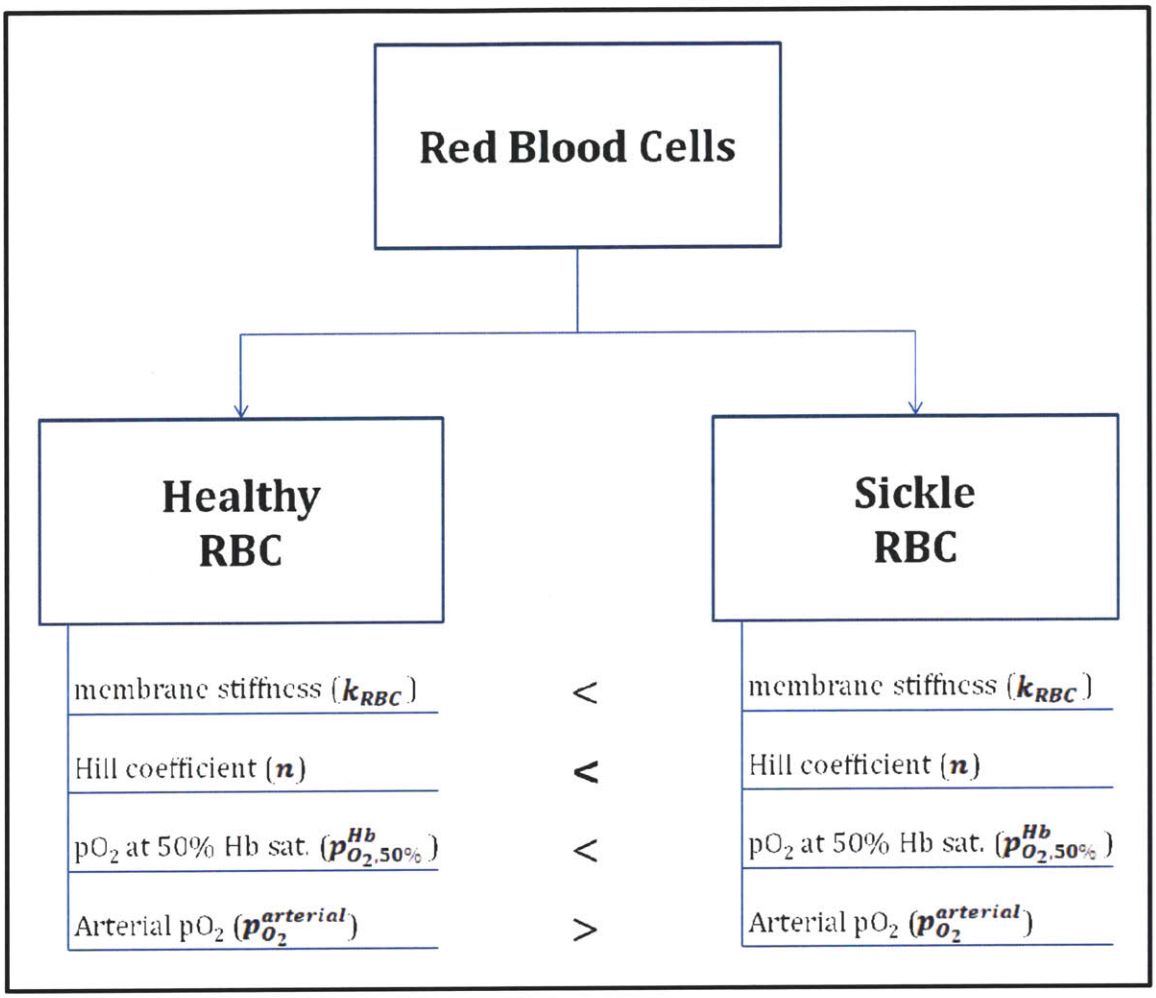

Figure 2.8 – Healthy vs. Sickle RBC

Notice the increased membrane stiffness, increased pO_2 at 50% Hb saturation, increased Hill coefficient, and decreased arterial pO_2 for the sickle RBC.

The changes in these values in the sickle case cause a right-shift in the hemoglobin oxygen saturation curve. Figure 1.9 shows the shifted hemoglobin saturation curve for the sickle case.

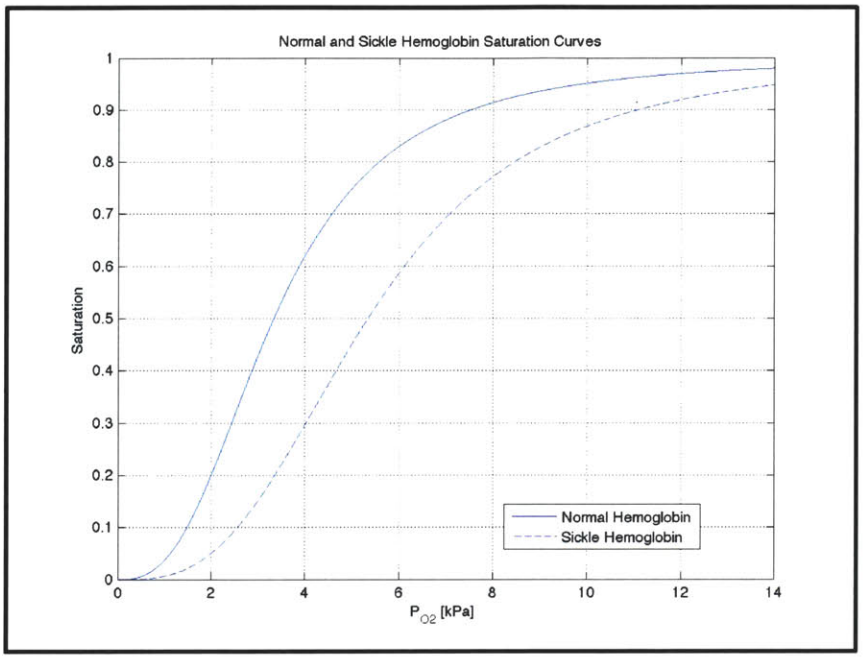

Figure 2.9 – Normal vs. Sickle Hemoglobin Saturation
The increased $p_{O_2,50\%}^{Hb}$, increased Hill coefficient, and decreased $p_{O_2}^{arterial}$ values cause a right-shift in the hemoglobin saturation curve.

3 Results

In this chapter, the data is presented for both the normal and sickle microcirculation. The simulations were run by varying the sickle microcirculation conditions, including the RBC membrane stiffness. The 24 test cases are explained in detail below.

3.1 Test Cases

The microcirculation numerical code was designed to run two simple cases, the normal microcirculation and the sickle microcirculation. The simulation for the normal and sickle cases are identical with the exception of four critical parameters. These four parameters and their values for both the normal and sickle blood scenarios are listed in Table 3.1.

Table 3.1 – Microcirculation Simulation Parameters

Parameter	Normal Case Value	Sickle Case Value
Hill coefficient ($\boldsymbol{n}$)	2.7	3.0
p_{O_2} at 50% Hb saturation ($p^{Hb}_{O_2,50\%}$)	$3.33 \times 10^3 Pa$ ($25\ mmHg$)	$5.33 \times 10^3 Pa$ ($40\ mmHg$)
p_{O_2} in arteries	$1.27 \times 10^4 Pa$ ($95\ mmHg$)	$1.07 \times 10^4 Pa$ ($80\ mmHg$)

$(p_{O_2}^{arterial})$		
stiffness index (j)	0.0	0.0; 0.2; 0.5; 1.0; 2.0

The stiffness index is zero for the normal case, meaning that the stiffness of the RBC membrane is a constant value everywhere, regardless of local oxygen concentration. The sickle case, however, is simulated at a variety of stiffness indices ranging between 0 and 2. At stiffness index values greater than 0, the RBC membrane stiffness is related to the local oxygen concentration. The sickle case is tested at five different stiffness indices, thereby creating six test cases in total – five sickle microcirculation test cases and one normal microcirculation test case.

The microcirculation model approximates the RBC's initial shape as an ellipse, which eventually reaches a steady shape. The geometry of the RBC membrane is defined by the function ϕ. The RBC is defined by the region $\phi < 0$. The function is initialized as an ellipse, according to the equation,

$$\phi(x,y) = \sqrt{b^2(x-x_0)^2 - a^2(y-y_0)^2} - ab \qquad (3.1)$$

where (x_0, y_0) are the coordinates for the center of the ellipse, and a and b are the semi-major and semi-minor axes. Before entering the capillary, the RBC at rest has a biconcave disc shape, which is approximated as an ellipse. In the simulation, as the RBC begins to move, it morphs into a biconcave shape. It would also be of

interest, for comparison, if the simulation began with the asymptotic value for the geometry as shown in Figure 3.1. The asymptotic shape may affect the speed at which the RBC traverses the capillary as well as its ability to deliver oxygen to its surroundings.

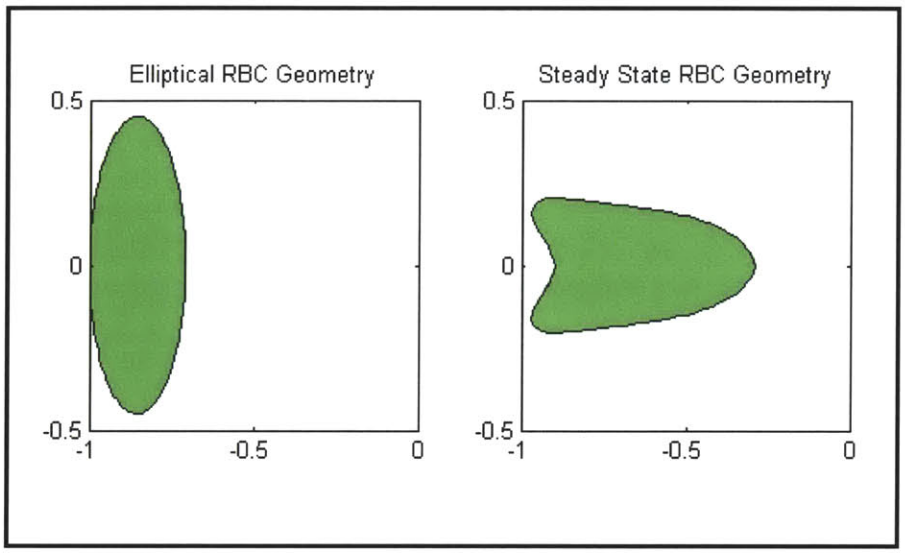

Figure 3.1 – RBC initial geometries

Test cases #01-#06 and #13-#18 use the elliptical geometry to define the RBC shape, while test cases #07-#12 and #19-#24 use the asymptotic RBC shape. The asymptotic geometry was obtained by running the elliptical RBC until the cell reached an asymptotic geometry.

Using two different initial geometries doubles the number of test cases, giving us 12 test cases.

The periodicity of our model allows the RBC to exit the frame of reference and enter on the opposite boundary. Although the plasma and cell in the capillary are flowing, the tissue does not, so the cell is flowing past same tissue segments repeatedly as its

oxygen content diminishes. The periodic boundary conditions will be used to analyze the oxygen consumption in a specific region of tissue, so for a portion of the test cases, a short, fixed-length segment of capillary will be used.

Table 3.2 – Microcirculation Test Cases

Channel Length (l_x) & Boundary Conditions	RBC initial geometry (ϕ)	Normal/Sickle Parameters	Stiffness index (j)	Test Case
l_x=2 Periodic East/West Boundary Conditions	elliptical	Normal	0.0	#01
		Sickle	0.0	#02
			0.2	#03
			0.5	#04
			1.0	#05
			2.0	#06
	asymptotic	Normal	0.0	#07
		Sickle	0.0	#08
			0.2	#09
			0.5	#10
			1.0	#11
			2.0	#12
l_x=10 Fixed East / Neumann West Boundary Conditions	elliptical	Normal	0.0	#13
		Sickle	0.0	#14
			0.2	#15
			0.5	#16
			1.0	#17
			2.0	#18
	asymptotic	Normal	0.0	#19
		Sickle	0.0	#20
			0.2	#21
			0.5	#22
			1.0	#23
			2.0	#24

It would also be interesting to see the behavior of the system as the cell flows beyond new segments tissue. Therefore, I present a test case in which the length of the channel the RBC flows through is increased. The new length must be long enough that the simulation will end before the RBC reaches the end. For this long capillary, a fixed boundary condition at the east boundary (arterial end of the capillary) will be enforced. The oxygen concentration at this boundary will be set to

the arterial oxygen concentration value. The west boundary will have a Neumann boundary condition.

Varying each of these parameters gives us a total of 24 test cases. These test cases are described in Table 3.2.

3.2 Simulation Results

Each test case was run for four seconds and data was collected at several intervals. Pressure, u-velocity, v-velocity, oxygen concentration, and RBC geometry were plotted.

3.2.1 Pressure

The pressure profiles for all test cases are nearly identical. The pressure variations due to the membrane reaction forces on the flow are small enough that the pressure gradient across the channel does not change. There is a large pressure gradient created by the pumping of the heart. Only this imposed pressure gradient is visible. Figure 3.2 shows the pressure profiles for the short and long capillaries.

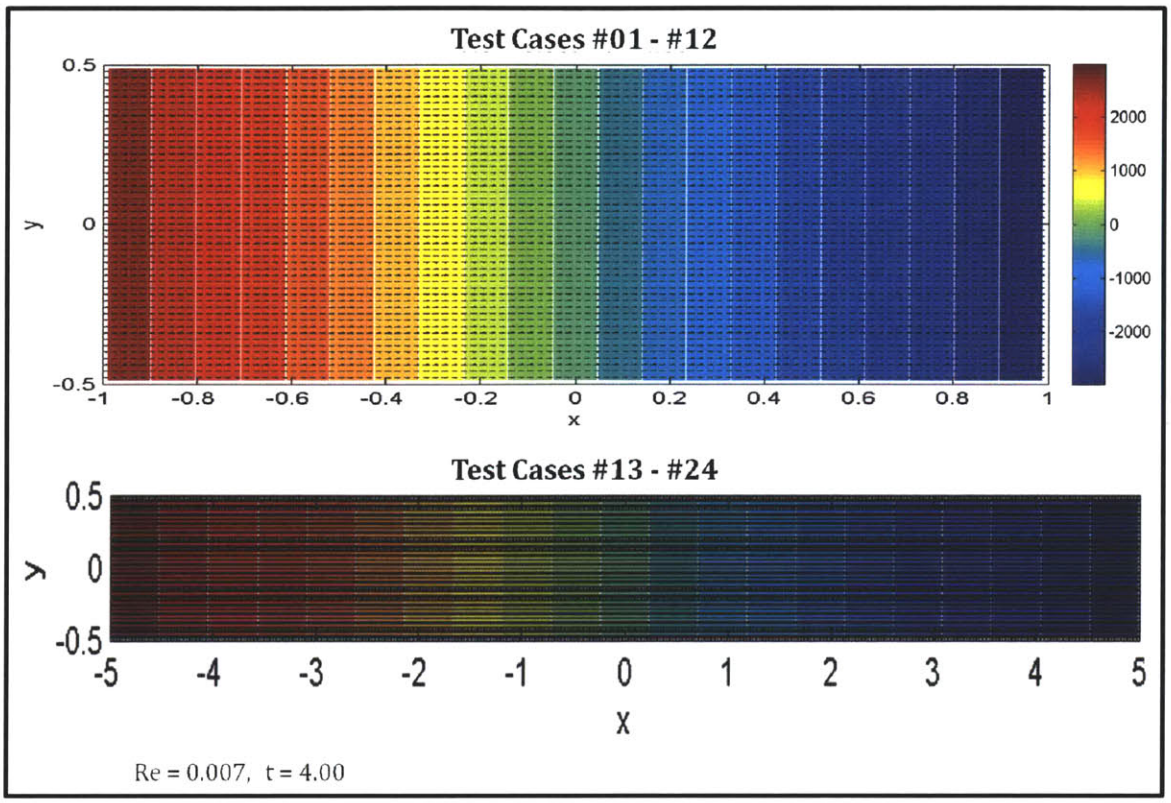

Figure 3.2 – Fluid Pressure Profile in Capillary

3.2.2 Velocity Profiles

The velocity profiles indicate a Poiseuille flow as expected in x-direction. Of the four different test case parameters (normal/sickle parameters, stiffness index, initial RBC geometry, channel length), the stiffness index has the largest impact on the U and V velocity. The V velocity values are orders of magnitude smaller than the U velocity. This is true for all test cases. The velocity profiles for both U and V are presented below. Only the normal cases, and the sickle cases with the smallest and

largest value for the stiffness index are presented in this section. A complete set of the data can be found in Appendix A.

Figure 3.3 – U-Velocity, Test Case #01, #02, #06
$L_X = 2$, Elliptical Initial RBC Geometry

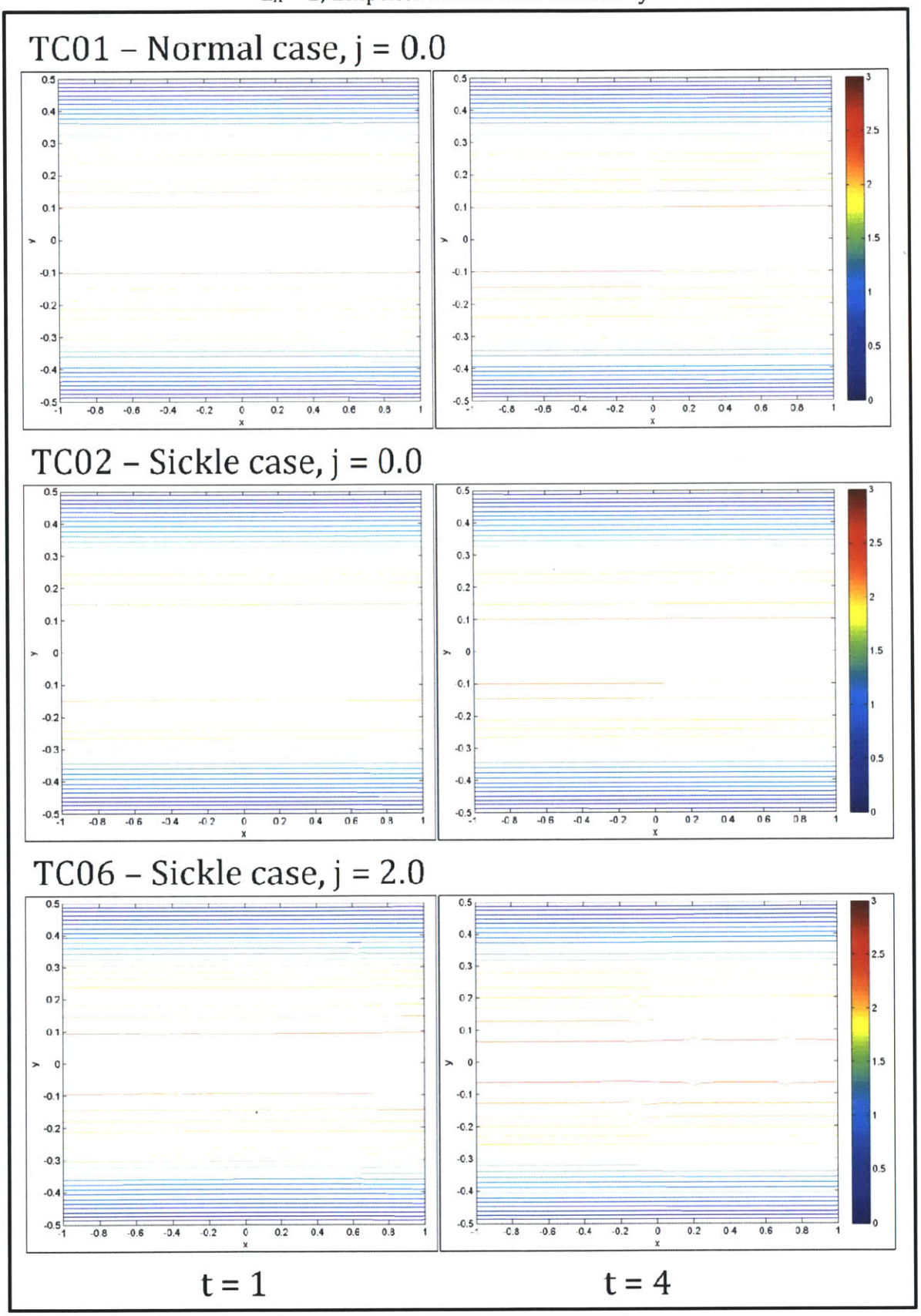

Figure 3.4 – U-Velocity, Test Case #07, #08, #12
L_X = 2, Asymptotic Initial RBC Geometry

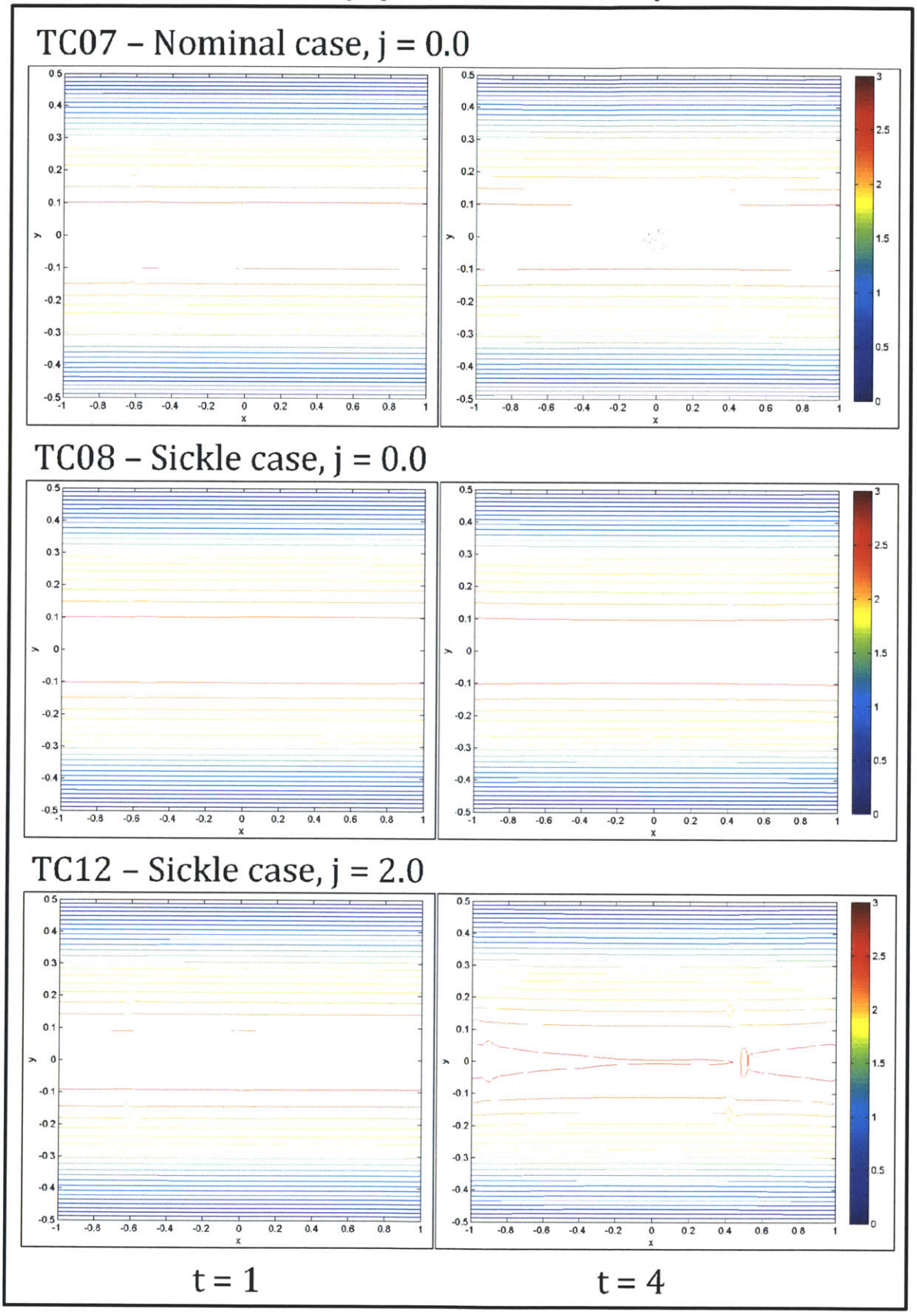

Figure 3.5 – U-Velocity, Test Case #13, #14, #18
L_X = 10, Elliptical Initial RBC Geometry

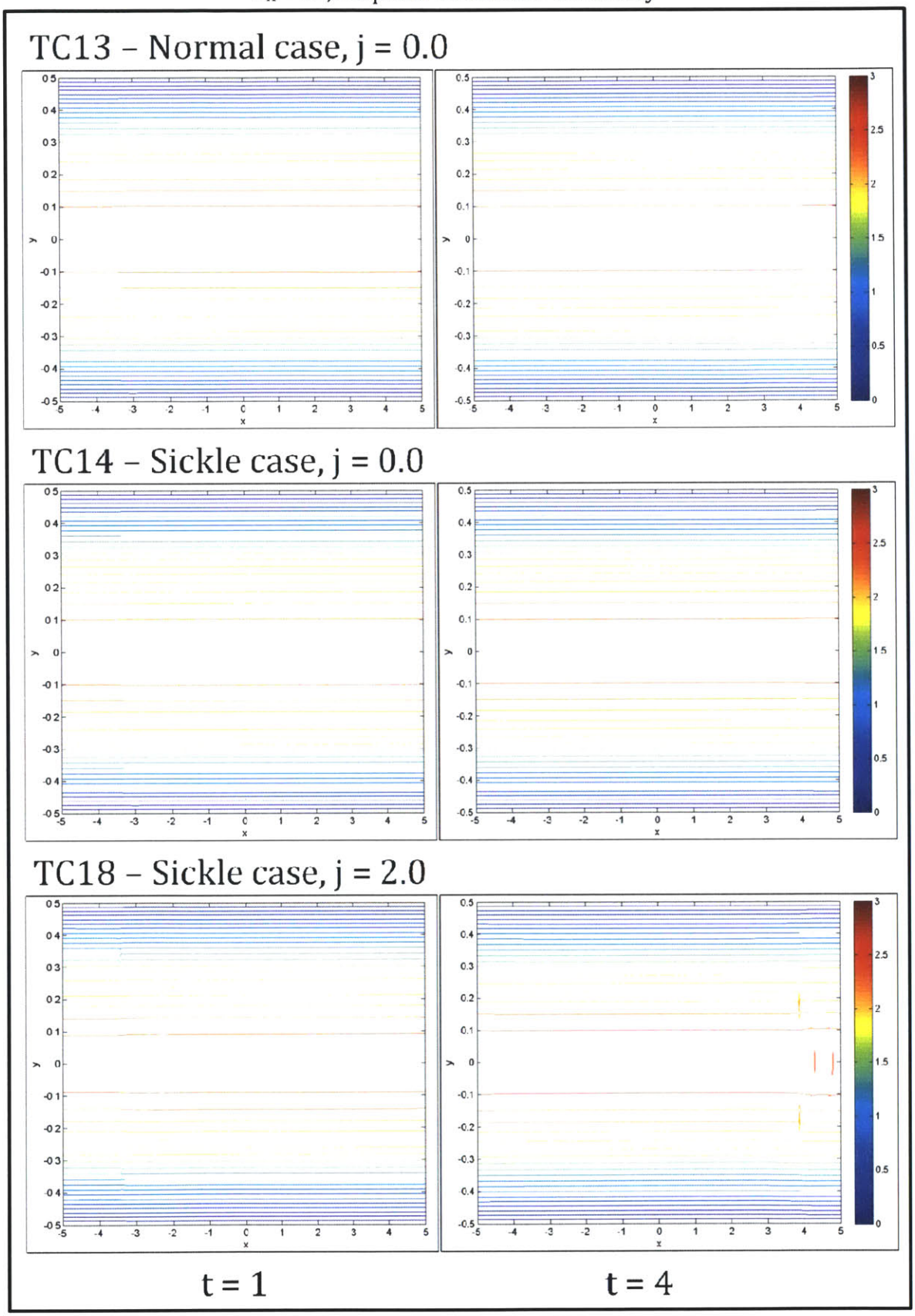

Figure 3.6 – U-Velocity, Test Case #19, #20, #24
L_X = 10, Asymptotic Initial RBC Geometry

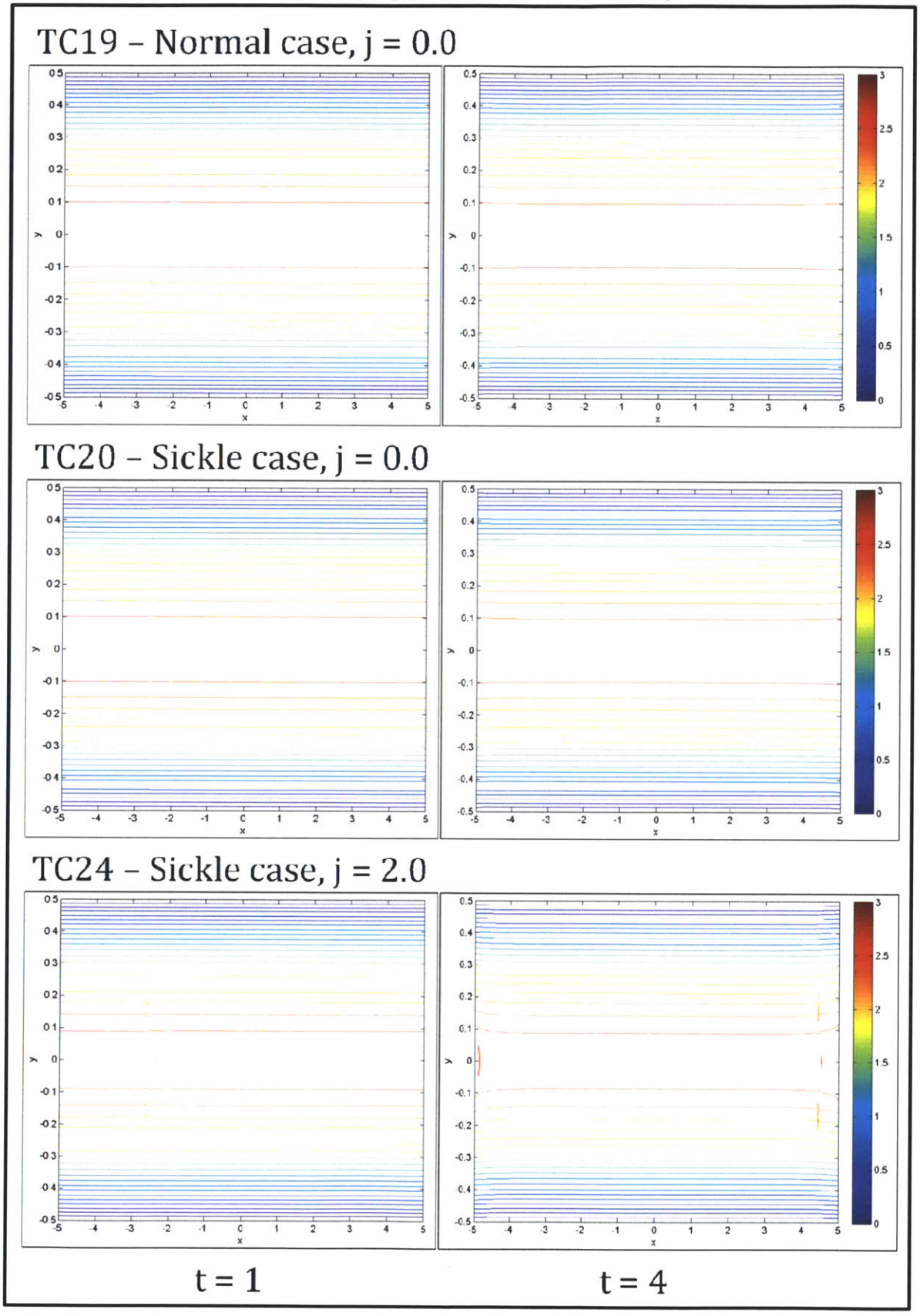

Figure 3.7 – V-Velocity, Test Case #01, #02, #06
L_X = 2, Elliptical Initial RBC Geometry

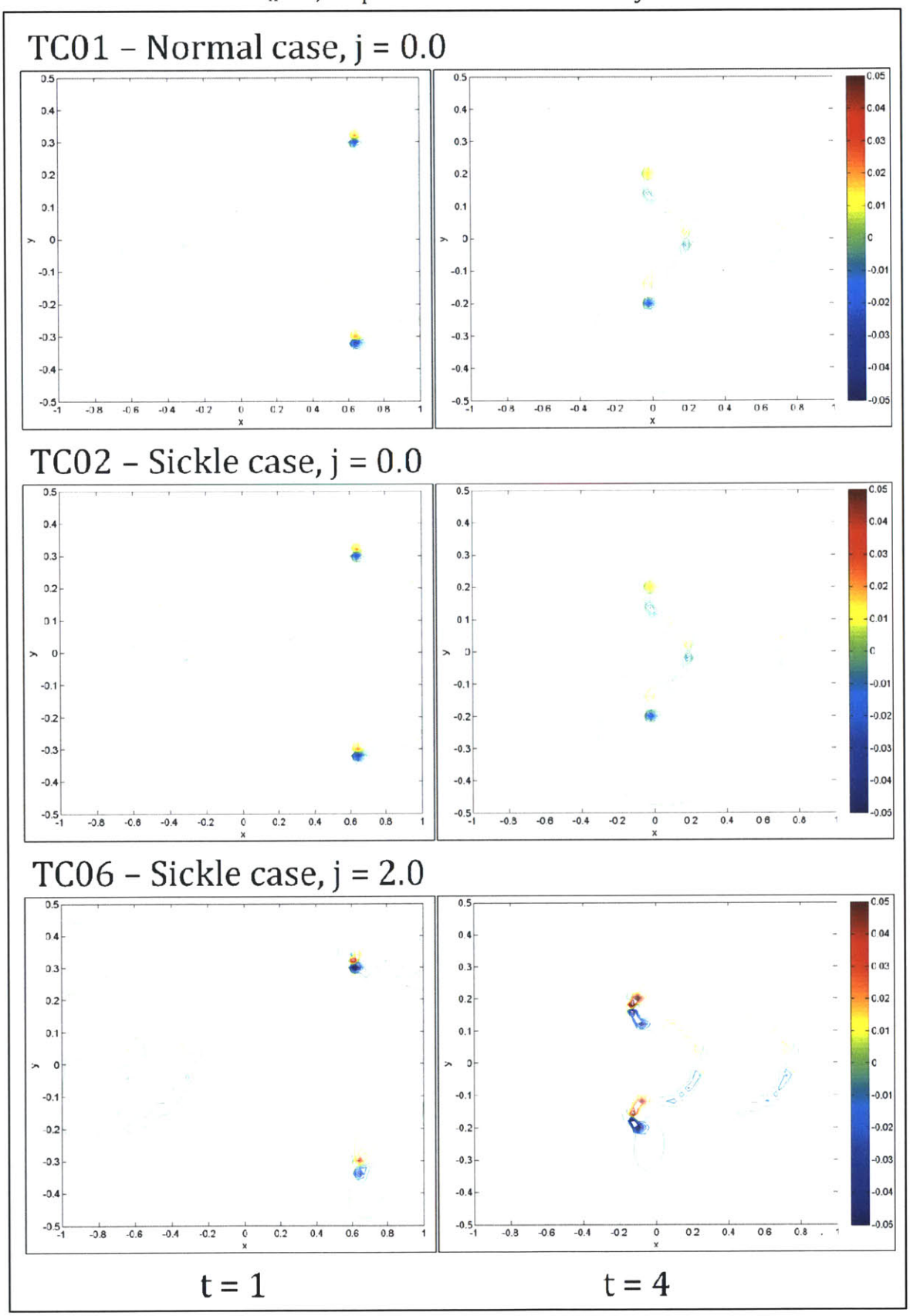

Figure 3.8 – V-Velocity, Test Case #07, #08, #12
$L_X = 2$, Asymptotic Initial RBC Geometry

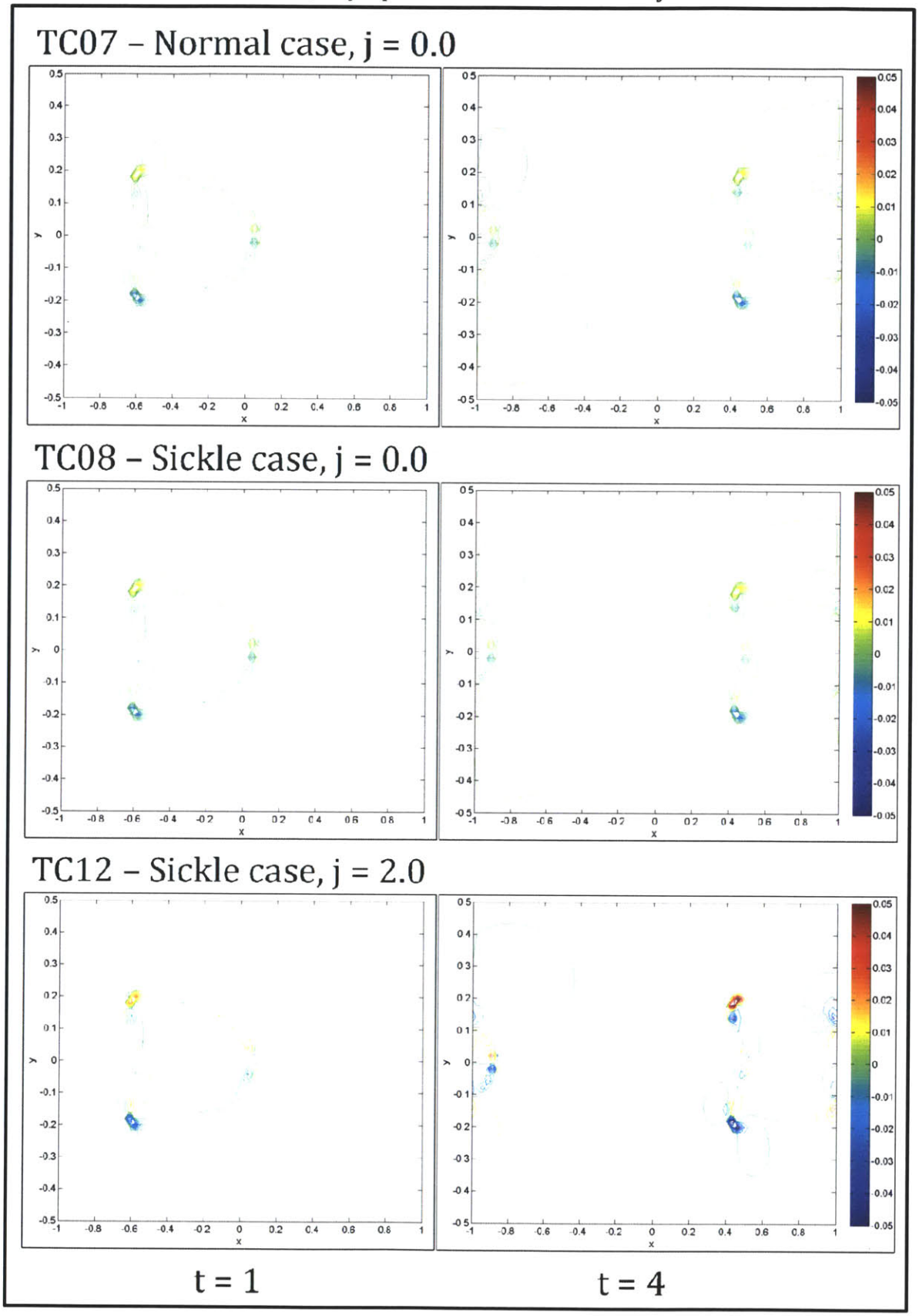

Figure 3.9 – V-Velocity, Test Case #13, #14, #18
L_X = 10, Elliptical Initial RBC Geometry

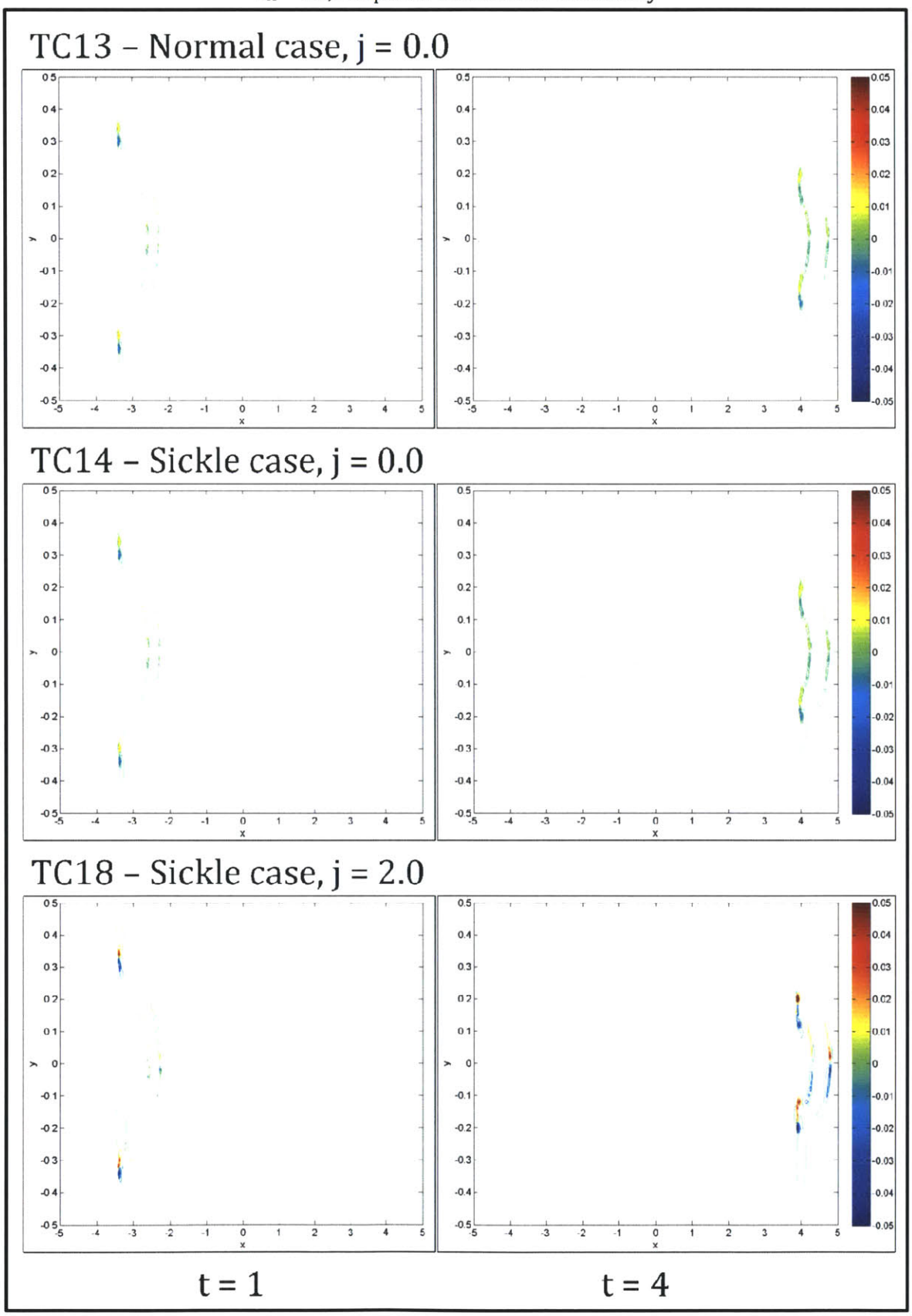

Figure 3.10 – V-Velocity, Test Case #19, #20, #24
L_X = 10, Asymptotic Initial RBC Geometry

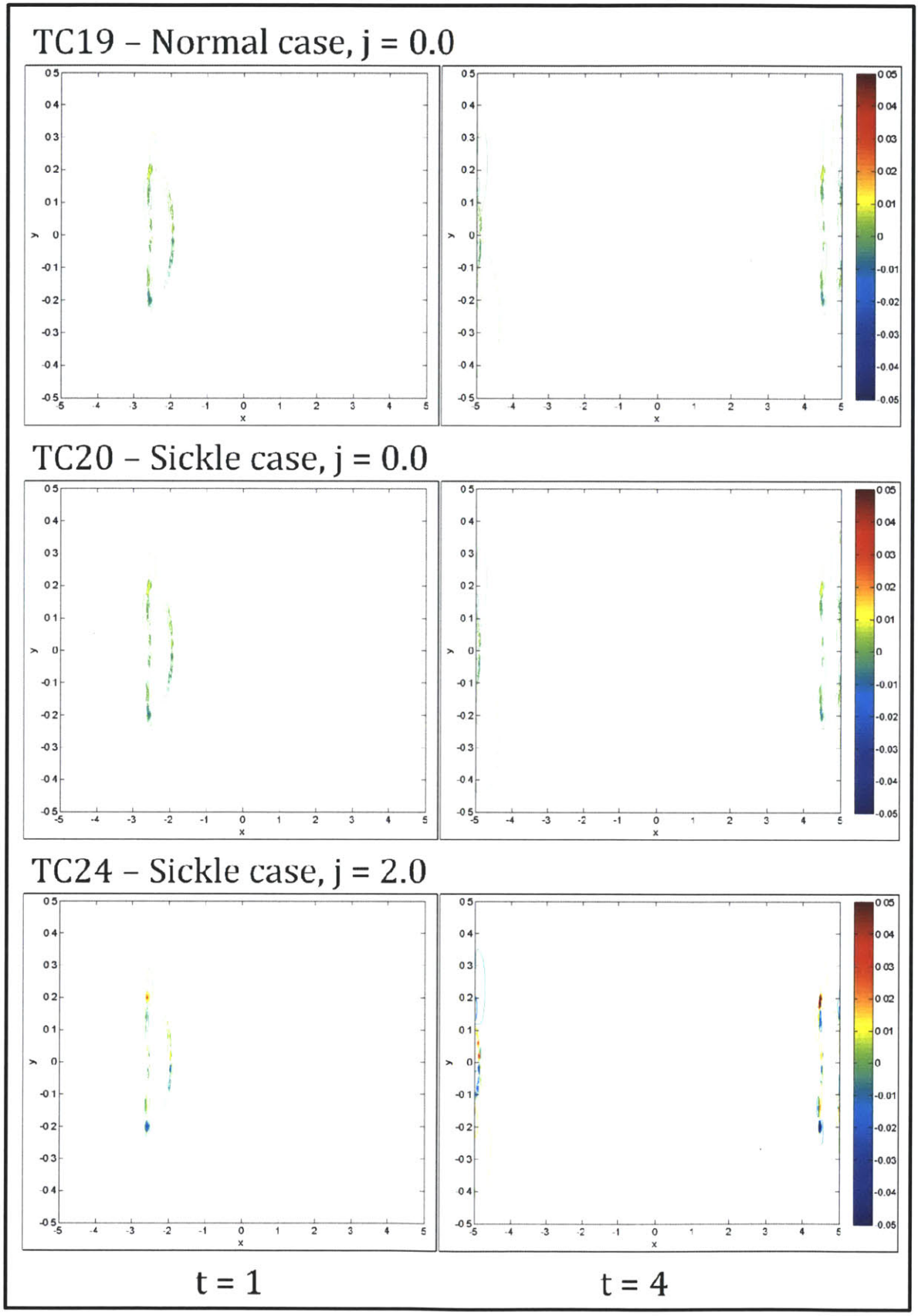

3.2.3 RBC Geometry and O_2 Concentration

The RBC Geometry and oxygen concentration profiles were superimposed onto one figure. This overlay will help identify the impact of the geometry on the oxygen concentration profile. Only the normal cases, and the sickle cases with the smallest and largest value for the stiffness index are presented in this section. A complete set of the data can be found in Appendix A.

Figure 3.11 – O_2 Concentration, Test Case #01, #02, #06
L_X = 2, Elliptical Initial RBC Geometry

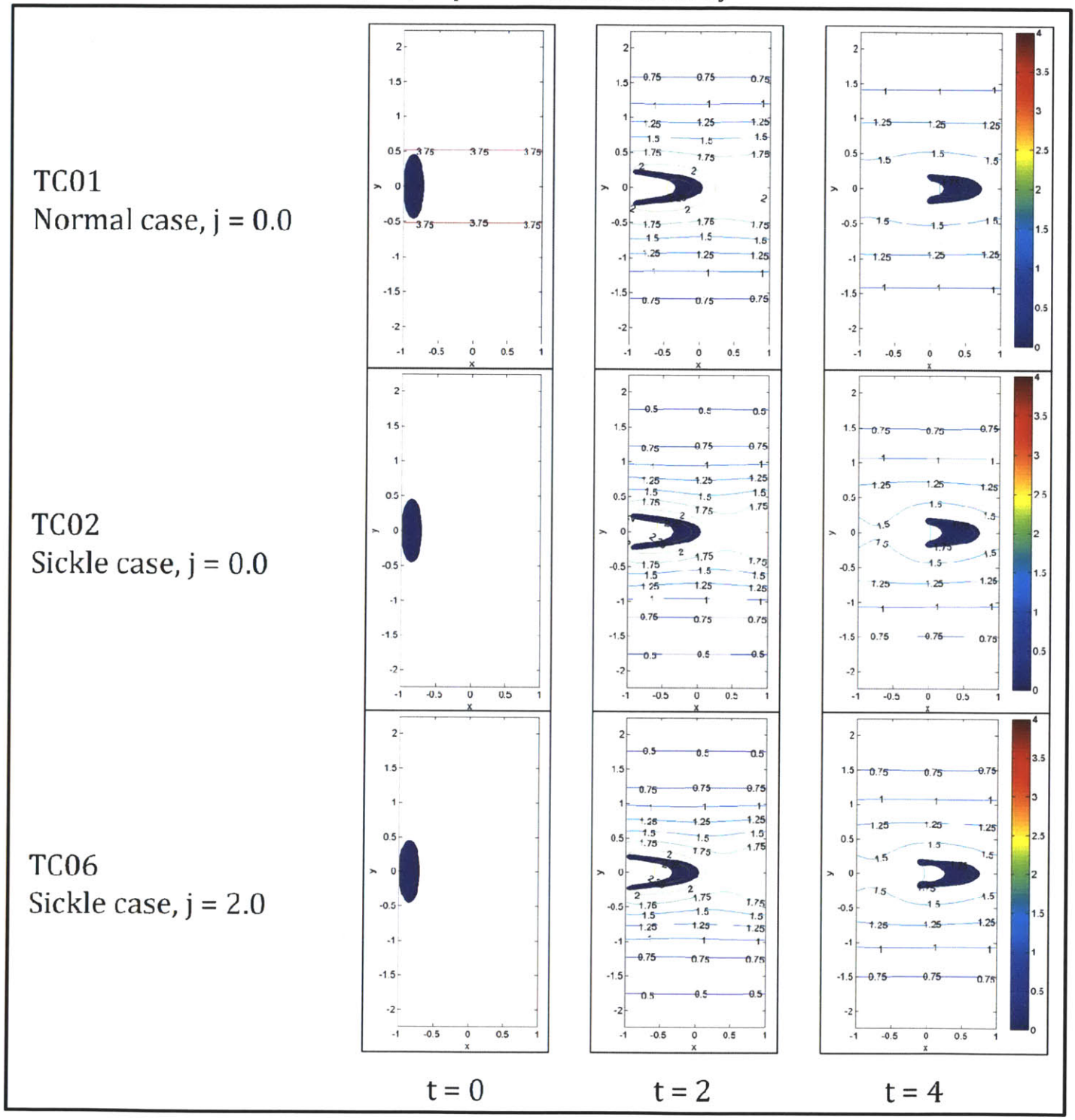

Figure 3.12 – O_2 Concentration, Test Case #07, #08, #12
$L_X = 2$, Asymptotic Initial RBC Geometry

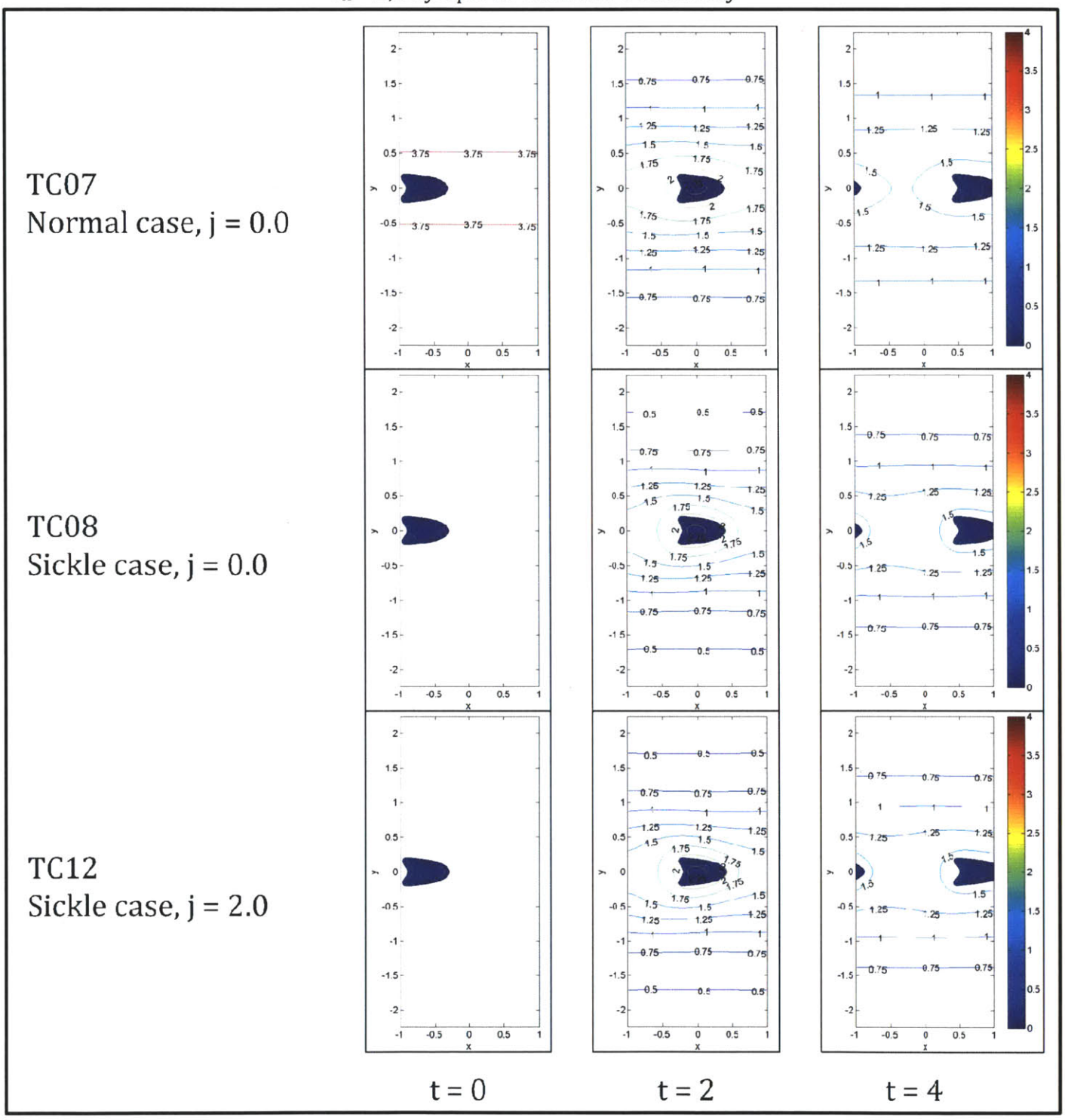

Figure 3.13 – O_2 Concentration, Test Case #13, #14, #18

L_X = 10, Elliptical Initial RBC Geometry

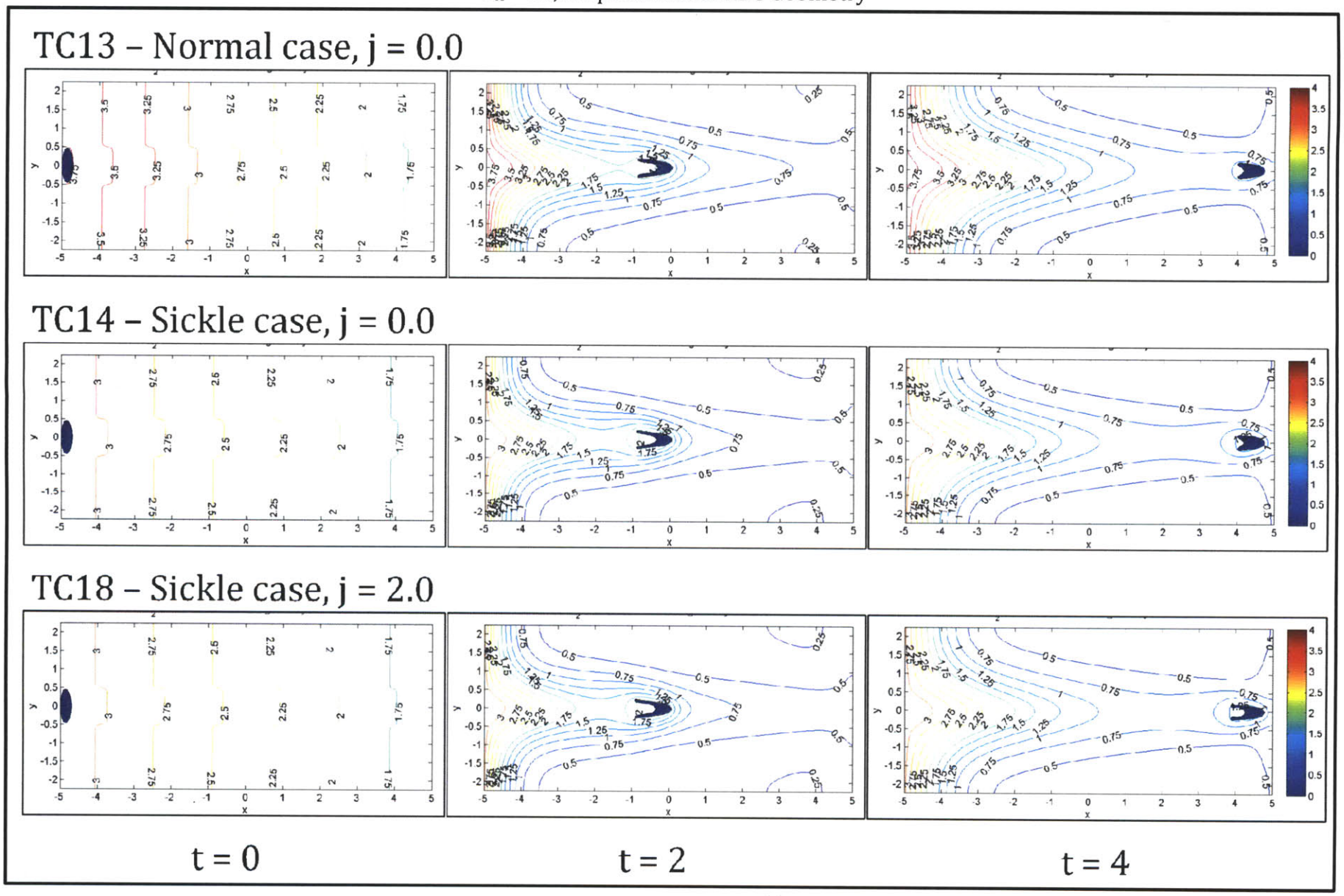

Figure 3.14 – O_2 Concentration, Test Case #19, #20, #24

L_X = 10, Asymptotic Initial RBC Geometry

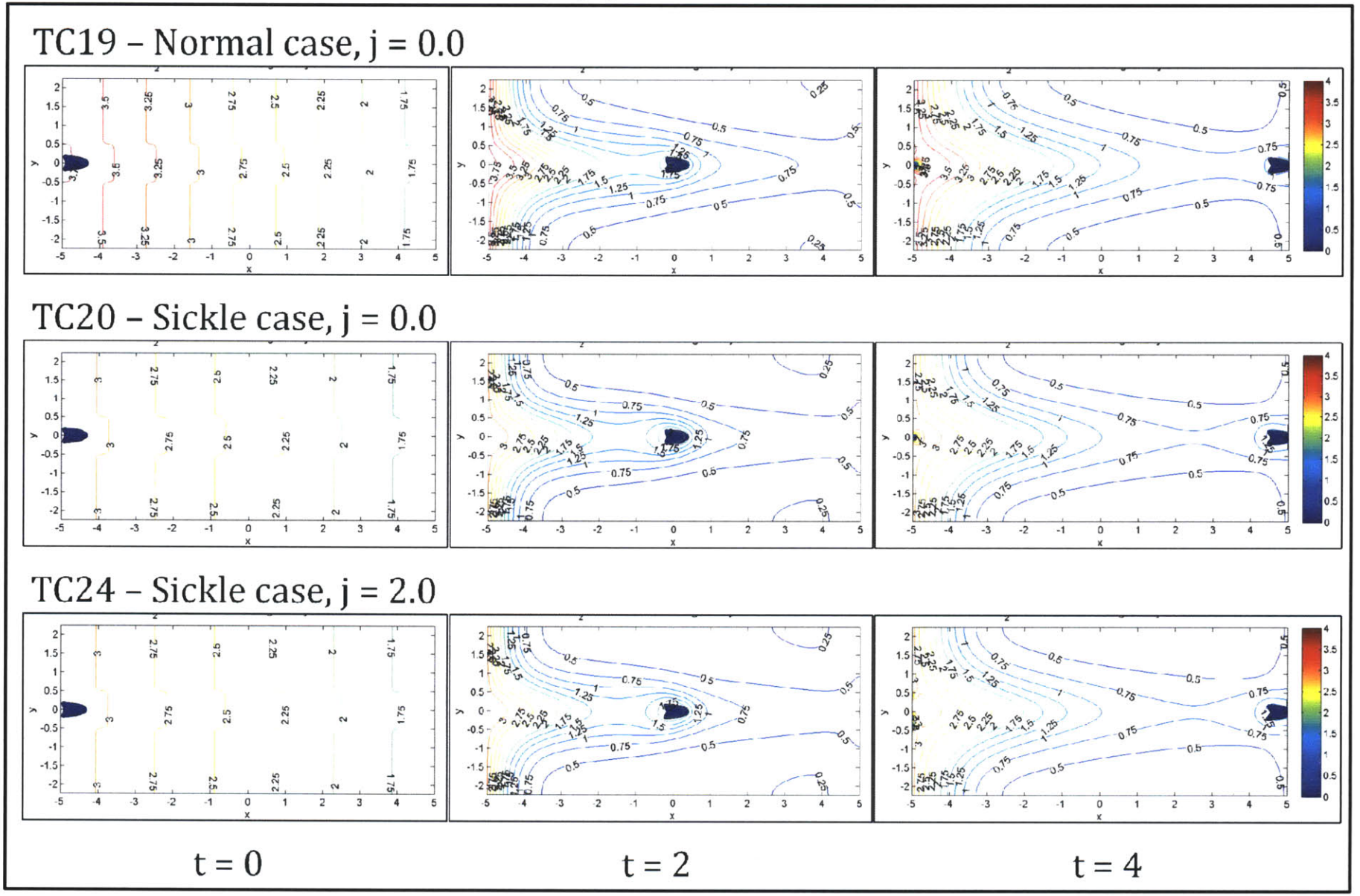

4 Discussion of Results and Implications

This section discusses the numerical simulations results and any conclusions we can draw from the data. Specifically, we investigate the RBC and its interaction with the surrounding environment. The plasma velocity profiles and oxygen concentration profiles are analyzed for both sickle and normal RBCs. This analysis helps us characterize the most influential factors that determine the flow of RBCs and the state of their surrounding environments.

4.1 Velocity Profiles

As stated previously, the velocity profiles indicate a quasi-steady Poiseuille flow. Virtually zero difference is seen in the velocity profile between the normal case and the sickle case with stiffness index $j = 0$. This similarity in the profiles can be explained by these two test cases having the same stiffness, and thus the same stress, across the RBC membranes. Because the membrane stress is directly correlated to the fluid pressure drop across the membrane, we do not expect there to be any difference between two test cases with identical stiffness indices.

Figure 4.1 and Figure 4.2 illustrate this point by comparing the normal test cases, #01 and #07, with their sickle case counterparts, test cases #02 and #08, both at a stiffness index values of zero (healthy RBC membrane stiffness). Although test cases

#03-#06 and #09-#12 are also sickle test cases, the stiffness indices is larger than that of the test cases #02 and #08, ranging from $j = 0.2$ to $j = 2.0$. By comparing these cases, we can assess the impact of the sickle parameters, independent of the RBC membrane stiffness. It is important to note that there is no perceivable difference between these plots, which indicates that the flow velocity perturbations are due purely to the stiffness index, and not an effect of the altered Hill coefficient, $p_{O_2,50\%}^{Hb}$, or $p_{O_2}^{arterial}$. It is important to note that other factors not tested in these simulations may also cause perturbations to the mean flow, for example RBC size or variability in capillary diameter. These variations may be tested with this model in the future.

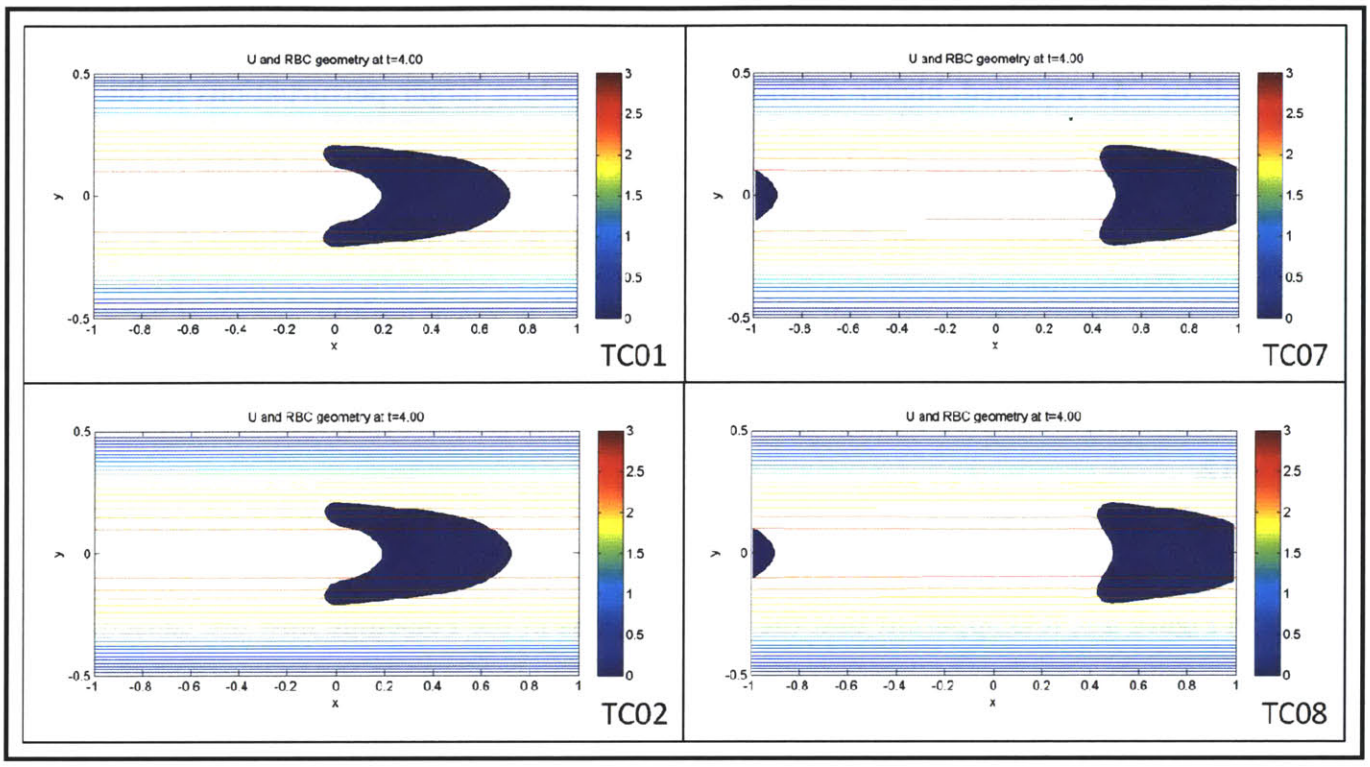

Figure 4.1 – U for Normal and Sickle cases

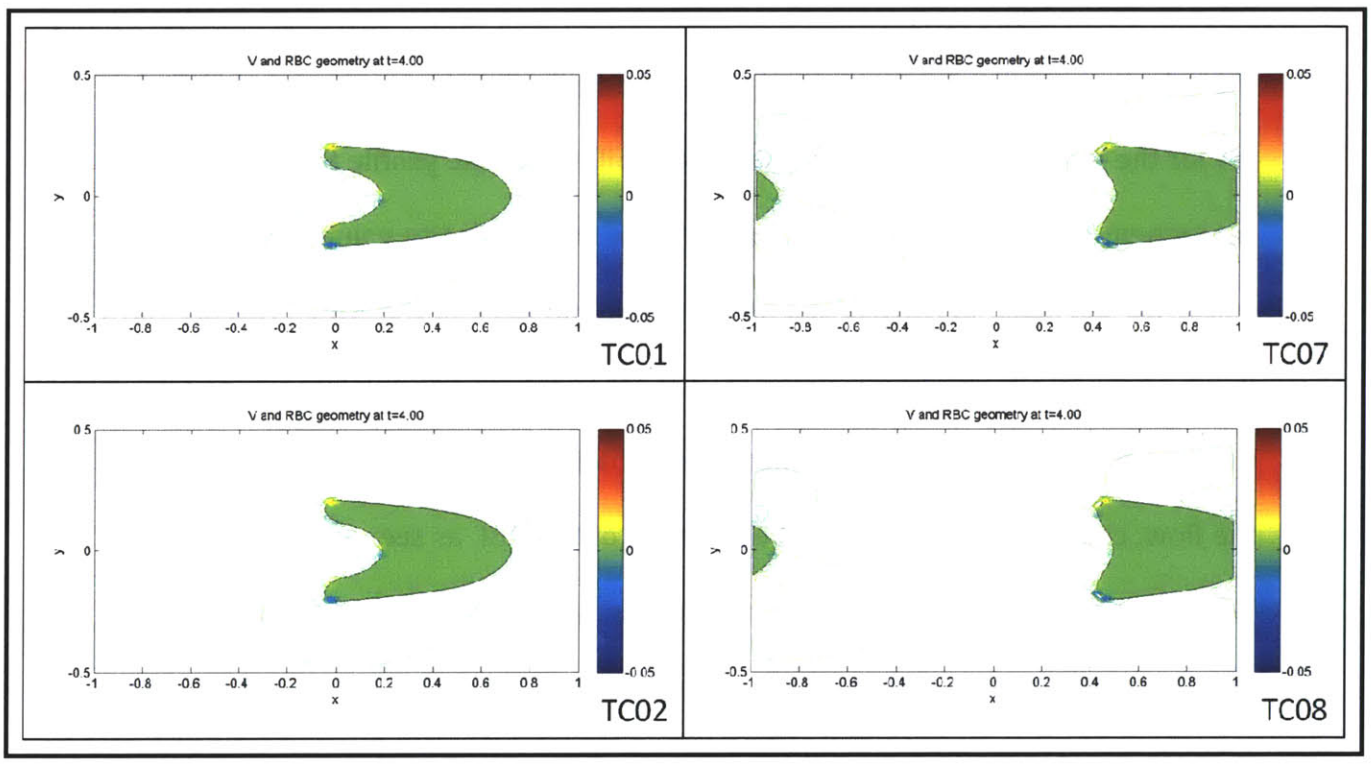

Figure 4.2 – V for Normal and Sickle cases

Differences are observed, however, between sickle test cases at different stiffness indices. As expected, higher stiffness indices produce larger perturbations in the Poiseuille flow because the less compliant sections of the cell membrane create greater resistances to the flow. The resistance to the flow is manifested as a pressure drop across the cell membrane. This is most readily apparent in a comparison between test cases #02 and #06, and also between test cases #08 and #12.

In Figure 4.3, it is apparent that the perturbations in the Poiseuille flow are caused by the RBC membrane stresses. Test cases #02 and #08 show nearly straight, horizontal U-velocity contour lines, with slight perturbations around the edges of the RBC membrane. Test cases #06 and #12, however, show very large changes in the velocity contours from a normal Poiseuille flow. This is also apparent in Figure 4.4 for the V-velocity profiles. In a true Poiseuille flow, the profile for the V-velocity component would be zero everywhere. While the V-velocity values are extremely small, we see some perturbations near the tail and nose of the RBC. The pressure jump across the membrane is greatest at these points due to the large curvature of the membrane at these points. These perturbations create small, weak vortices in the flow, causing small eddies at the tail ends of the RBC as seen in Figure 4.4. The V-velocity values are an order of magnitude larger in test cases #06 and #12 (greatest stiffness index) than they are in #02 and #08 (smallest stiffness index) due to the increase in the RBC membrane stiffness.

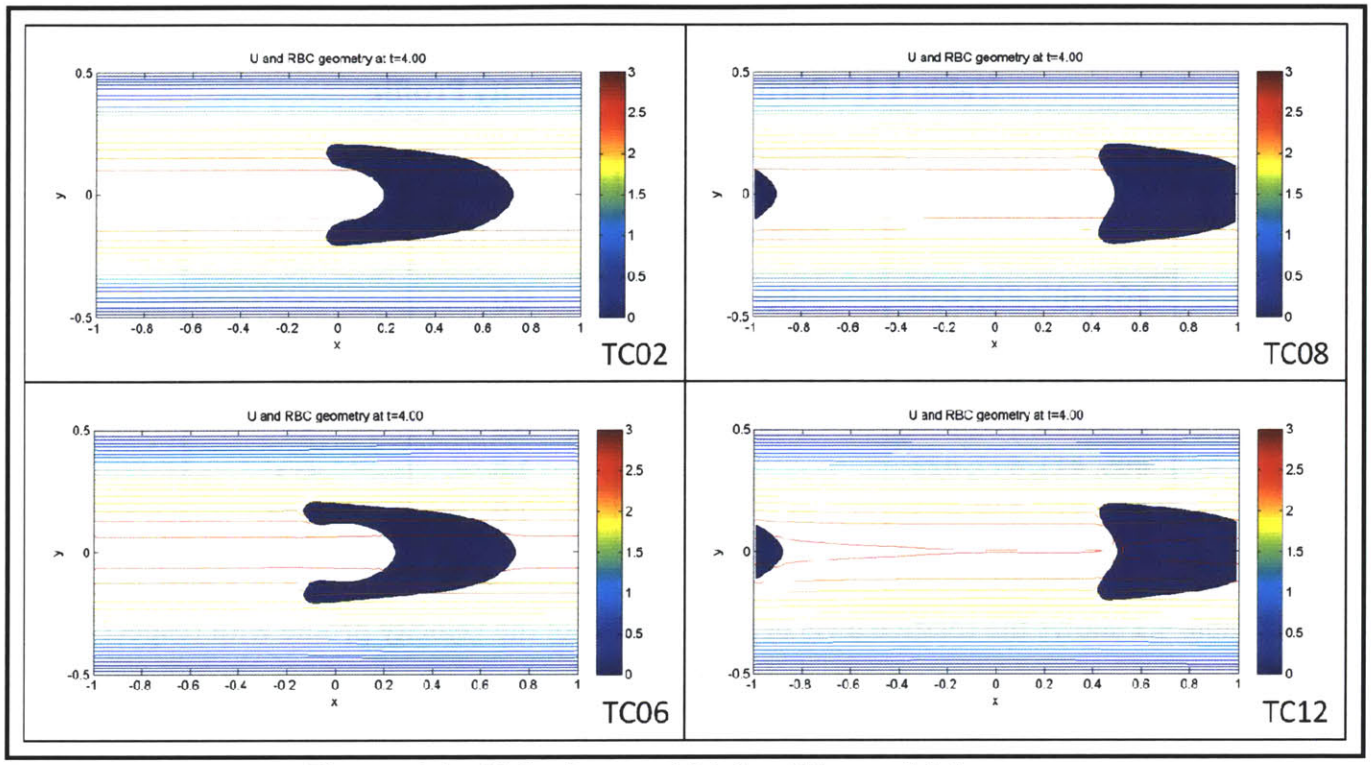

Figure 4.3 – U for low and high stiffness sickle cases

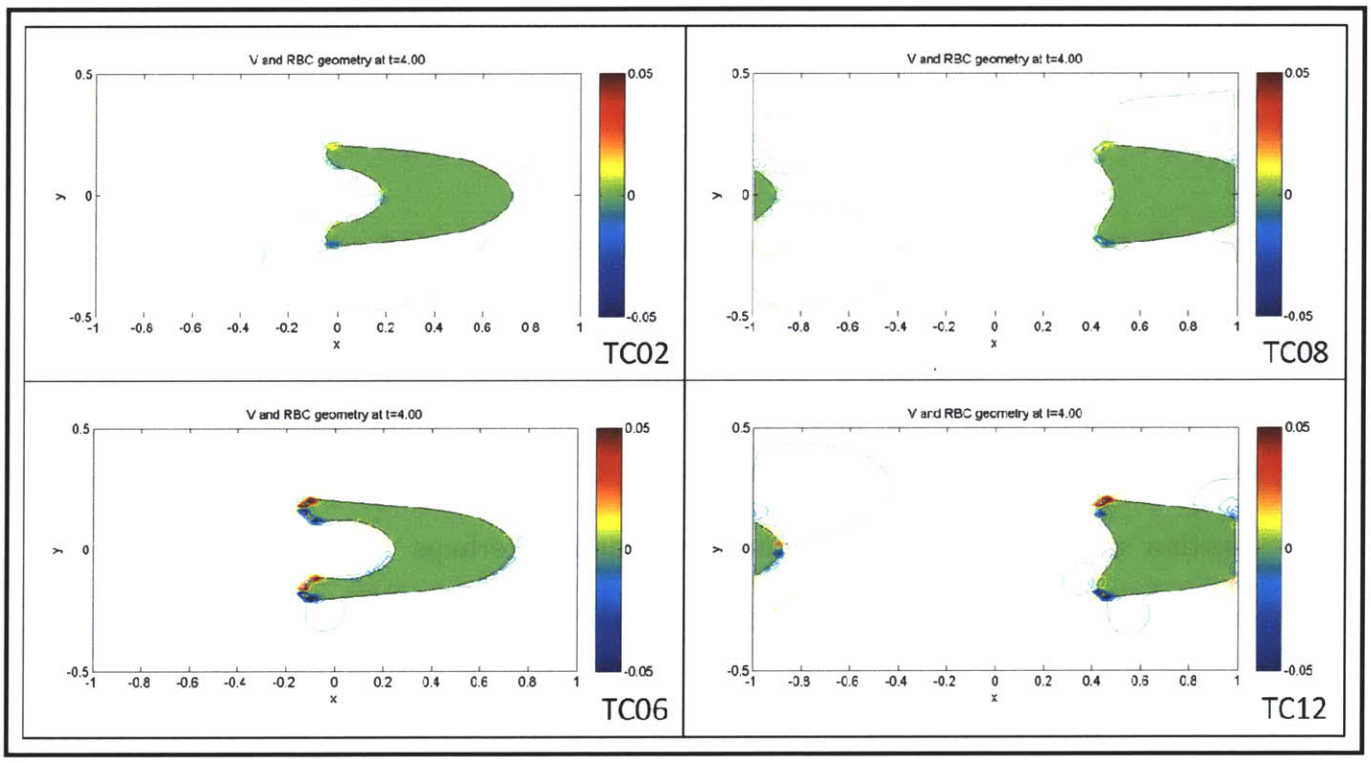

Figure 4.4 – V for low and high stiffness sickle cases

Table 4.1 – Perturbation in Velocity Profile

Test Cases	Normal/Sickle Parameters	Stiffness index (j)	Perturbation in Velocity Profile
#01, #07, #13, #19	Normal	0.0	-
#02, #08, #14, #20	Sickle	0.0	-
#03, #09, #15, #21		0.2	+
#04, #10, #16, #22		0.5	++
#05, #11, #17, #23		1.0	+++
#06, #12, #18, #24		2.0	++++

Table 4.1 shows the relative level of perturbation of the velocity profile with respect to the normal RBC case. From the U and V-velocity profiles we can determine the level of perturbation from the mean flow. The normal case has some level of perturbation; however it is much smaller than the sickle cases with higher levels of membrane stiffness.

From these observations we can conclude that the stiffness index has an impact on the profile. High stiffness regions of the membrane can cause perturbations in the flow. However, we do not see a perturbation to the mean flow large enough to retard the motion of the RBC. In all cases, the RBC reaches approximately the same position at any time point in the simulation. Perhaps for longer duration simulations, we may notice a small difference, although it most likely would not be a significant change.

4.2 O_2 Concentration Profiles

The oxygen concentration profile is constant throughout the system initially, at t=0. Over the next 1600 iterations through t=4, the oxygen dissipates from the system as it is consumed by the tissue. The flow of oxygen from the RBC, through the plasma and into the tissue is represented by contour lines in the plots of Figure 4.5. These plots show the system early in the simulation at t=1 and at later time t=4. Notice the highest concentration of oxygen is inside the RBC. These profiles only consider free oxygen, and not hemoglobin bound oxygen.

The oxygen profiles for all sickle RBC cases, regardless of the stiffness index, are almost identical. There are slight differences very close to the sickle RBC due to the difference in shape of the membrane; however, far away from the sickle RBC, in the tissue, we find that the profiles are very similar. The normal RBC case however, shows a very different oxygen profile from the sickle RBC case. The oxygen concentration throughout the system is significantly higher in the normal case except very close to the cell center. This indicates that the impact of the sickle parameters (increased Hill coefficient, increased $p_{O_2,50\%}^{Hb}$, and decreased $p_{O_2}^{arterial}$) is much greater than that of the membrane stiffness.

This is consistent with our understanding of the dynamics of the cell and oxygen transport. Although the increased stiffness of the cell causes membrane rigidity and

changes the flow velocity near the cell, these changes are very small in the oxygen transport equations. The oxygen transport equation has a diffusion term, a advection term, and a generation/consumption terms for the different regions of the plasma. The changes in the velocity profile caused by the increased stiffness are only found inside the plasma. However, the slight perturbations that we observe are small enough that the diffusion, and generation/consumption terms dominate the oxygen concentration profile in the system. In larger vessels with higher speed flows and greater levels of turbulence, this may not be the case.

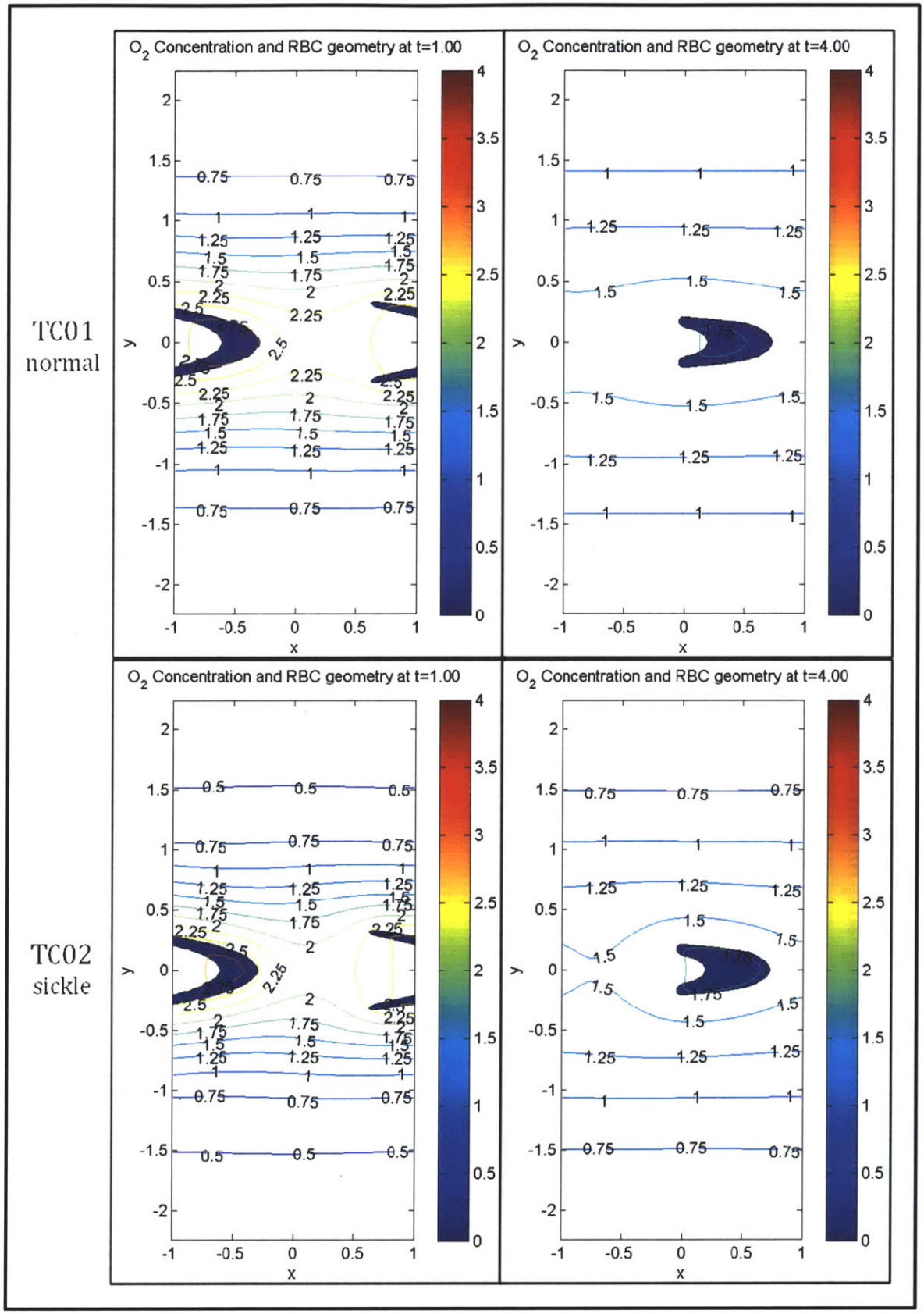

Figure 4.5 – Normal and Sickle O_2 concentration for short, periodic capillary

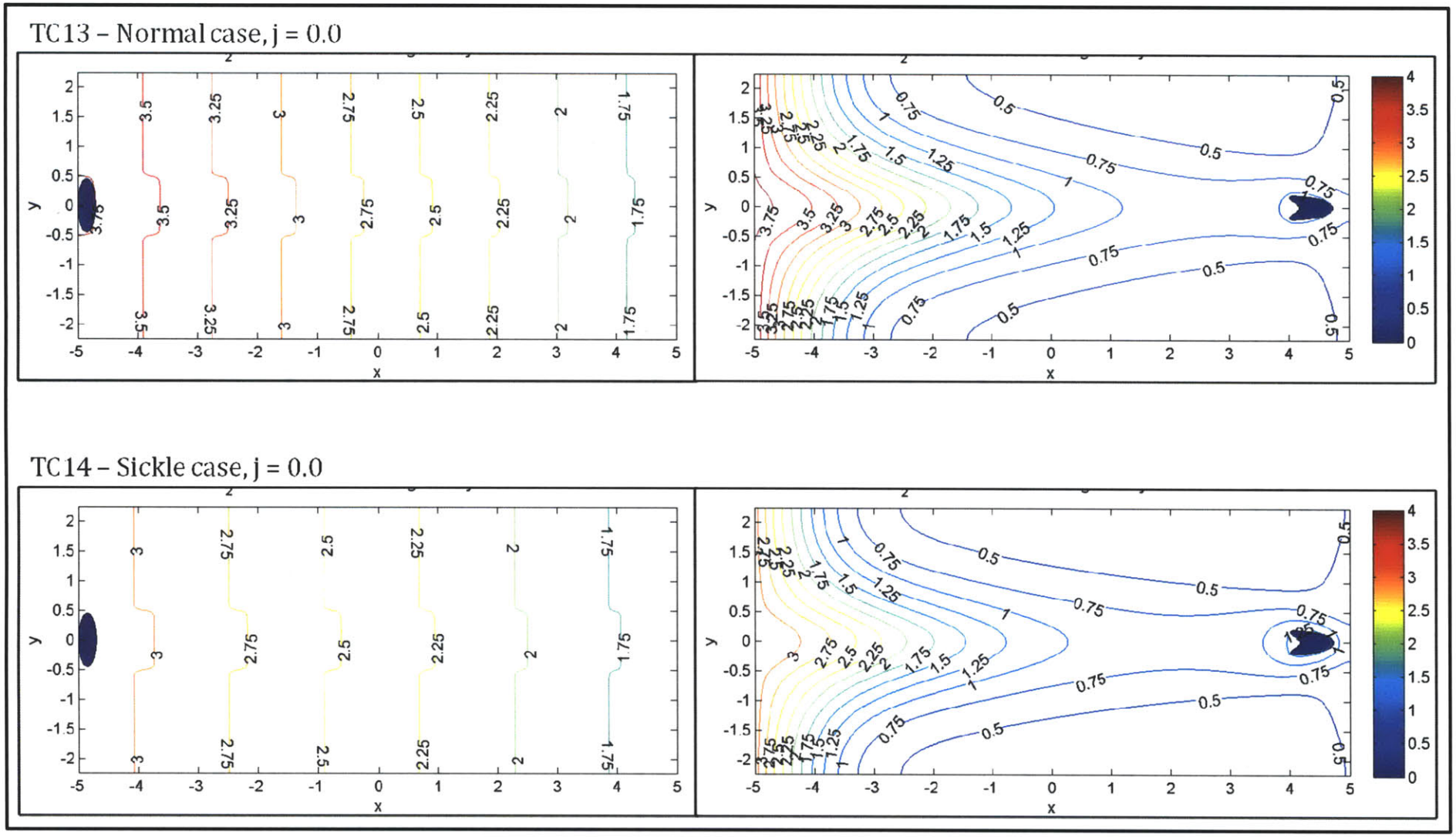

Figure 4.6 – Normal and Sickle O_2 concentration for long, fixed left B.C. capillary

As seen in Figure 4.5, the oxygen concentration profile of the normal RBC case indicates higher oxygen concentration values at all points in the tissue and most of the plasma with respect to the sickle RBC case. Near the cell, however, the sickle RBC case shows higher values of oxygen as time elapses. This seems counter intuitive due to the lower initial (arterial) pressure in the RBC. In fact, at earlier times, we notice the normal case has higher oxygen concentration values everywhere with respect to the sickle RBC case. These increased levels of free oxygen inside the sickle RBC occur because the hemoglobin saturation levels drop more quickly than in the normal RBC. This happens because the increased Hill coefficient and increased $p_{O_2,50\%}^{Hb}$ cause a right-shift in the hemoglobin saturation curve. The relationship between the two curves can be seen in Figure 4.7.

Although there is a lower amount of total oxygen content in the sickle RBC case, both bound and unbound, the low saturation of the sickle RBCs yields more free oxygen around the cell. This occurs because the sickle hemoglobin proteins are much weaker at binding oxygen molecules, so they lose whatever oxygen they may have rather quickly. After releasing the oxygen molecules, the sickle oxyhemoglobin change conformation, becoming sickle deoxyhemoglobin. The sickle deoxyhemoglobin bind to one another, creating long branches in the RBC, and thus have a much lower probability of rebinding other oxygen molecules in their surroundings. Therefore, we expect to see more free oxygen around the cell, but not throughout the system.

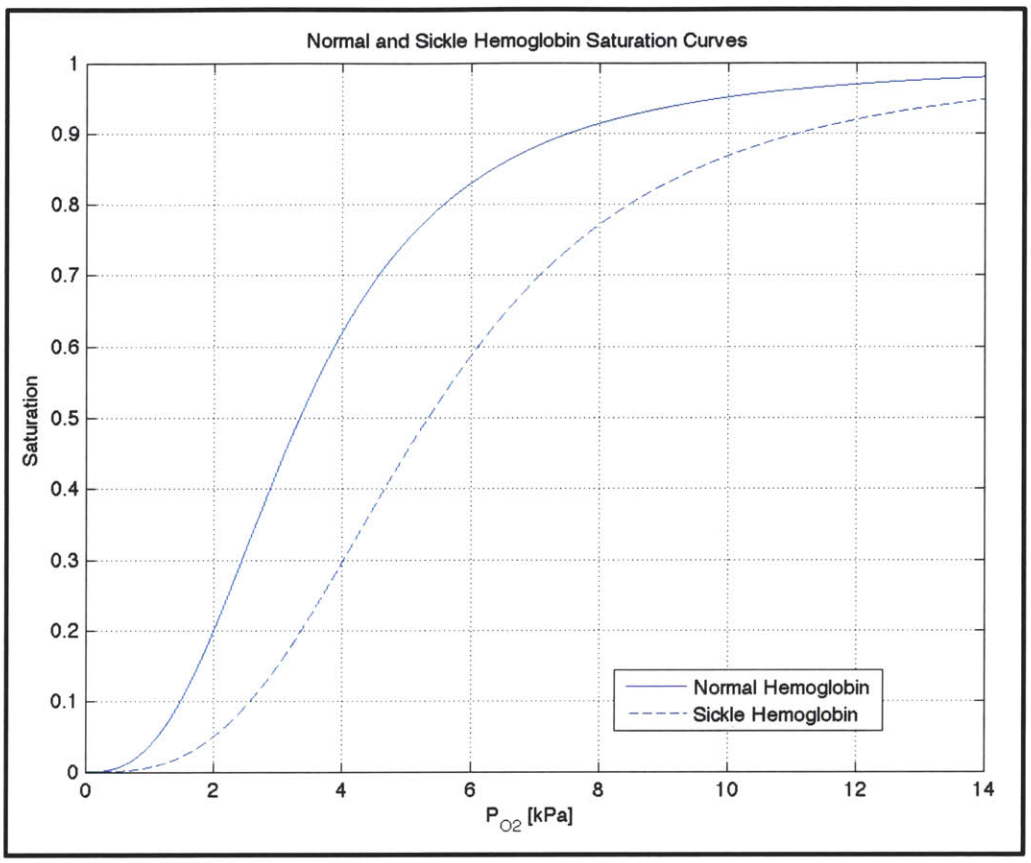

Figure 4.7 – Normal and Sickle Hemoglobin Saturation Curves
The sickle Hemoglobin curves shifts right due to a higher Hill coefficient and an increased $p_{O_2,50\%}^{Hb}$.

Figure 4.6 shows the simulation for a longer, non-periodic capillary with one cell flowing down the channel. In this case, the left boundary is fixed at the arterial pressure value, which represents the arterial end of the capillary. The initial condition is a linear oxygen concentration gradient across the capillary. As the simulation runs, the oxygen is consumed by the tissue and advected by the plasma flow. Although the profile looks different from the short, periodic capillary, the results are consistent. The oxygen concentration throughout the system is much higher in the normal case except very near to the center of the RBC.

4.3 Comparisons with Previous Models

It is important to compare our model to previous models. The Le Floch-Harris model **[8]** and Secomb's model **[4]** are used for comparison. Although this model simulates capillary blood flow, there are several differences between this model and the two models to which it is being compared. These differences must be taken into consideration when comparing the results. First, the major difference in this model is that we only look at an individual erythrocyte traveling down the axis, and its impact on the oxygen profile, whereas the Le Floch-Harris and Secomb models account for multiple cells, periodically spaced along the length of the capillary. The spatial period is based on the hematocrit level.

$$L = \frac{4\,V_{RBC}}{Hct\;\pi\;D_{cap}^2}\;, \tag{4.1}$$

Despite these differences, in both cases we should see a drop in P_{O2} along the length of the capillary as well as radially outward from the centerline of the capillary, into the tissue. First, let's examine the Le Floch-Harris model. In Figure 4.8, Le Floch demonstrates the experimental results from case (4a), which is most similar to this model.

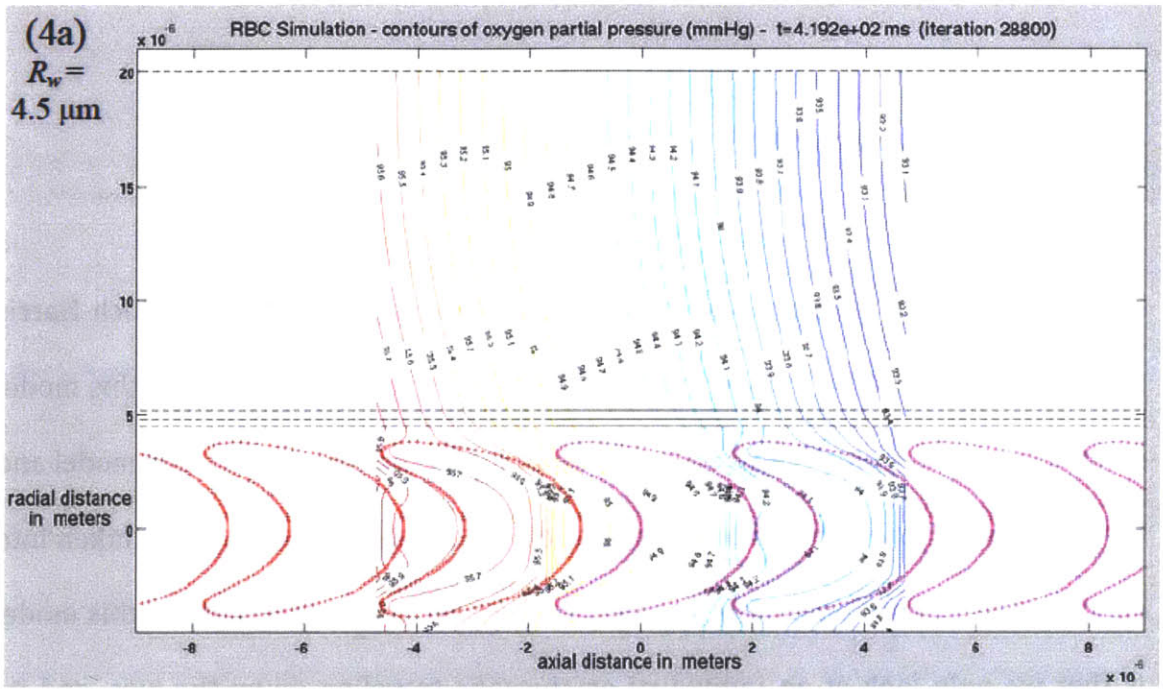

Figure 4.8 – Le Floch's results

O_2 contours show the P_{O2} in the RBC, capillary, and tissue.

The oxygen partial pressure contour lines indicate a significant drop in P_{O2} downstream, both in the capillary as well as in the tissue, and a slight radial drop in the oxygen levels.

Secomb's model shows similar behavior as seen in Figure 4.9.

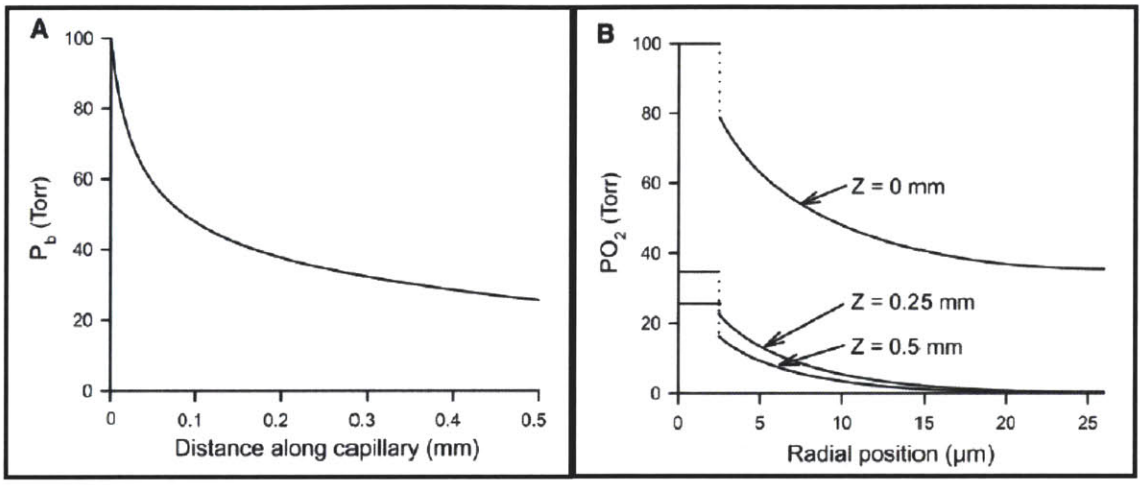

Figure 4.9 – Secomb's results

A: Drop in average P_{O2} along the length of the capillary.
B: P_{O2} at radial sections of the capillary. Z indicates position along length of capillary

The differences in the models are readily apparent when comparing the oxygen contour lines from our model. For comparison, we will use test case #19. Figure 4.10, shows the oxygen concentration and RBC geometry.

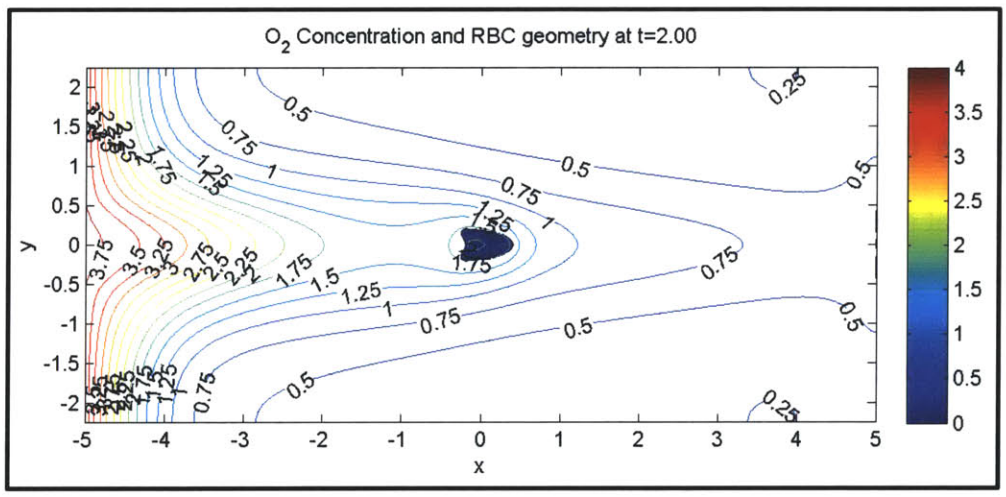

Figure 4.10 – Test Case #19 Oxygen Concentration

By looking at Figure 4.8, Figure 4.9, and Figure 4.10, we can identify major differences in the oxygen concentration profiles in the capillary and tissue. Let us first consider the profile in the axial direction. In Secomb's figure, this data would be represented by plot A. All three figures show an axial decrease in oxygen concentration (directly proportional to oxygen partial pressure). Le Floch's data shows a nearly constant, linear drop in oxygen concentration axially, both in the tissue and in the capillary. Further away from the capillary, the values are slightly lower, but the axial trend is consistent. Secomb's data, along with the data from this model, indicates a non-linear decrease in oxygen concentration. In fact, they both report a higher drop in oxygen concentration towards the entrance of the capillary. As the RBC moves further down the capillary, the oxygen concentration begins to slowly level off. Therefore in the axial direction, our data is more consistent with that of Secomb than Le Floch. However, the concentration drop in our data is much more significant than that of both Secomb and Le Floch. This is primarily due to the fact that our model can only account for one RBC in the capillary. This is a major difference in these models. In order to make a more fair comparison between the models in the future, it must be updated to account for multiple RBCs in the capillary at once.

Next let us consider the profiles in the radial direction. In Secomb's figure, this data would be represented by plot B. In the radial direction, there are major difference between our data and that of Le Floch and Secomb. Secomb's and Le Floch's data

both show a logarithmic drop from the capillary wall into the tissue. The radial concentration drops are consistent along the axis of the capillary, but the values are lower as you move downstream. In the data from this model, there is also a radial drop from the capillary into the tissue, however, the oxygen concentration levels are much lower with more significant drops further away from the entrance of the capillary. The region closest to the capillary entrance is least affected because a fixed oxygen concentration boundary condition is used on the left boundary. This significant drop is in large part due to the fact that our model has only one RBC. This idea is supported by the fact that we can see small increases in the regions closest to the RBC. Notice that in Figure 4.10, at $x = 0$, the oxygen concentration values are slightly higher than a little further upstream at $x = -1$. Further into the tissue, this is less apparent because it takes some time for the oxygen to diffuse into that region.

It appears that most of the differences between this model and Le Floch's and Secomb's models arise from the fact that the tissue everywhere is consuming oxygen, while only the tissue near the single red blood cell is receiving oxygen. Notice the higher regions of oxygen near the entrance of the capillary have contour lines that are more vertical like that of Le Floch. Because only one cell is used, less oxygen is being diffused throughout the system. Also, the middle regions of the tissue ($-2 < x < 2$), has lower oxygen levels than the region near the entrance of the capillary at the right boundary as seen in Figure 4.10. Using a multi-cell model

may produce results that are even more consistent with that of Secomb and Le Floch.

5 Conclusion

This model was designed to serve as a fast and efficient method for calculating capillary flow conditions and local oxygen concentration for both healthy and sickle RBCs. The model utilizes computational domain representative of a capillary surrounded by muscle tissue. Given specific initial and boundary conditions, the model produced overall results consistent with the basic understanding of flow conditions and oxygen concentration profiles in human capillaries. Perturbation analysis allows us to determine differences in flow conditions and oxygen profiles from the mean flow. For the purpose of this perturbation analysis, the *mean* was determined to be ideal flow conditions and oxygen concentration levels found in healthy RBCs systems.

5.1 Findings

Comparing the simulation results between the various test cases have led to several conclusions. First, the perturbations in the flow velocity are due primarily to an increase in cell membrane stiffness. A variety of RBC membrane stiffness values were simulated in different test cases. Regardless of initial and boundary conditions used, the flow velocities showed similar trends between the test cases. It was clear that perturbations to the mean Poiseuille flow were more apparent as the stiffness of the membrane was increased.

The perturbations in the oxygen concentration are largely a function of the three sickle parameters, the Hill coefficient ($\boldsymbol{n}$), $p_{O_2,50\%}^{Hb}$, and $p_{O_2}^{arterial}$. The cell membrane stiffness does however, play a small role in the oxygen concentration very close to the RBC. Of the 24 test cases, the first half were simulated with periodic boundary conditions using a smaller computational grid while the second half were simulated with a fixed boundary on the left end and a Neumann boundary condition on the right end. In both sets of test cases, the sickle parameters played the largest role in the oxygen concentration. In the sickle RBC case, the system as a whole has noticeably lower oxygen content than the healthy RBC case. The concentration values are lower in the tissue and the plasma region far from the RBC. This, however, is not the case very close to the RBC. In the plasma region very close to the RBC, and inside the RBC, we observe higher oxygen concentration levels than the healthy case, due to the sickle RBC's poor ability to carry oxygen. The sickle RBC cannot saturate its hemoglobin as much as a healthy RBC due to the right-shift in the saturation curve as illustrated in Figure 4.7.

The oxygen concentration follows general trends as seen in Le Floch's and Secomb's work. As we move downstream in the system, the oxygen content of the RBC, the plasma, and the surrounding tissue diminish. Additionally, at any axial cross section in the capillary, the highest level of oxygen can be found at the center and it diminishes radially such that the tissue furthest away has the lowest concentration.

5.2 Recommendations

To gain a better understanding of the dynamics of sickle cell using this model, several test cases can be developed. In these simulations, the flow parameters were unchanged, such as the density and viscosity of plasma. It may be of interest to test whether small changes in these values in both the sickle and healthy cases may impact the perturbations in the flow or the oxygen concentrations. It may also be interesting to simulate moderate exercise, in which there may be slightly faster speed flows and larger oxygen consumption rates in the tissue.

Several modifications can be made to improve this microcirculation model. The first suggested modification would be to change the model to allow multiple cells. We would then be able to more accurately replicate the oxygen delivery system in real human capillaries. We would be able to vary the hematocrit level for sickle and healthy cases, as well as any other stressing cases we may like to consider.

The capillary in this system is model as a two-dimensional fluid flow between two flat plates, using a Cartesian coordinate system. Although it may be more computationally intensive, in the future we might consider creating a model that uses a three-dimensional axisymmetric flow, using a cylindrical coordinate system.

Capillaries in the human body do not have constant diameters. In reality, they have converging and diverging cross sections. Allowing variable capillary radius (diverging or converging capillaries) would make the model more authentic.

In a real sickle RBC, the membrane stiffness is not fixed throughout its life, or even the duration it traverses a capillary. In fact, it is indirectly related to the hemoglobin saturation levels. As the RBC releases oxygen, the membrane becomes more rigid. By creating a time-dependent, or oxygen saturation dependent membrane stiffness model, we would be able to capture the dynamic nature of the membrane stiffness.

With these changes to the model, it would be good to see how the data compares to that of other models, such as Le Floch's or Secom's model. These changes would allow more direct comparisons to be made. It would also be very insightful to compare our data to experimental data conducted either in microfluidic devices or in biological samples.

Appendix A – Full Data Set

Figure A.1 – U-Velocity, Test Case #01 - #03

$L_X = 2$, Elliptical Initial RBC Geometry

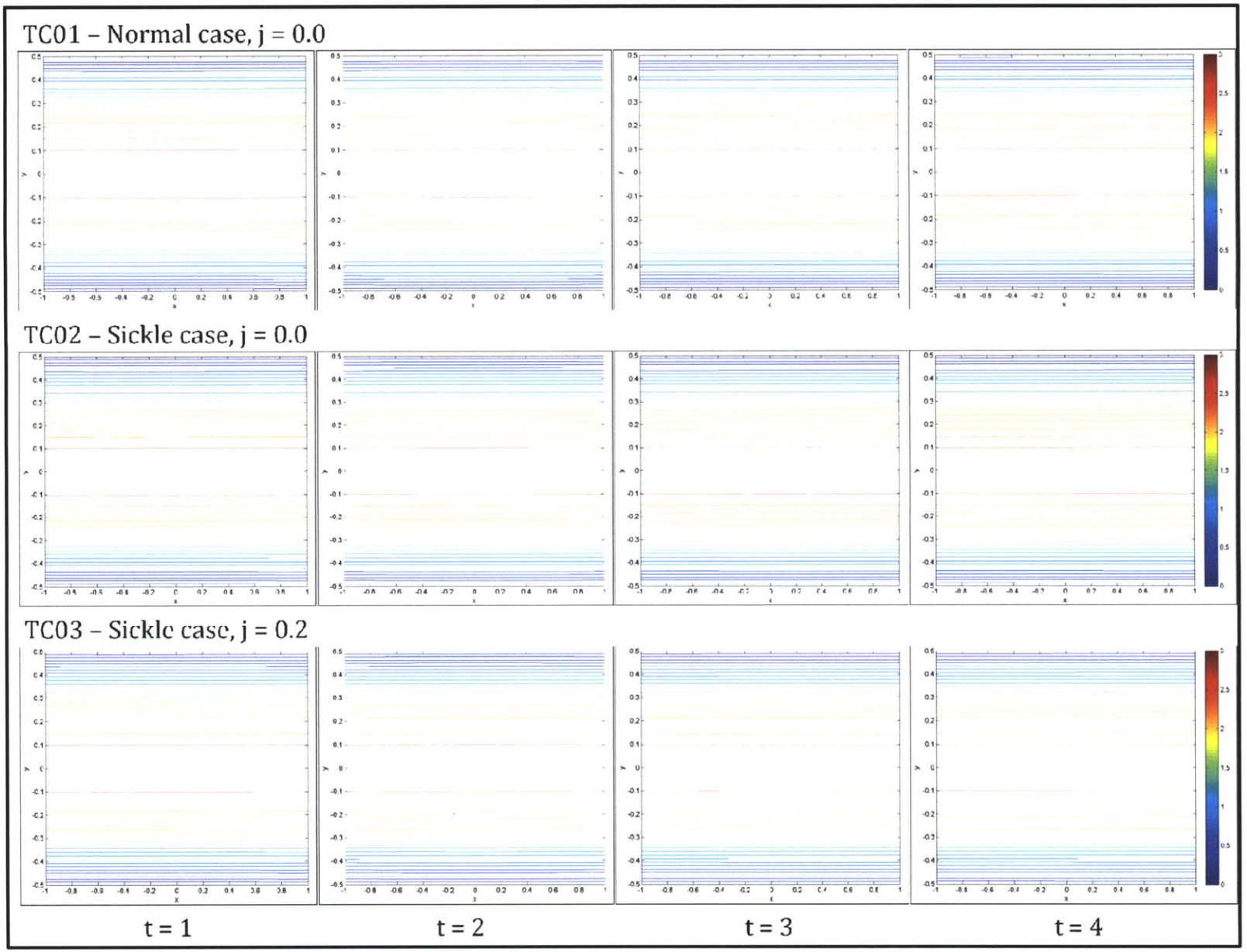

Figure A.2 – U-Velocity, Test Case #04 - #06

L_X = 2, Elliptical Initial RBC Geometry

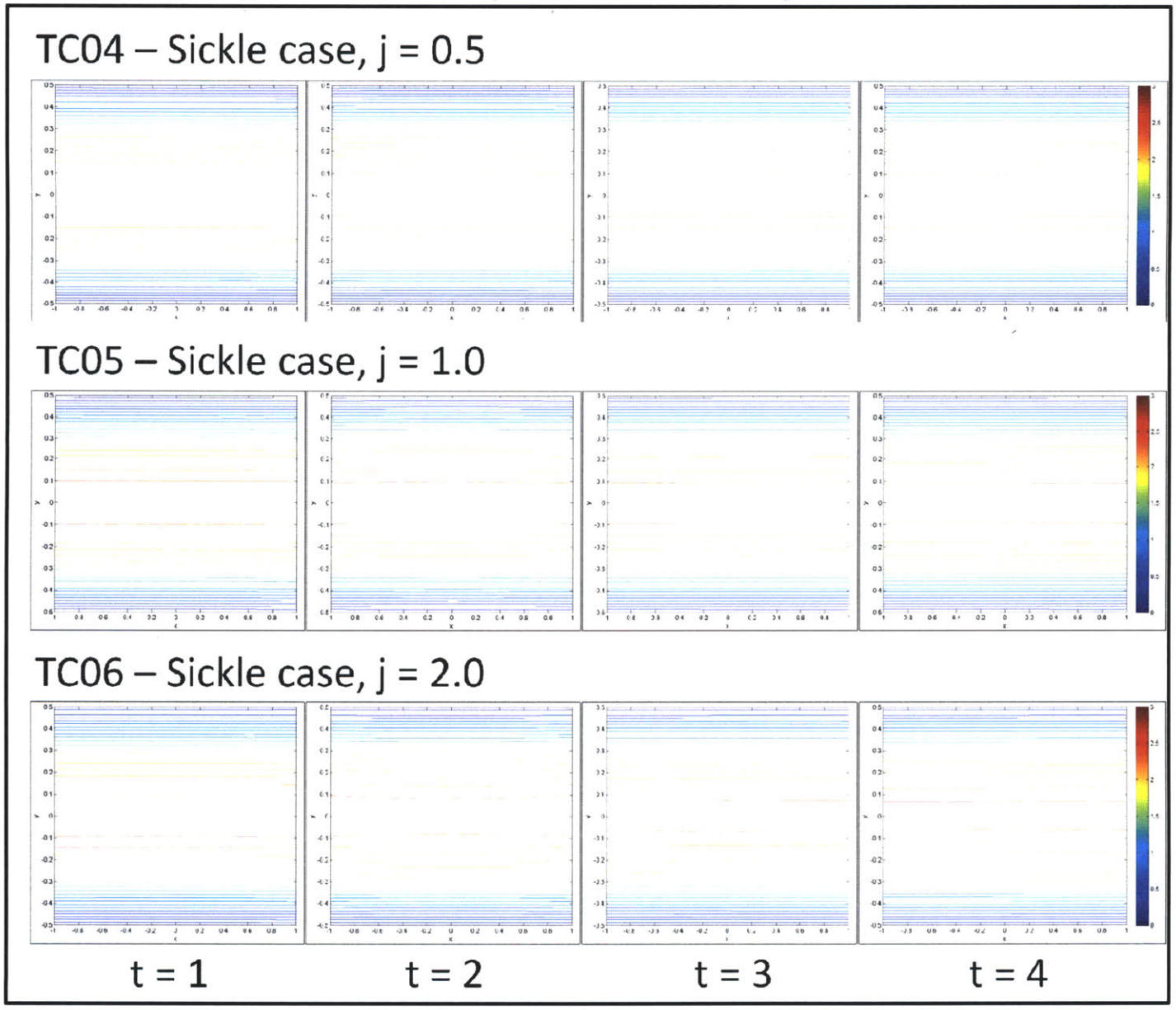

Figure A.3 – U-Velocity, Test Case #07 - #09
L_X = 2, Steady State Initial RBC Geometry

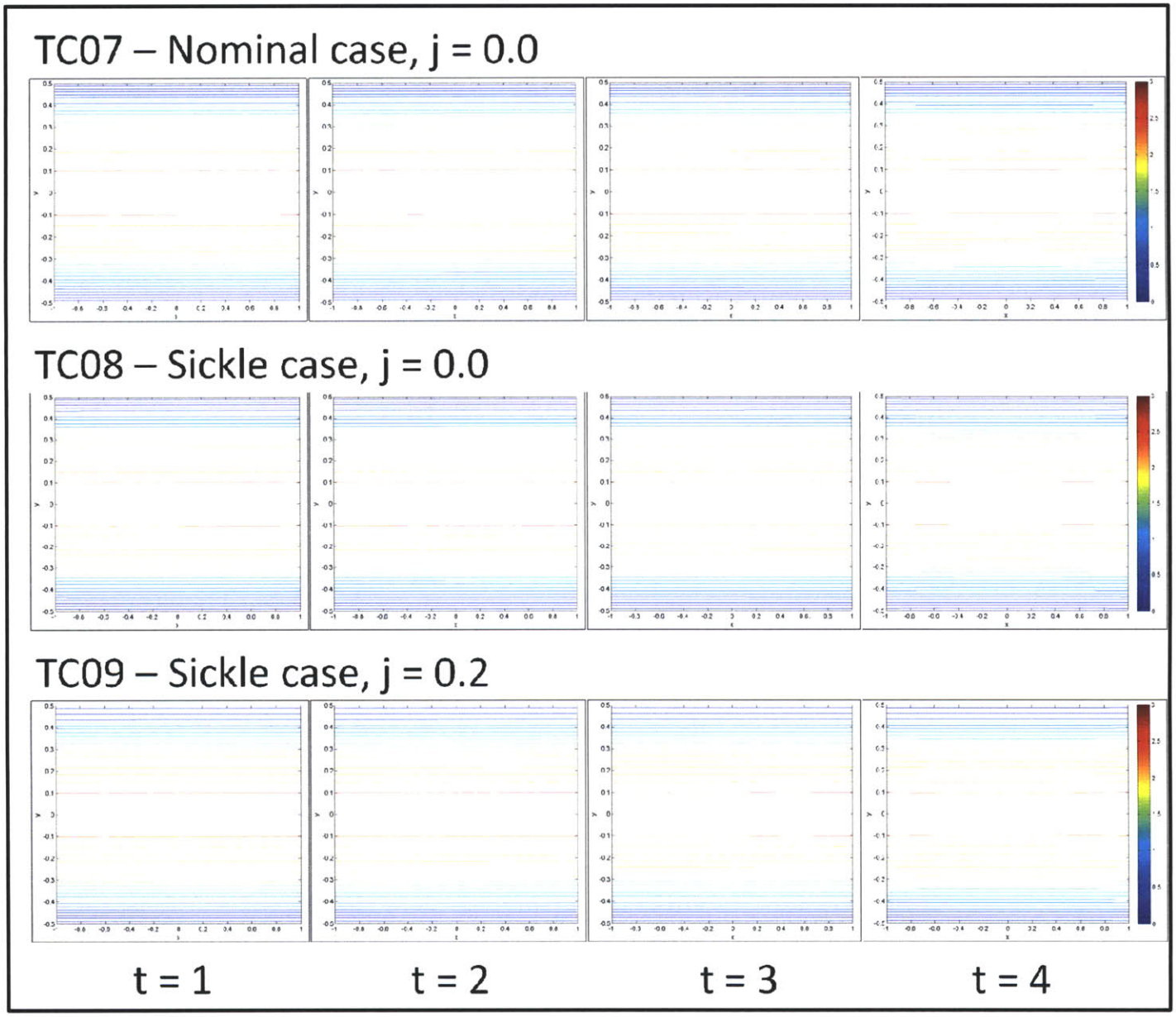

Figure A.4 – U-Velocity, Test Case #09 - #12

L_X = 2, Steady State Initial RBC Geometry

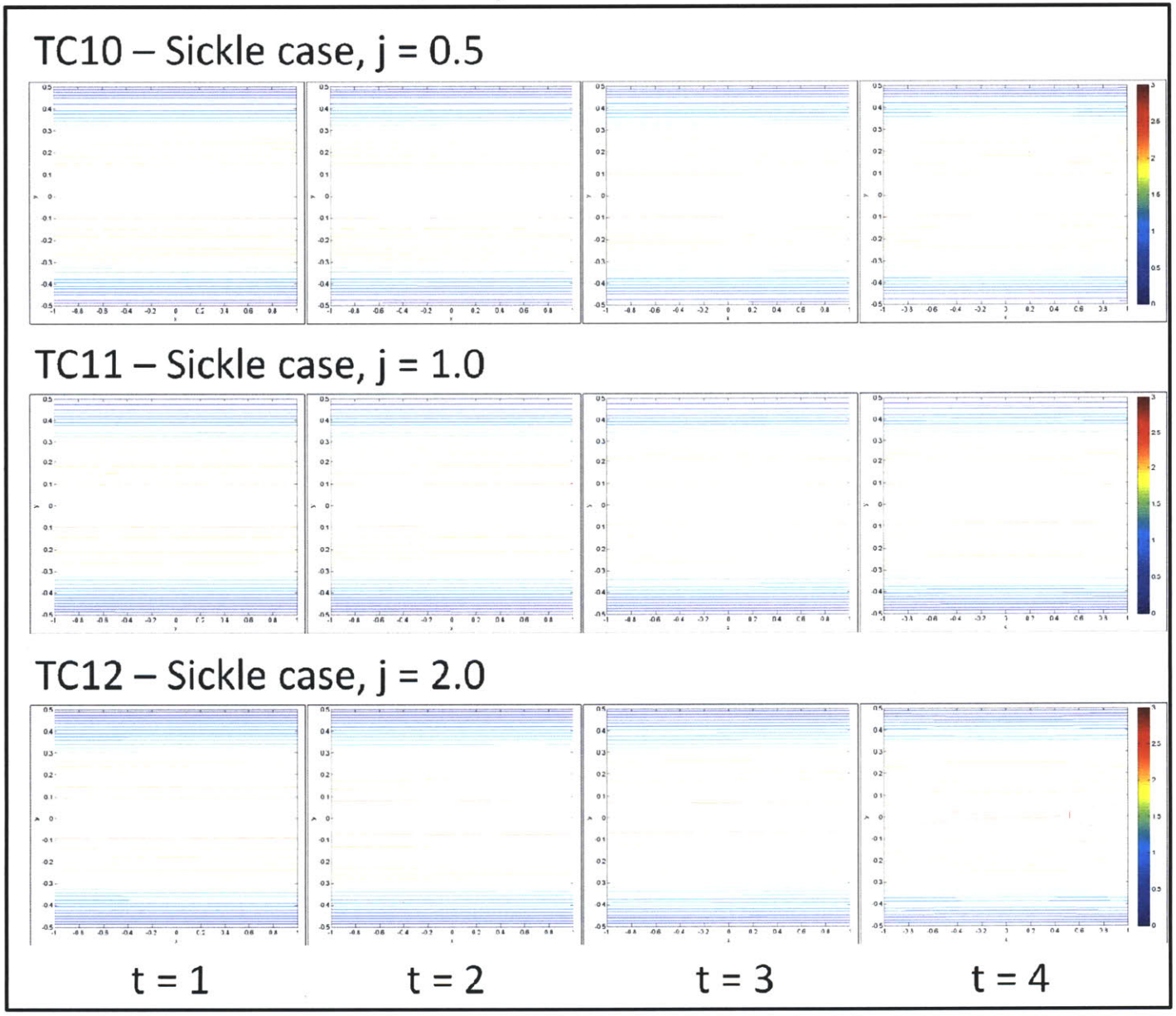

Figure A.5 – U-Velocity, Test Case #13 - #15

L_X = 10, Elliptical Initial RBC Geometry

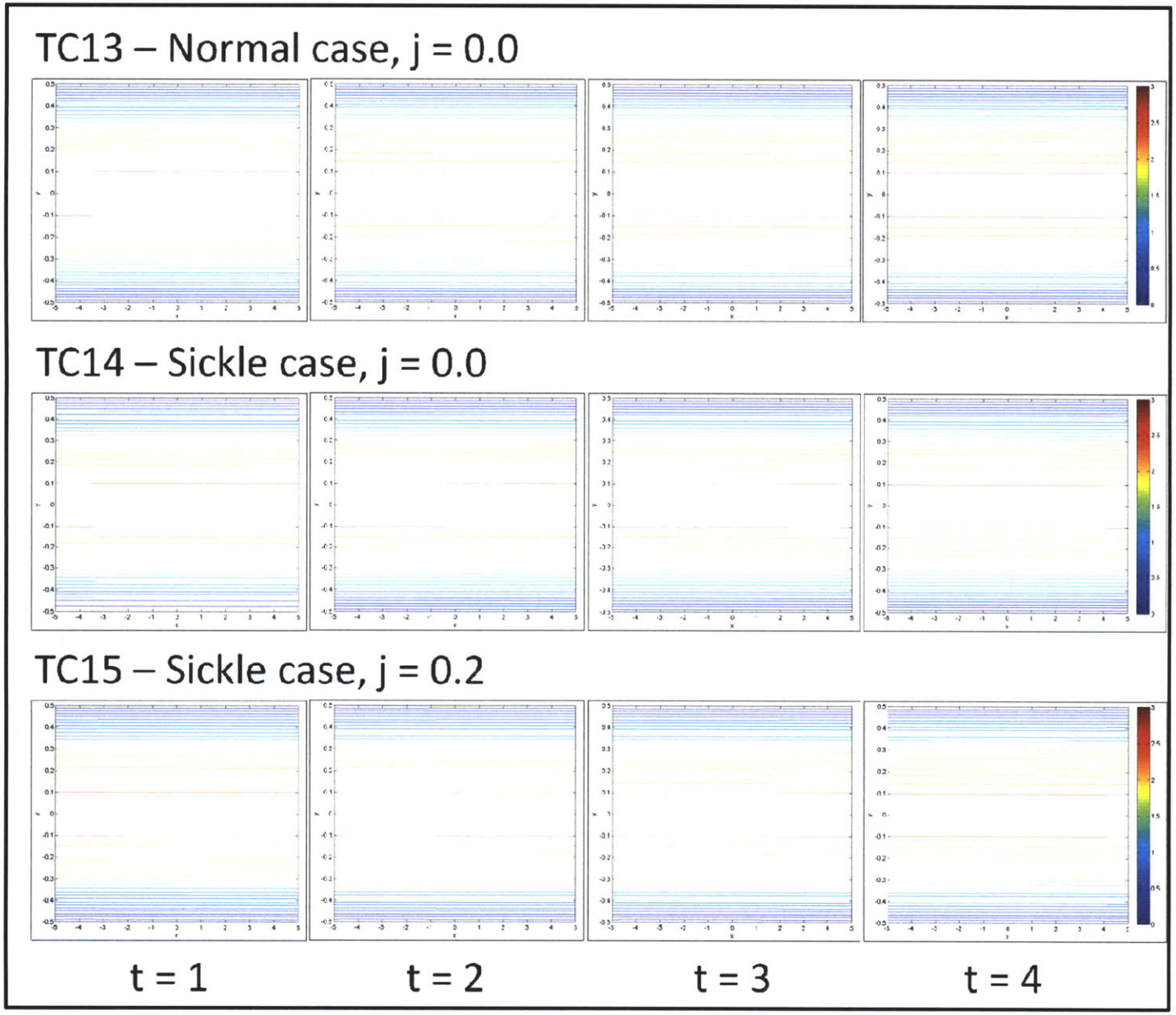

Figure A.6 – U-Velocity, Test Case #16 - #18

L_X = 10, Elliptical Initial RBC Geometry

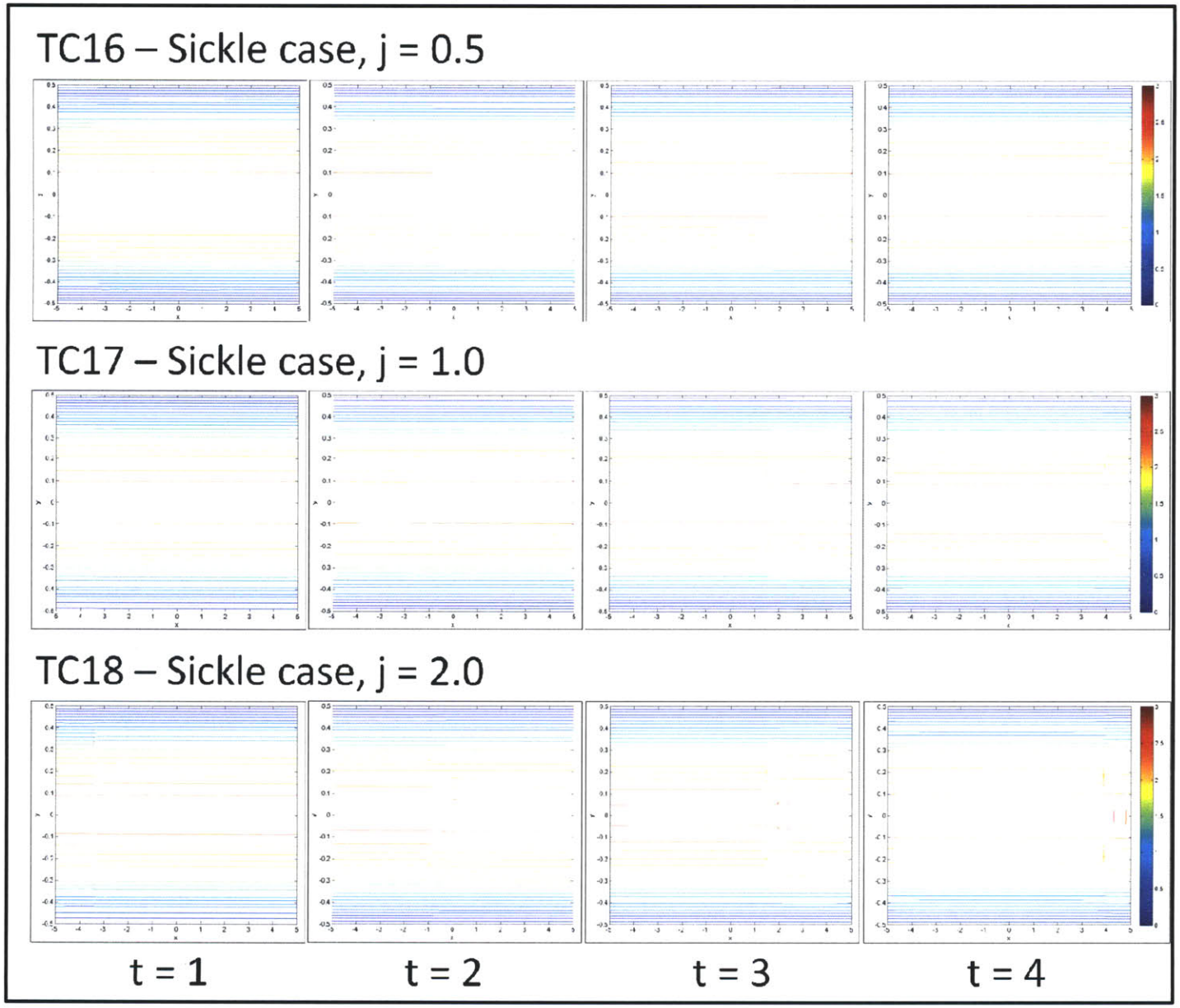

Figure A.7 – U-Velocity, Test Case #19 - #21

L_X = 10, Steady State Initial RBC Geometry

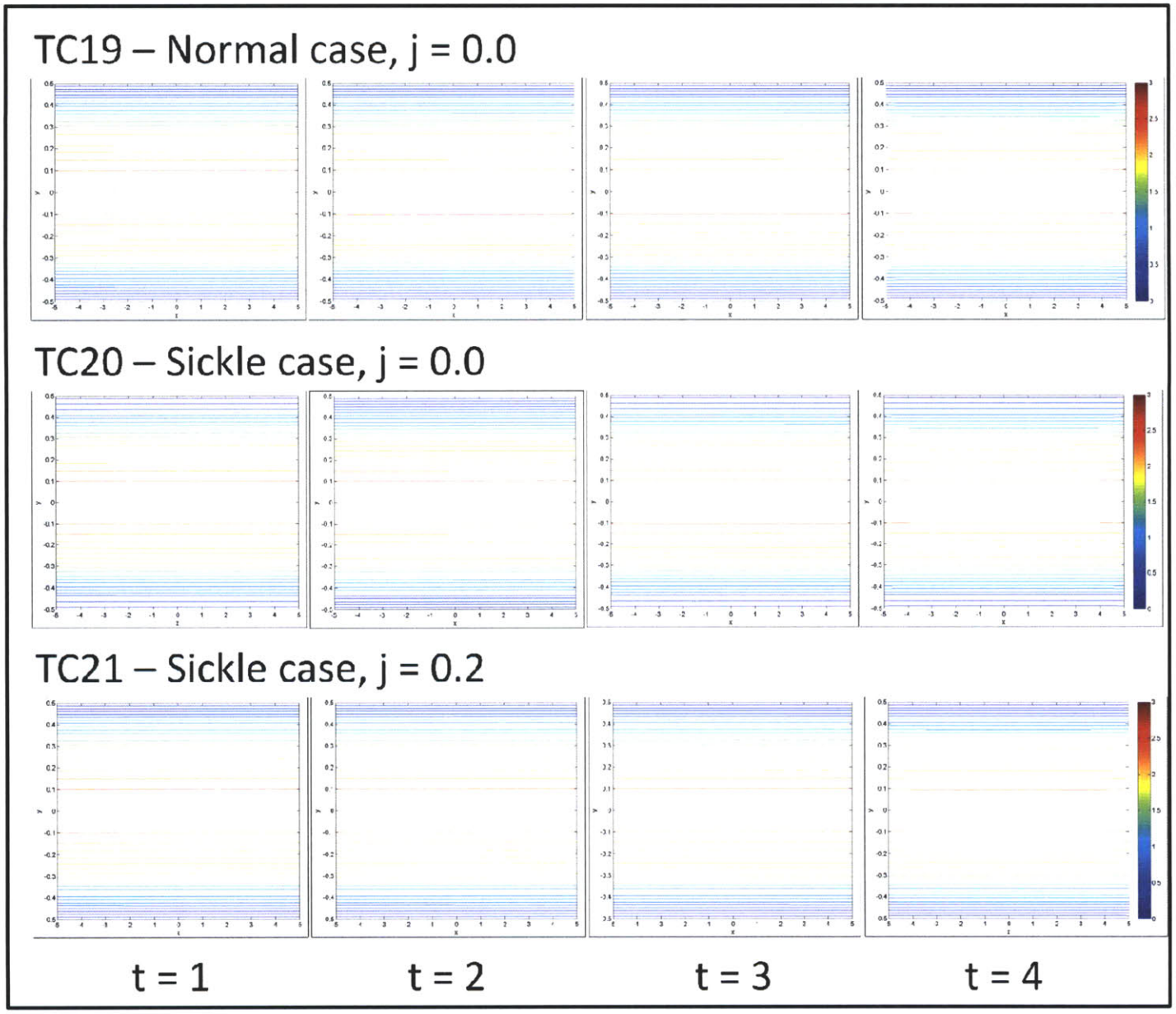

Figure A.8 – U-Velocity, Test Case #22 - #24

L_X = 10, Steady State Initial RBC Geometry

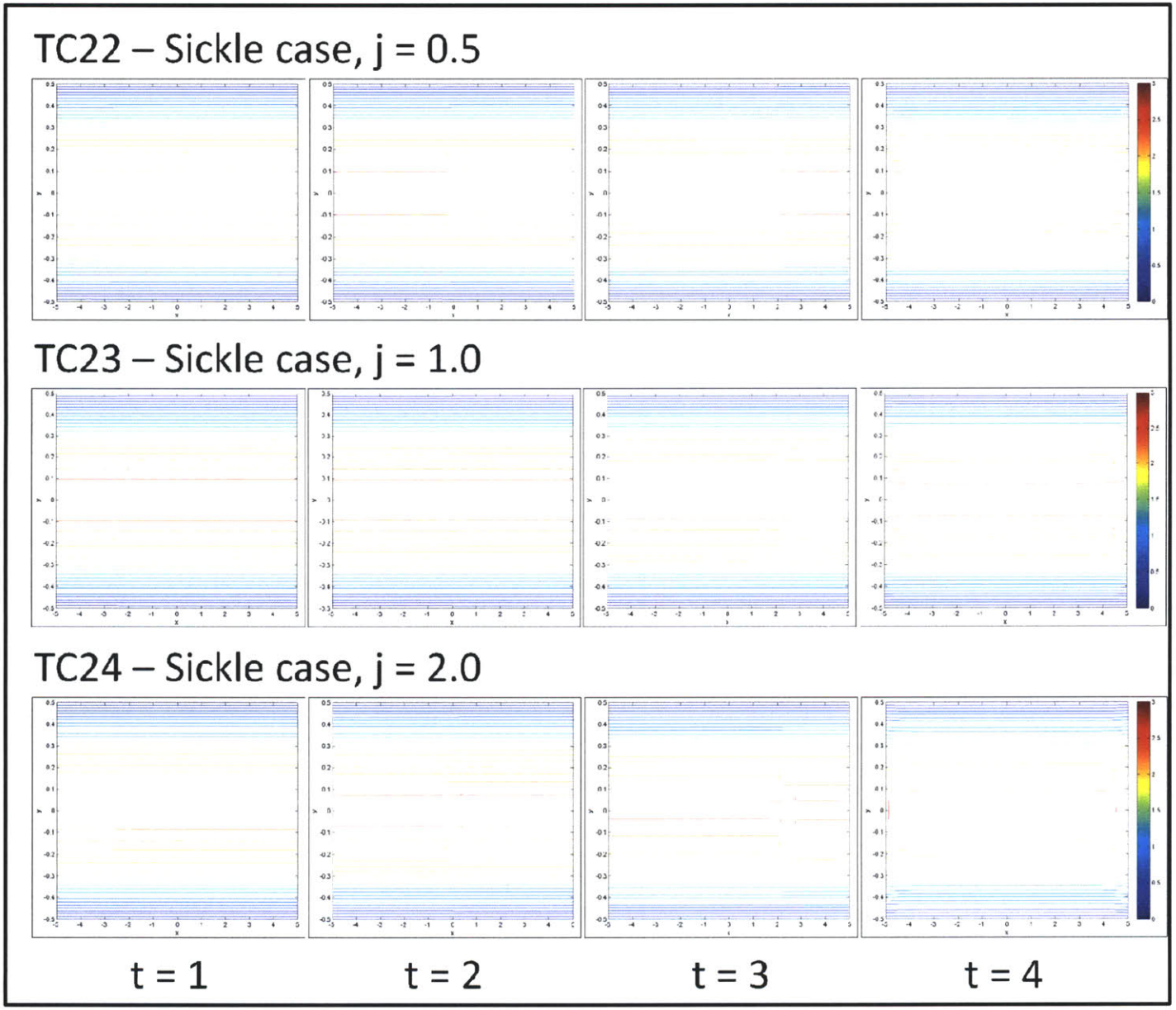

Figure A.9 – V-Velocity, Test Case #01 - #03
L_X = 2, Elliptical Initial RBC Geometry

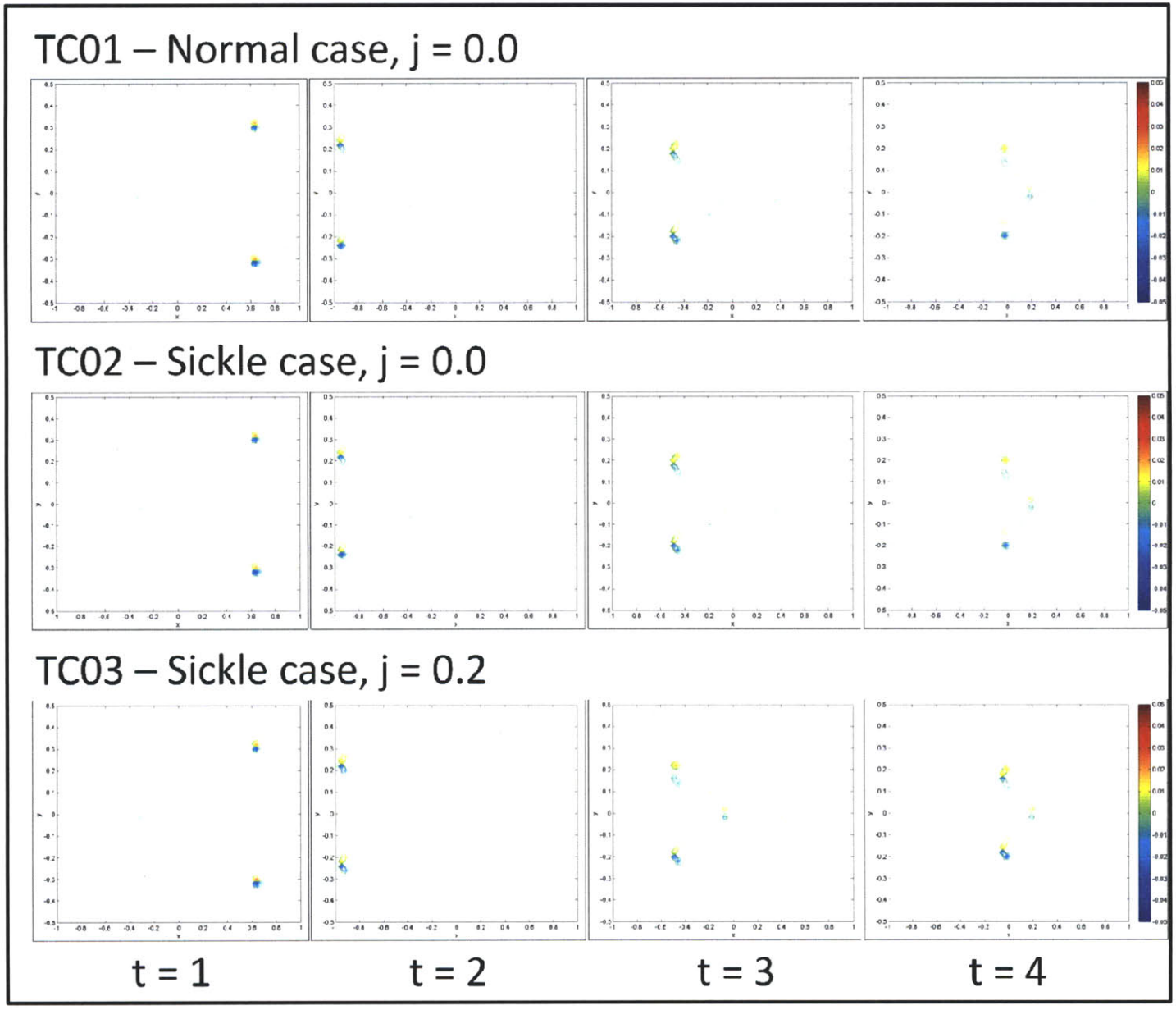

Figure A.10 – V-Velocity, Test Case #03 - #06

L_X = 2, Elliptical Initial RBC Geometry

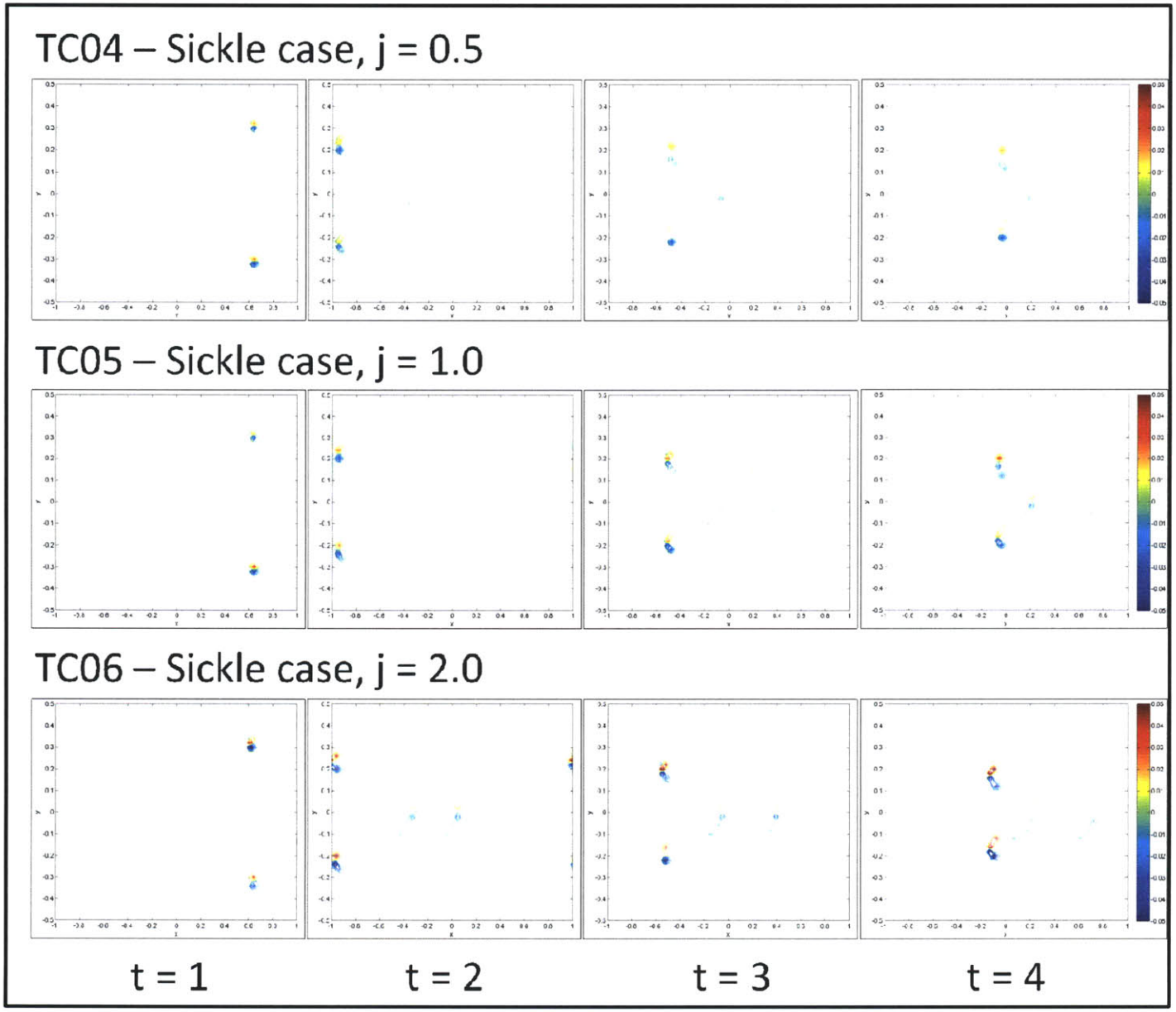

Figure A.11 – V-Velocity, Test Case #07 - #09
L_X = 2, Steady State Initial RBC Geometry

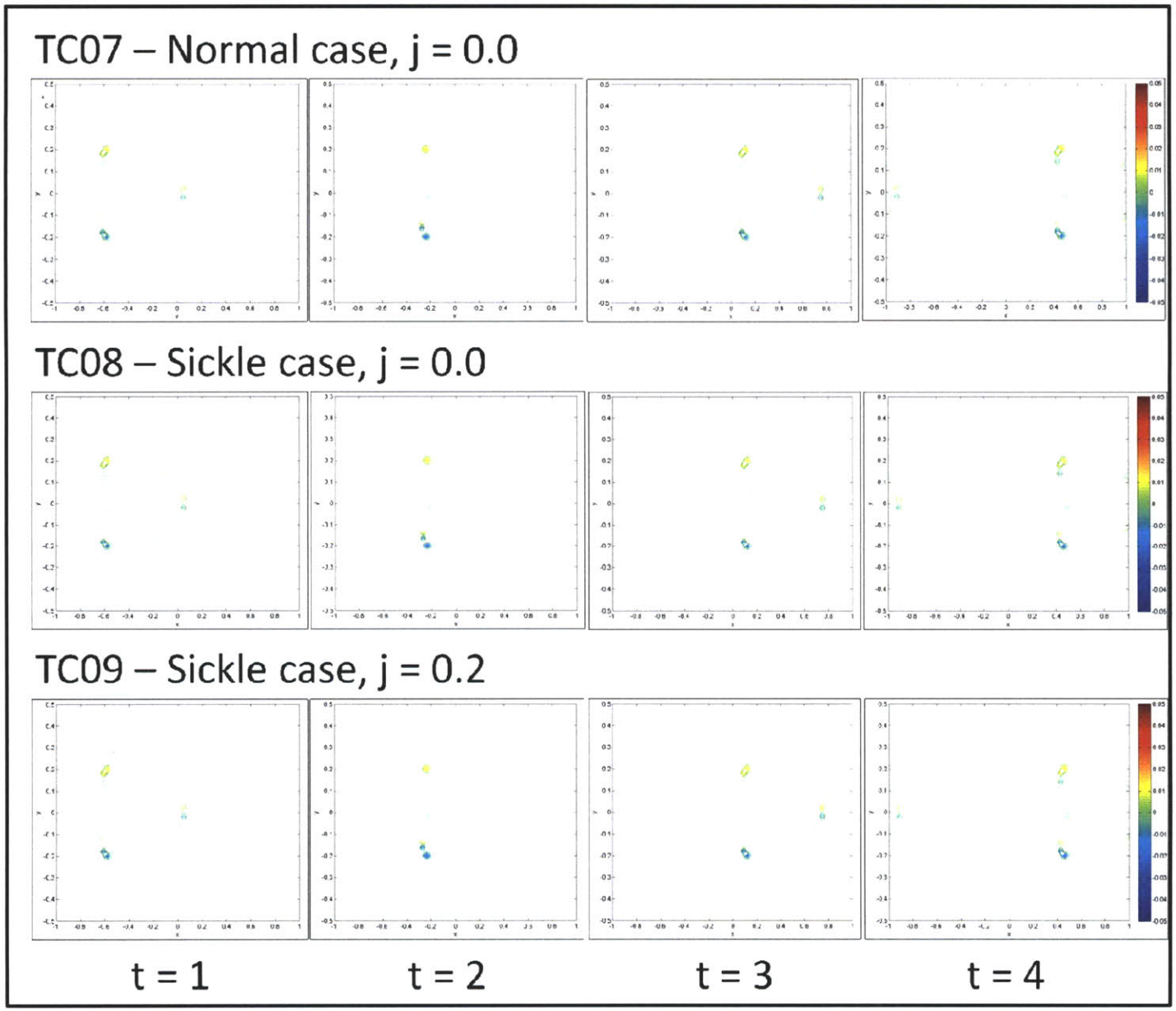

Figure A.12 – V-Velocity, Test Case #10 - #12
L_X = 2, Steady State Initial RBC Geometry

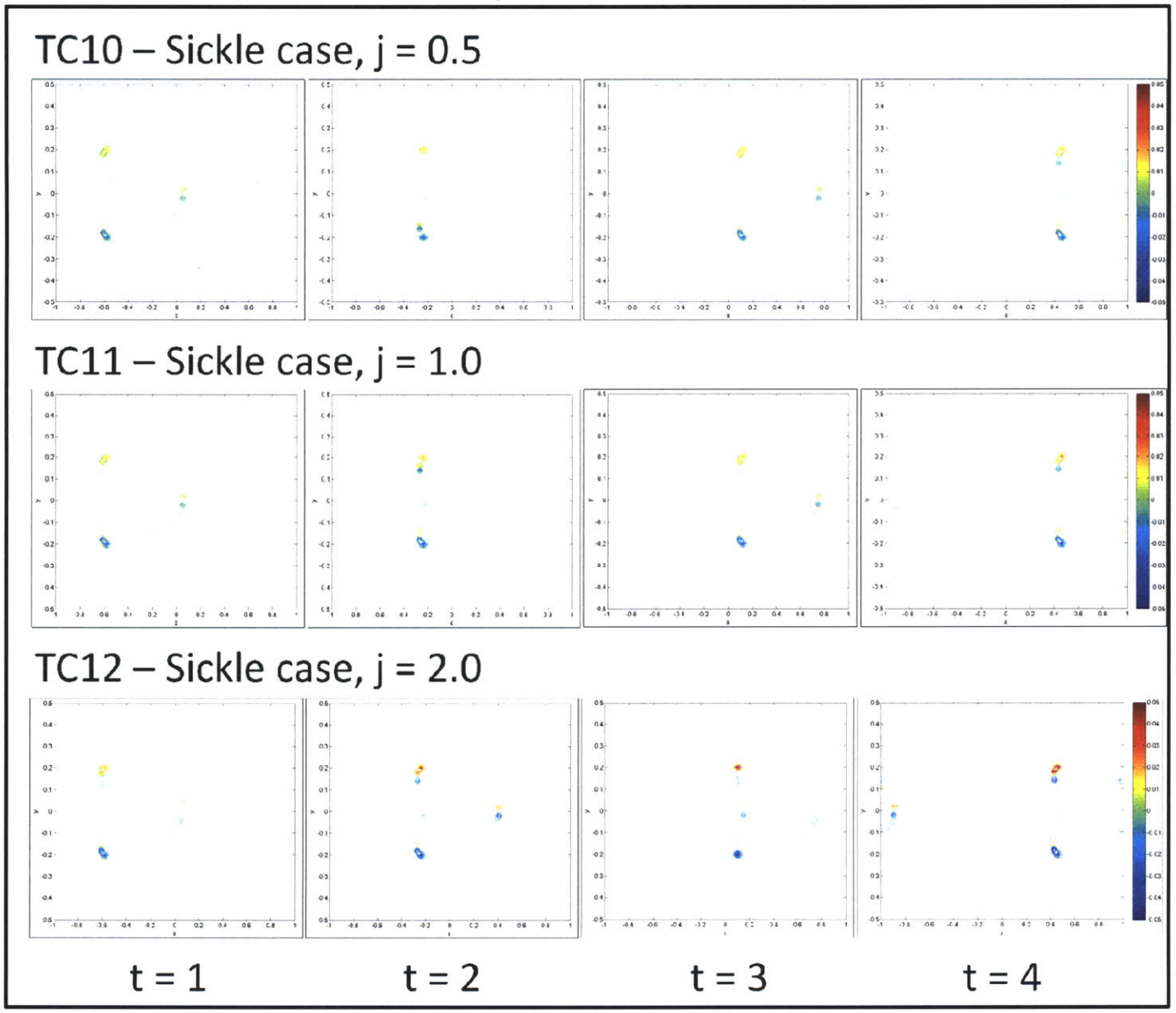

Figure A.13 – V-Velocity, Test Case #13 - #15

L_X = 10, Elliptical Initial RBC Geometry

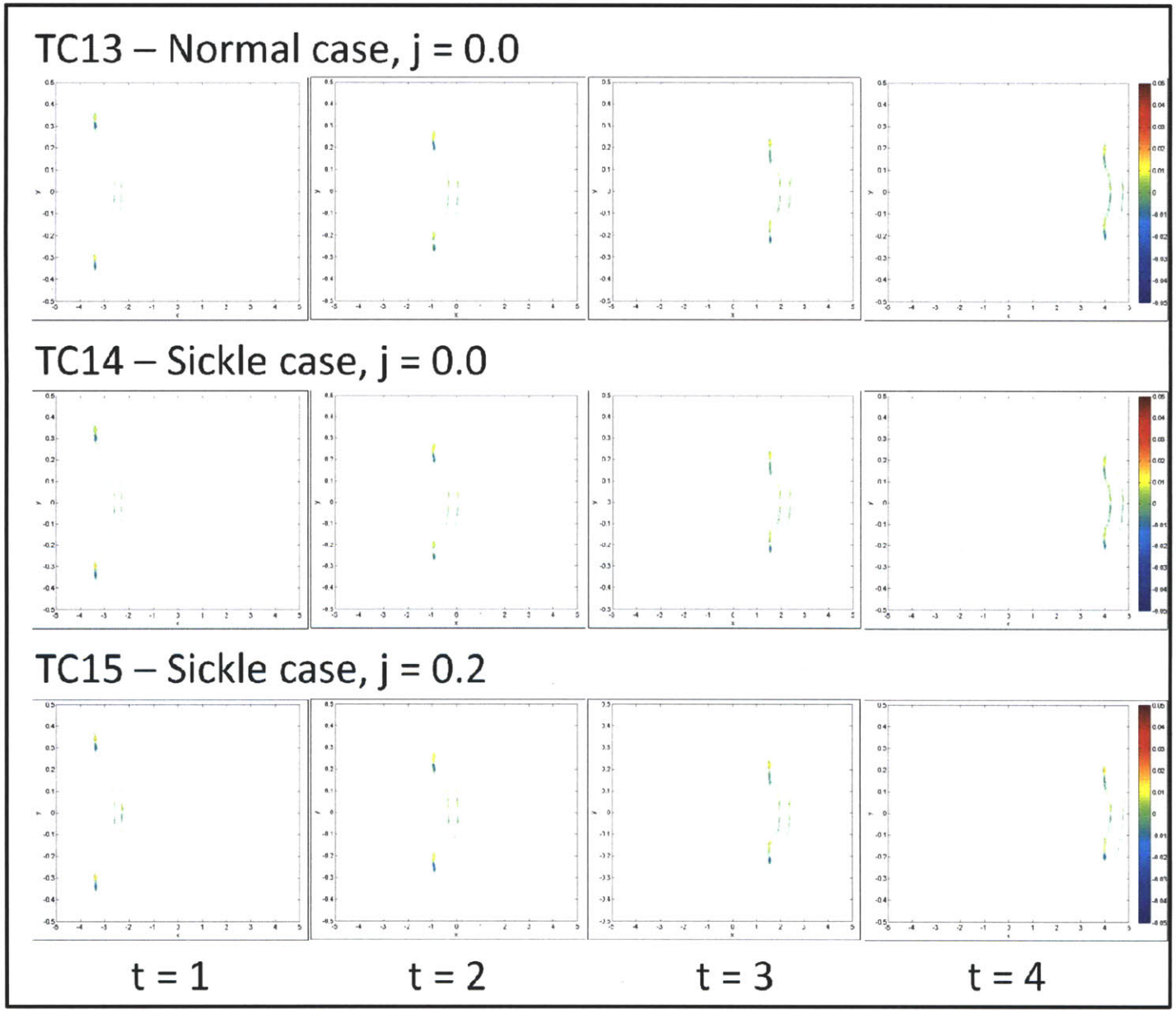

Figure A.14 – V-Velocity, Test Case #16 - #18

L_X = 10, Elliptical Initial RBC Geometry

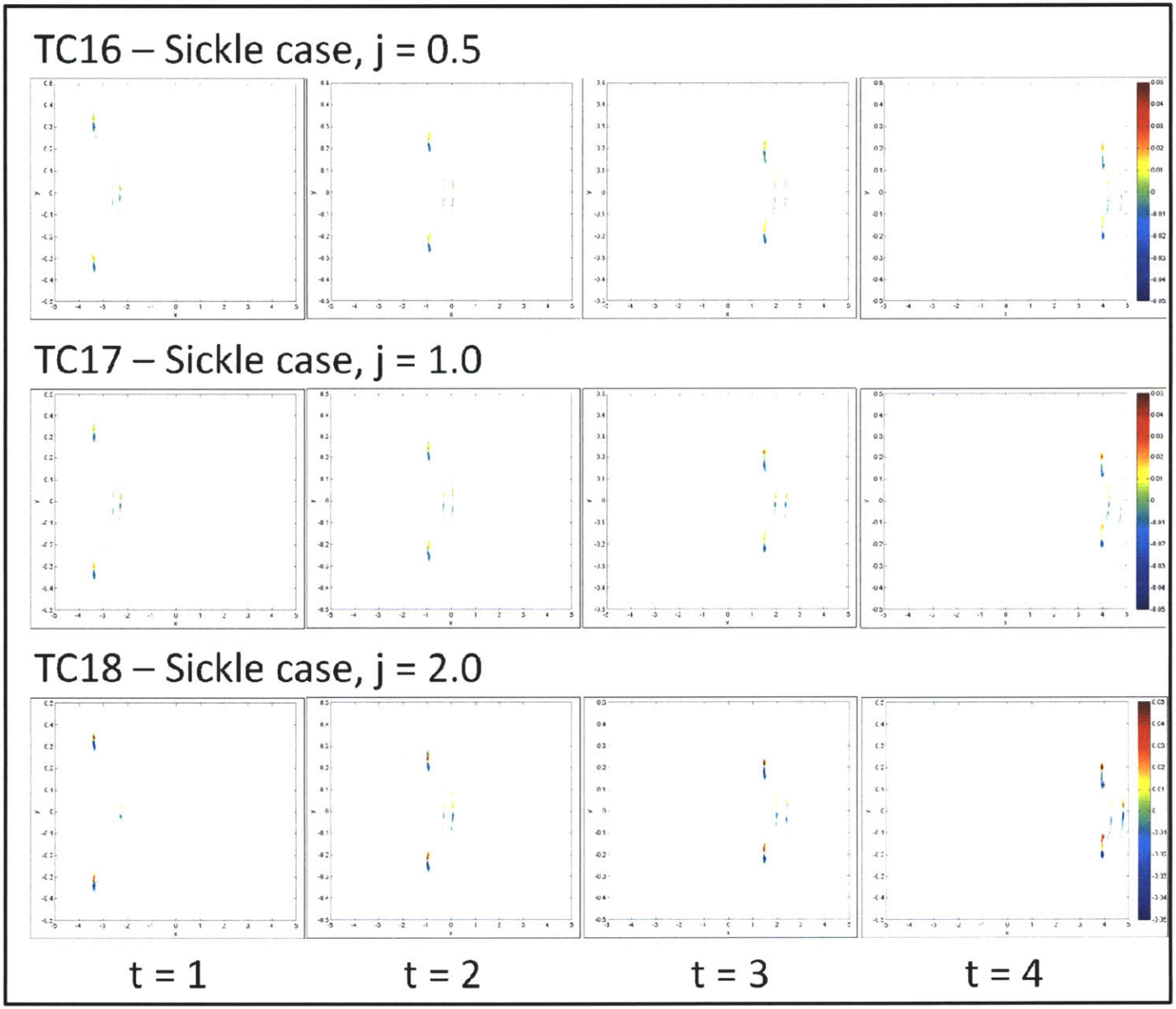

Figure A.15 – V-Velocity, Test Case #19 - #21
L_X = 10, Steady State Initial RBC Geometry

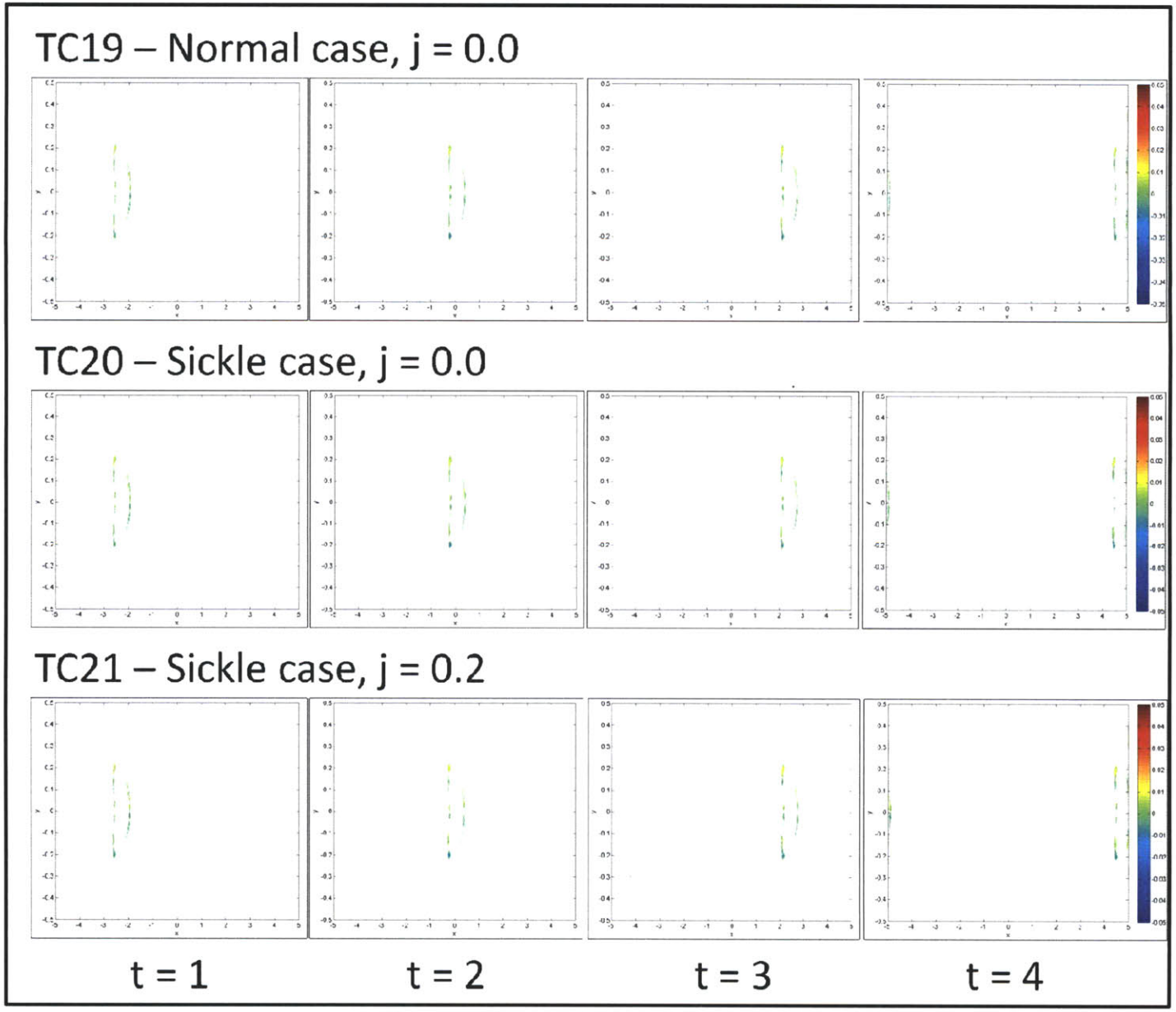

Figure A.16 – V-Velocity, Test Case #22 - #24

L_X = 10, Steady State Initial RBC Geometry

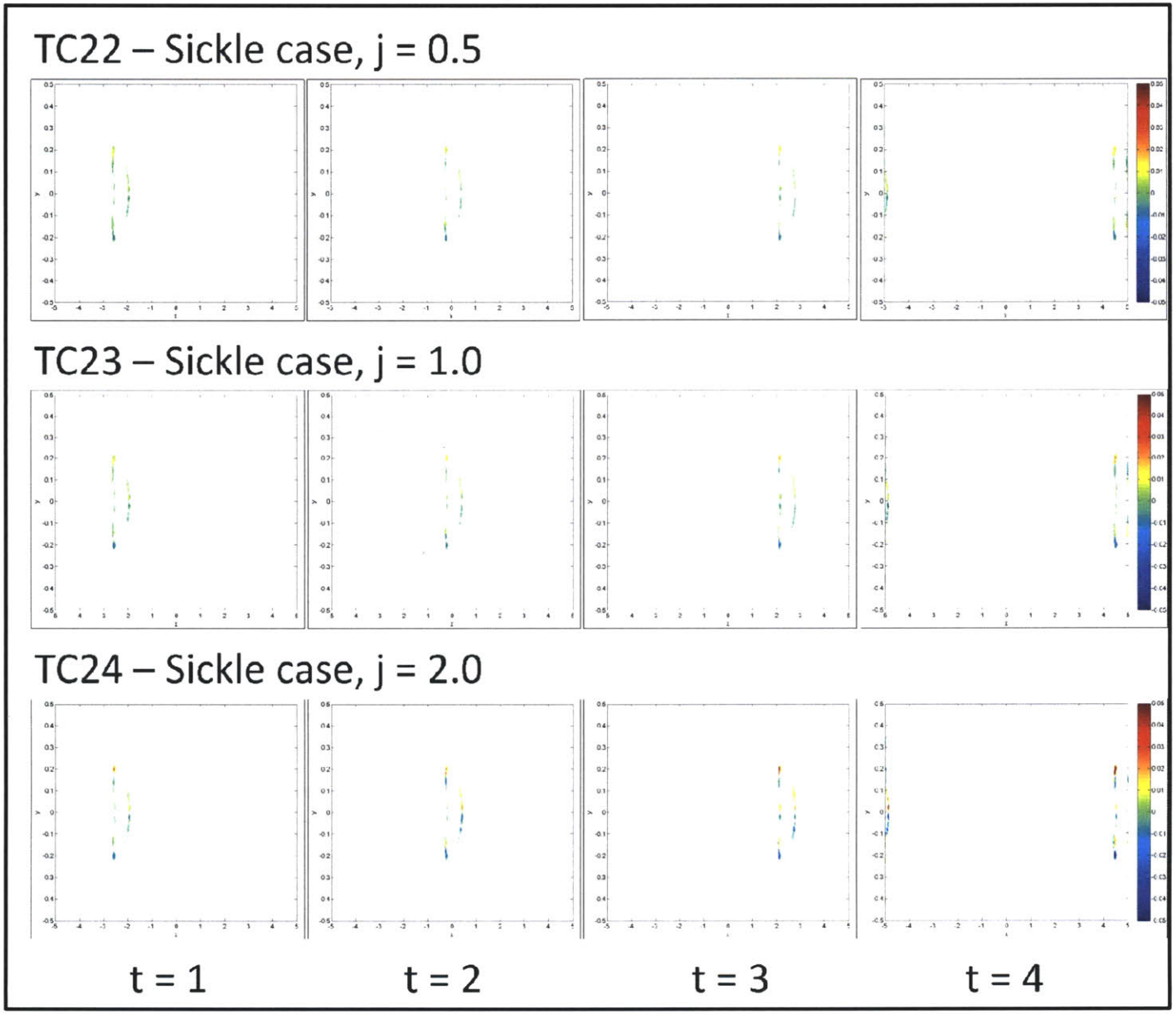

Figure A.17 – O_2 Concentration, Test Case #01 - #03
L_X = 2, Elliptical Initial RBC Geometry

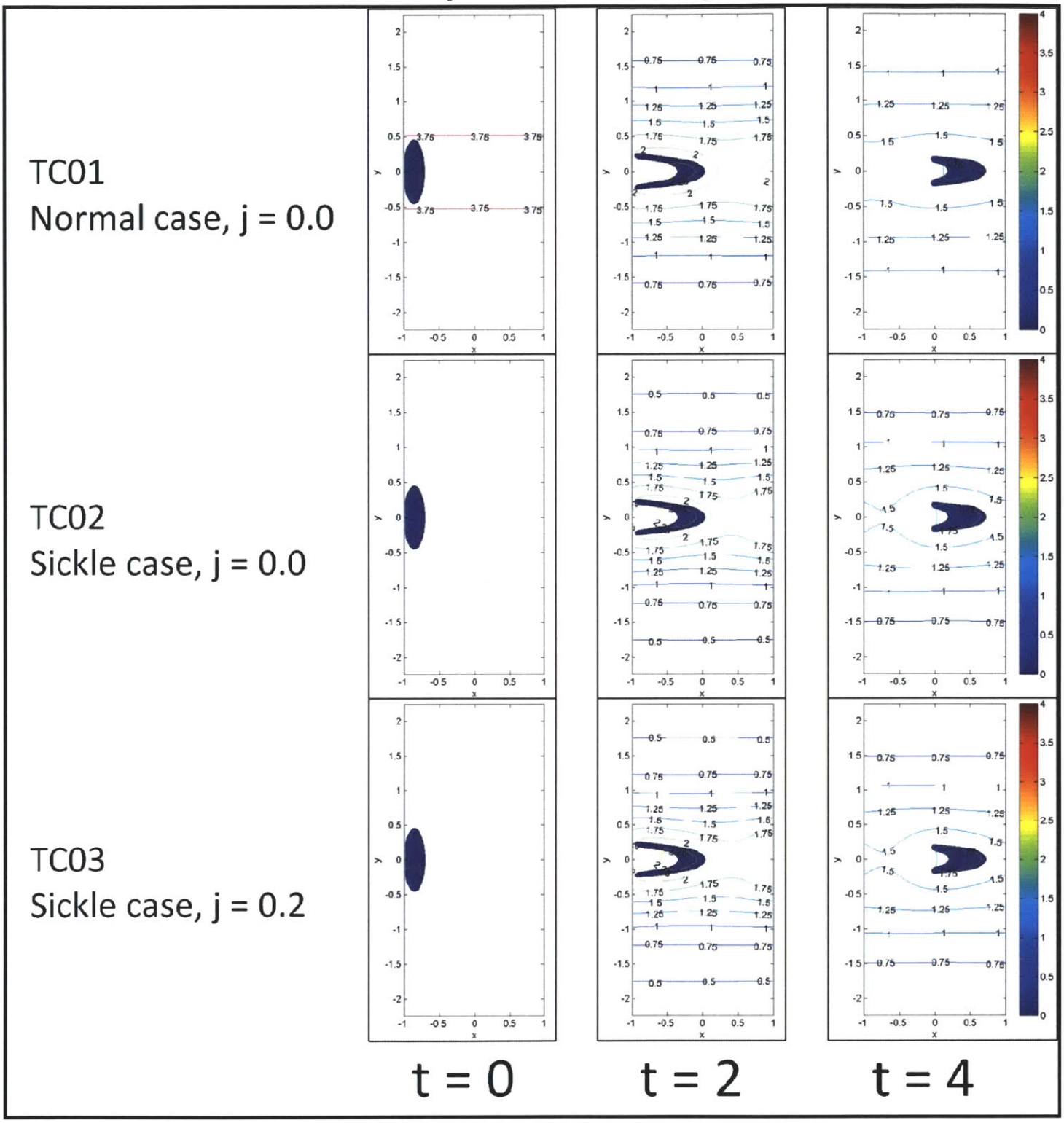

Figure A.18 – O_2 Concentration, Test Case #04 - #06
L_X = 2, Elliptical Initial RBC Geometry

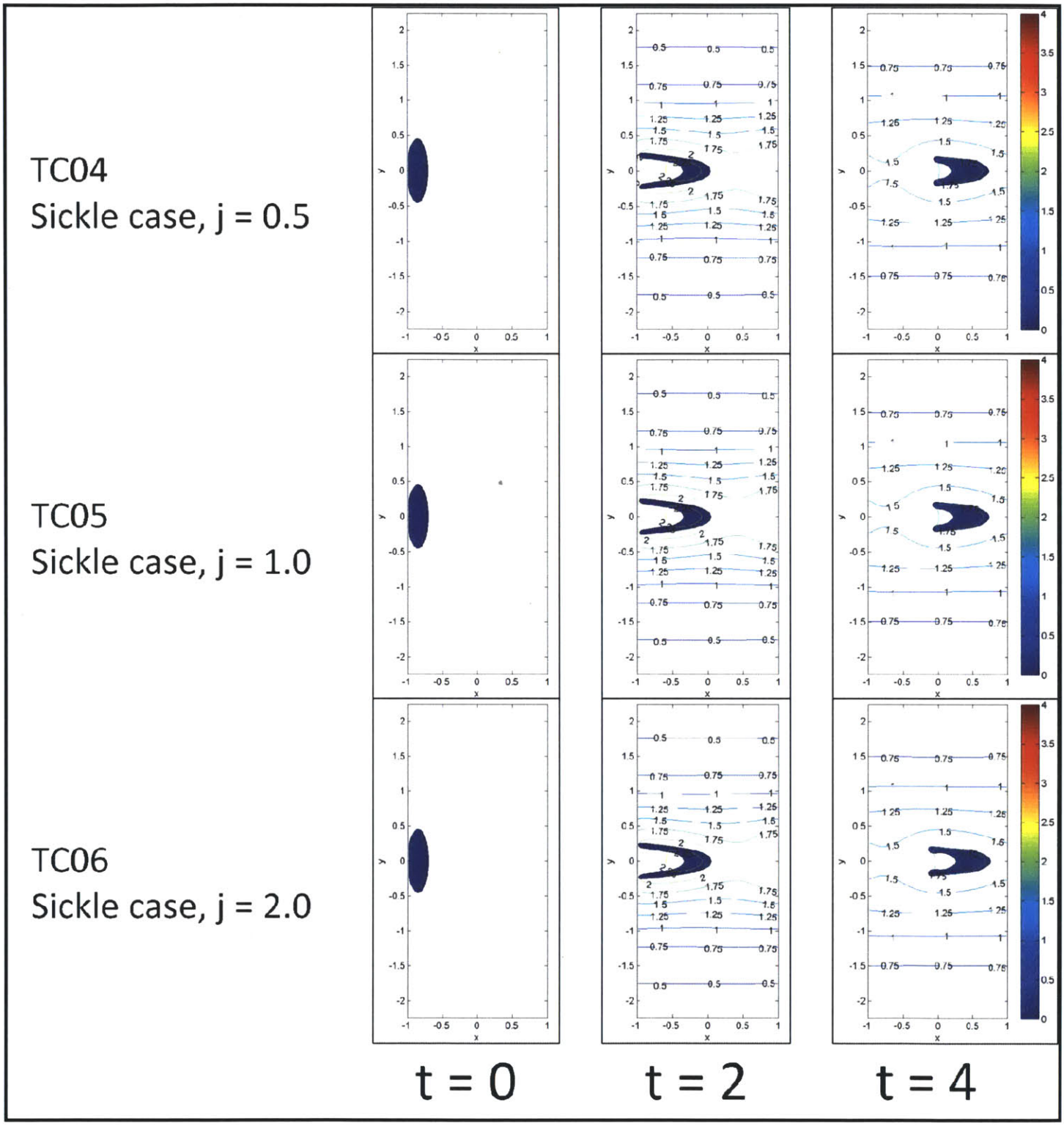

Figure A.19 – O_2 Concentration, Test Case #07 - #09
L_X = 2, Steady State Initial RBC Geometry

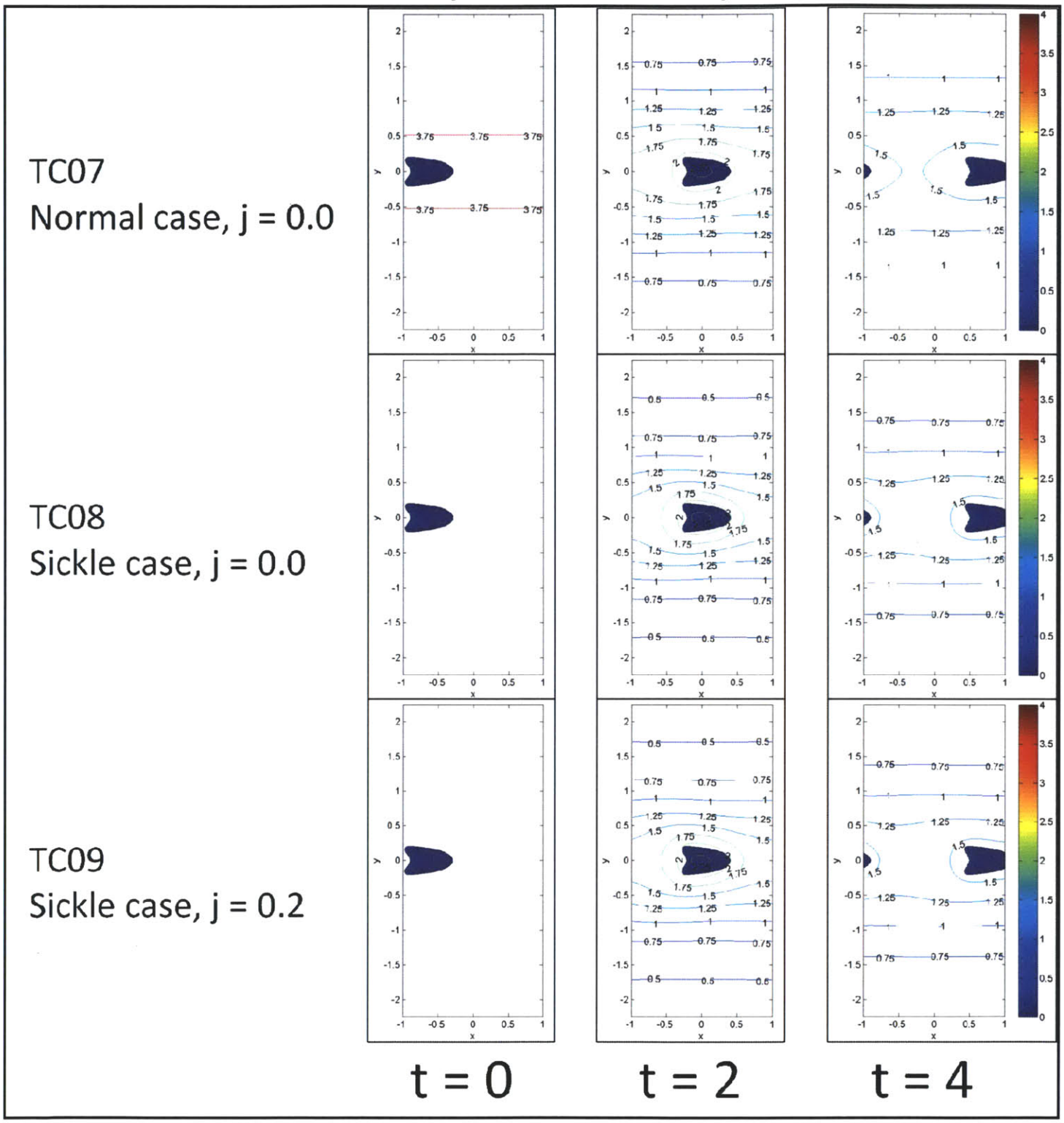

Figure A.20 – O_2 Concentration, Test Case #10 - #12
L_X = 2, Steady State Initial RBC Geometry

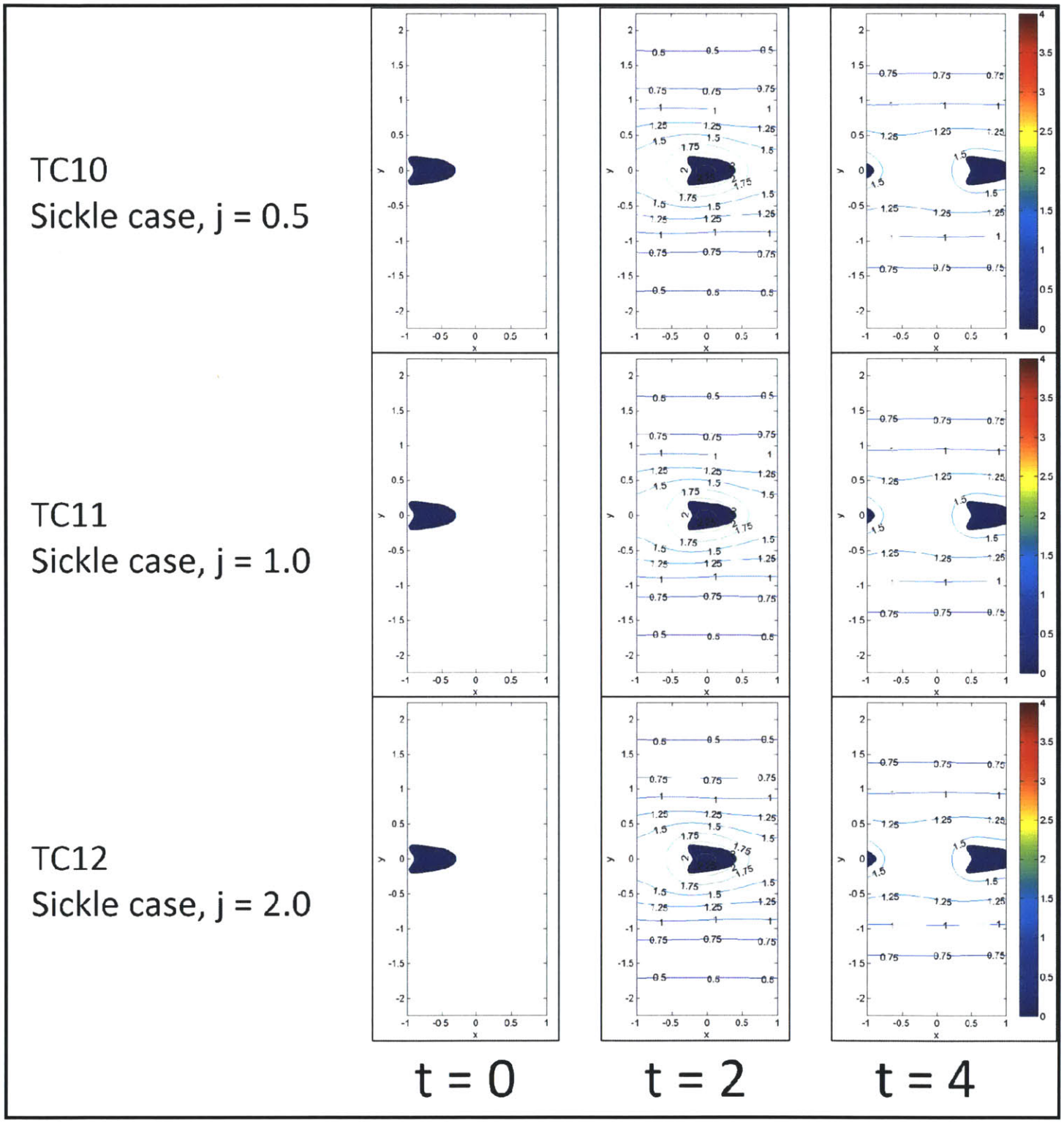

Figure A.21 – O_2 Concentration, Test Case #13 - #15

L_X = 10, Elliptical Initial RBC Geometry

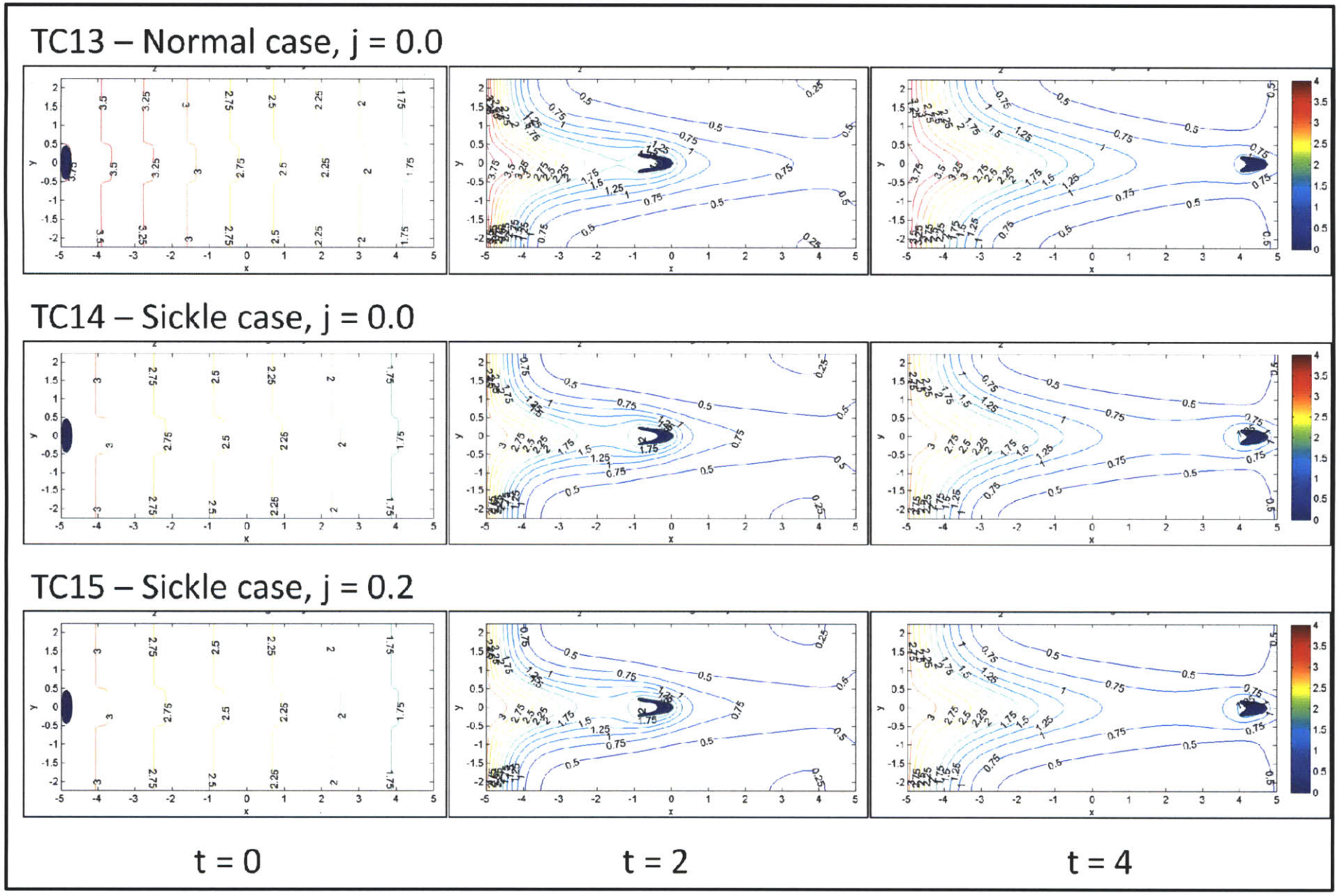

Figure A.22 – O_2 Concentration, Test Case #16 - #18

L_X = 10, Elliptical Initial RBC Geometry

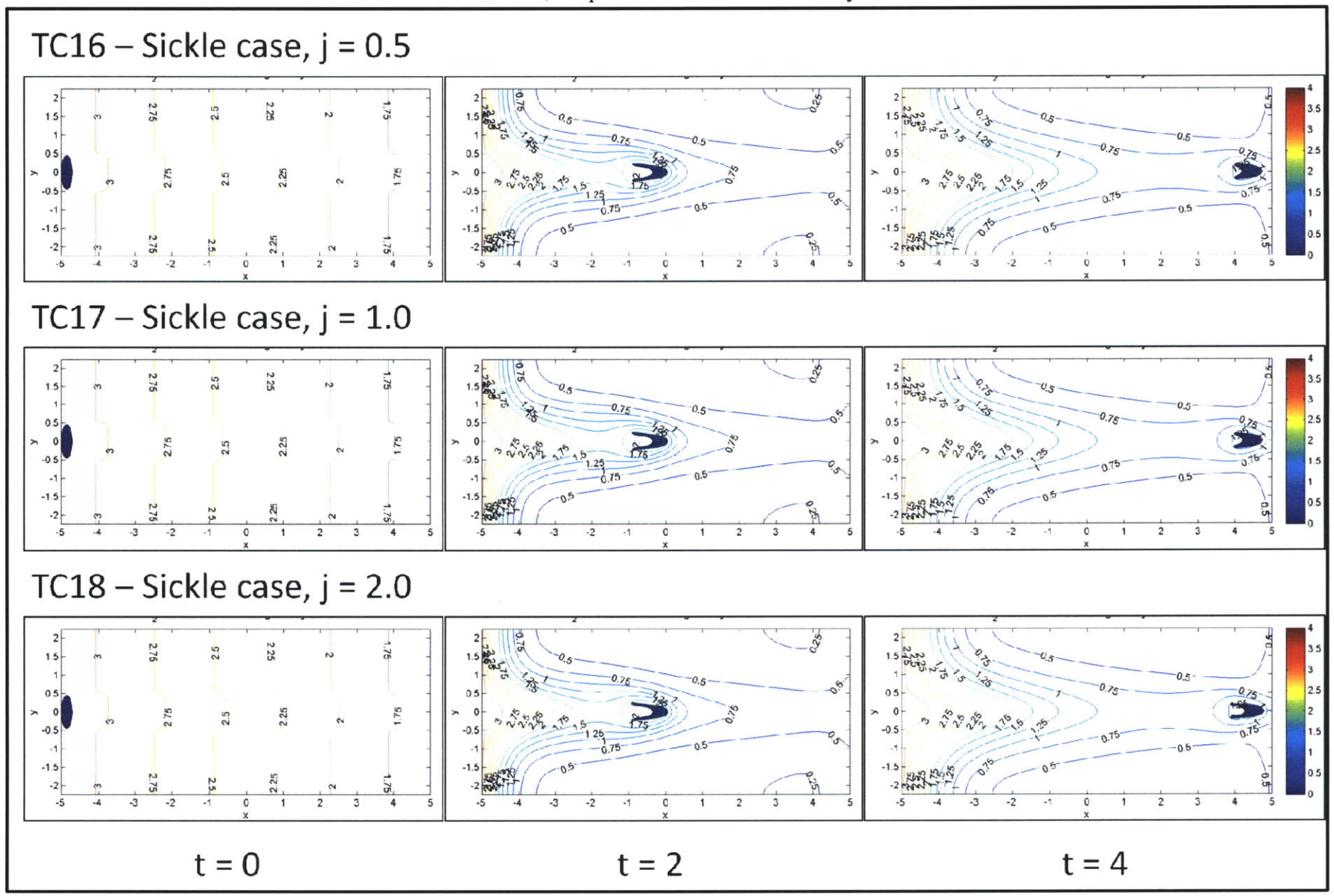

Figure A.23 – O_2 Concentration, Test Case #19 - #21

L_X = 10, Steady State Initial RBC Geometry

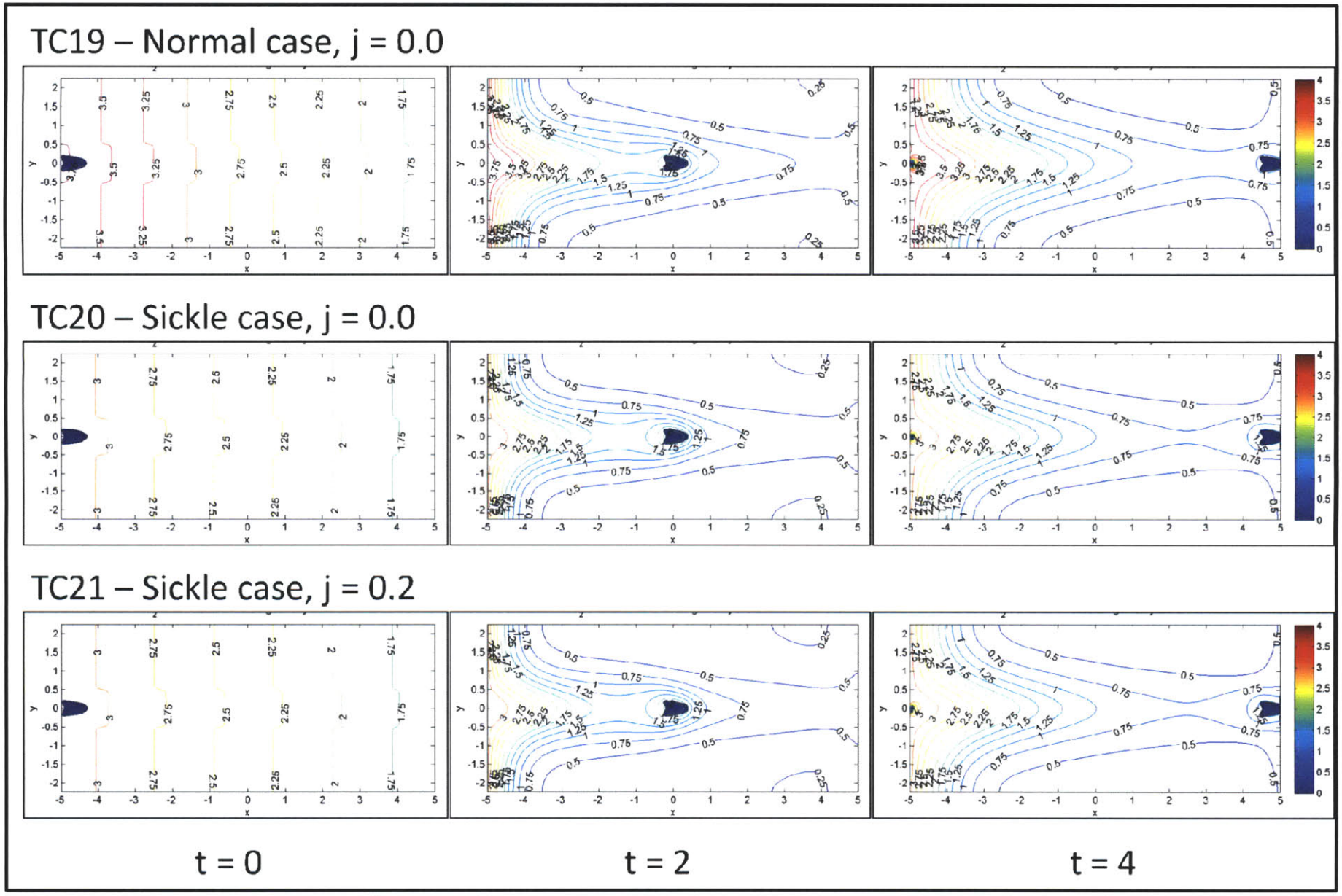

Figure A.24 – O_2 Concentration, Test Case #22 - #24

L_X = 10, Steady State Initial RBC Geometry

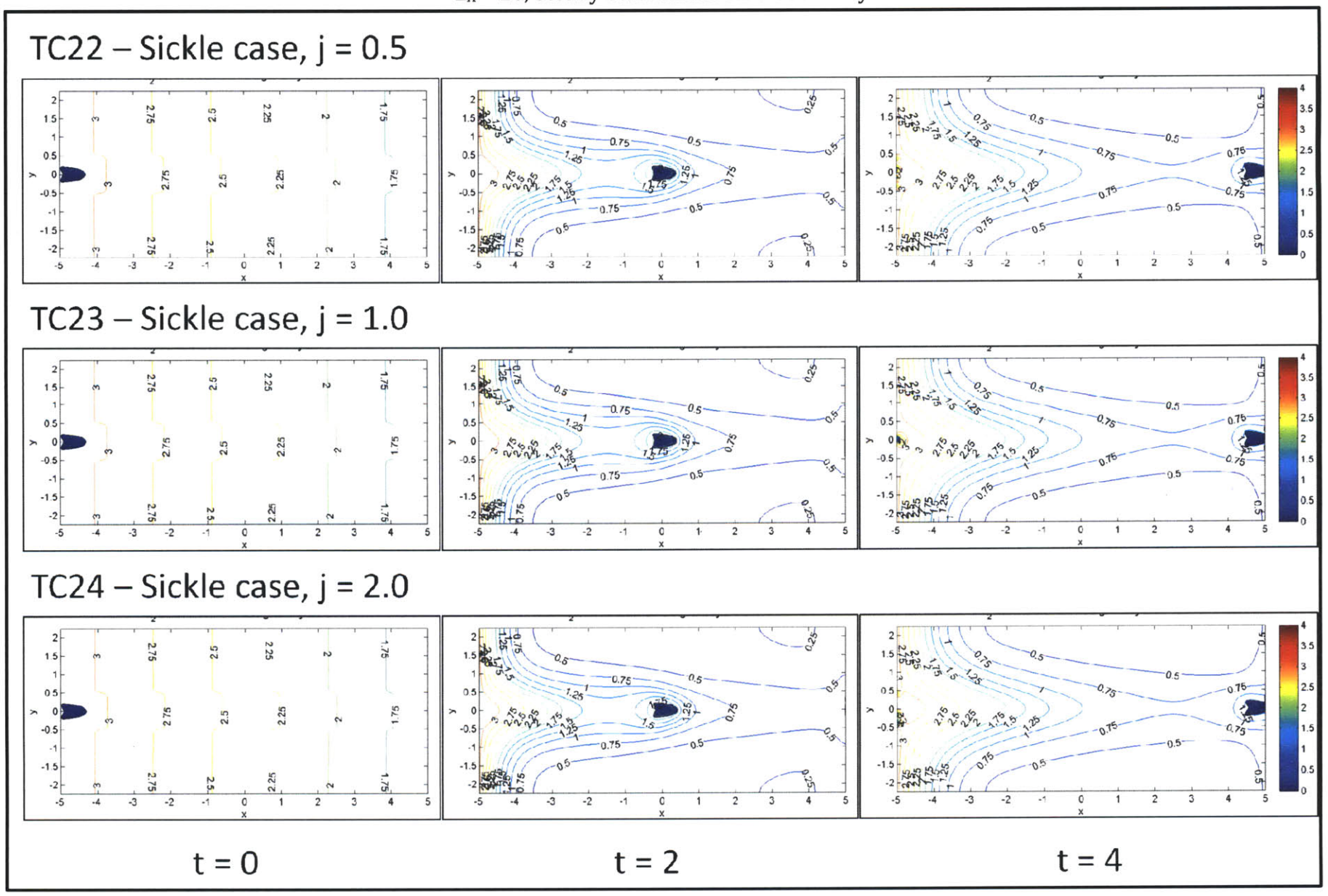

Appendix B – Code

```
function microcirculation(lx,ss, periodic_flag)
%NAVIERSTOKES --> MICROCIRCULATION
%    Solves the incompressible Navier-Stokes equations in a rectangular
%    domain with prescribed velocities along the boundary.  The solution
%    method is finite differencing on a staggered grid with implicit
%    diffusion and a Chorin projection method for the pressure.
%    Visualization is done by a colormap-isoline plot for pressure and
%    normalized quiver and streamline plot for the velocity field.
%    The standard setup solves a lid driven cavity problem.
%
% 07/2007 by Benjamin Seibold, http://www-math.mit.edu/~seibold/
% Feel free to modify for teaching and learning.
%
% 04/2010 Modified by Yonatan Tekleab (ytekleab)
%    This code has been modified to simulate the flow of a red blood cell
%    (RBC) within a capillary.
%       -level-set method implemented to create RBC boundary
%       -jump matrix to incorporate jump in fluid pressure due to membrane
%          stresses
%       -boundary conditions changed to periodic flow on the E & W
%          boundaries and no-flux/no-slip along N & S boundaries
%       -axial pressure gradient applied
%       -oxygen diffusion incorporated
%
% Last modified: ytekleab Jan 23, 2011 16:25:00
%-------------------------------------------------------------------------
close all; clc;
if nargin < 3
    periodic_flag = 0;
end
if nargin < 2
    ss = 0;
end
if nargin < 1
    lx = 10;
end

% DEFINE MICROCIRCULATION PARAMETERS
% reference values
pHb50_0 = 3.333e3;      % reference pHb50 [Pa]
pO2a_0 = 1.2666e4;      % reference pO2a [Pa]

% sickle/normal RBC, O2 parameters
sickle = ~logical(input('Sickle RBC [0] or Normal RBC [1--default] case? '));
if ~sickle,
   fprintf(['\n***NORMAL RBC CASE***\nEntering stiffness index of "0"',...
      ' will give normal RBC Membrane stiffness\n']);
   n = 2.7;             % Hill coefficient for normal blood
   pHb50 = pHb50_0;     % pO2 at 50% Hb saturation [Pa] for normal blood
   pO2a = pO2a_0;       % Arterial pO2 [Pa] for normal blood
else
   fprintf(['\n***SICKLE RBC CASE***\nEntering stiffness index of "0"',...
```

```
      ' will give normal RBC Membrane stiffness\n']);
   n = 3.0;              % Hill coefficient for sickle blood
   pHb50 = 5.333e3;      % pO2 at 50% Hb saturation [Pa] for sickle blood
   pO2a = 1.0666e4;      % Arterial pO2 [Pa] for sickle blood
end
index = 0;               % Stiffness index (0 for normal RBC)
in = input('\nEnter the stiffness index (between 0 and 2): ');
if in > 2 || in < 0,
   fprintf(['\nBad index! Must be [0 2]\nWill proceed using index value of
',num2str(index)]);
else
    index = in; clear in;
end

% fluid, capillary & RBC parameters
rho = 1025;                                % plasma density [kg/m^3]
Vavg = 1e-3;                               % mean plasma velocity [m/s]
Dcap = 9e-6;                               % capillary diameter [m]
mu = 1.4e-3;                               % plasma viscosity [Pa-s]
Re = rho*Vavg*Dcap/mu;                     % reynolds number
Rk = 20.10e-6;                             % capillary centerline to end of
tissue [m]
V_rbc = 9e-17;                             % RBC volume [m^3]
a = 0.45;                                  % semi-major axis (vertical
direction)
b = V_rbc/((4/3)*pi*(a^2)*Dcap^3);         % semi-minor axis (horizontal
direction)
k_mem = 1.9e-5;                            % membrane stiffness [N/m]
dpdx = -(3.4e5)*(Dcap/(rho*Vavg^2));       % pressure gradient [Pa/m] (Non
dimensionalized)

% oxygen concentration parameters
Dox = 2.40e-9;              % O2 diffusivity in plasma/tissue [m^2/s]
DHb = 1.40e-11;             % diffusivity of oxyhemoglobin [m^2/s]
DMb = 6.10e-11;             % diffusivity of oxymyoglobin [m^2/s]
alpha = 1.029e-5;           % Henry's law constant [mol/(m^3-Pa)]
pMb50 = 3.179e2;            % pO2 at 50% Mb saturation [Pa] (Schenkman et.
al.)
cHb50 = pHb50*alpha;        % O2 concentration at 50% Hb saturation [mol/m^3]
cMb50 = pMb50*alpha;        % O2 concentration at 50% Mb saturation [mol/m^3]
cHb_const = 21.099;         % Hb concentration in RBC [mol/m^3]
cMb_const = 0.4;            % Mb concentration in Tissue [mol/m^3]
kinvHb = 44;                % Hb inverse rate constant [sec^-1]
kinvMb = 15.6;              % Mb inverse rate constant [sec^-1]
M = -6.1321e-3;             % tissue O2 consumption rate [mol/(m^3-s)]
cO2a = pO2a*alpha;          % arterial cO2 [mol/m^3]
cHb50_0 = pHb50_0*alpha;    % reference cHb50 [mol/m^3]
cO2a_0 = pO2a_0*alpha;      % reference cO2a [mol/m^3]

pO2v = 5.333e3;
cO2v = pO2v*alpha;

%-------------------------------------------------------------------------
% DISCRITIZATION
```

```
dt = 1e-2;                  % time step
tf = 0.4e+1;                % final time
ly = 1;                     % height of capillary
nx = lx*50;                 % number of x-gridpoints
ny = ly*50;                 % number of y-gridpoints
nsteps = tf;                % number of steps with graphic output
nyc = round(ny*(2*Rk/Dcap)/2)*2;
lyc = nyc/ny;

x = linspace(-lx/2,lx/2,nx+1); hx = lx/nx;
y = linspace(-ly/2,ly/2,ny+1); hy = ly/ny;
yc = linspace(-lyc/2,lyc/2,nyc+1);
[X,Y] = meshgrid(y,x);
ax = [min(x) max(x) min(y) max(y)]; axc = [min(x) max(x) min(yc) max(yc)];

k_cfl = 1; Umax = 4;
if tf/ceil(tf/(k_cfl*min(hx,hy)/(2*Umax)))<dt;
   dt = k_cfl*min(hx,hy)/(2*Umax);
end
nt = ceil(tf/dt); dt = tf/nt;

% fine grid discritization (f times finer than coarse grid)
f = 2;   dtf = dt/f;
xf = linspace(min(x),max(x),f*nx+1); hxf = lx/(f*nx);
yf = linspace(min(y),max(y),f*ny+1); hyf = ly/(f*ny);
[Xf,Yf] = meshgrid(yf,xf);

%-------------------------------------------------------------------------
% INITIALIZE RBC BOUNDARY - using level-set method
num_shift0 = 0; num_shift1 = 0;
nr = 3;                                          % number of
reinitialization steps
x0 = -(lx/2)+b; y0 = 0;                          % ellipse center
phi = sqrt((b^2)*((X-y0).^2)+(a^2)*(Y-x0).^2)-a*b;  % eqn of ellipse
if ss ~= 0,
    if lx == 2,
        load('lx2_phi_ss.mat');
    elseif lx == 10,
        load('lx10_phi_ss.mat');
    else
        sprintf(['Steady State geometry only saved for lx=2 and lx=10\n'...
            'Using elliptical geometry']);
    end
end
phif = interp2(X,Y,phi,Xf,Yf); volf_0 = length(find(phif<0));

%-------------------------------------------------------------------------
% INITIAL/BOUNDARY CONDITIONS
% initial conditions
if periodic_flag ~= 0,
    C = (cO2a/cHb50_0)*ones(nx,nyc);
else
    C = linspace(cO2a/cHb50_0,cO2v/cHb50_0,nx)'*ones(1,nyc);
end
```

```
SHb = Hb_Sat(pO2a,pHb50,n)*ones(nx,nyc);
SMb = 0.57*ones(nx,nyc);
U = ones(nx-1,ny); V = zeros(nx,ny-1);
Pmax = abs(dpdx*lx/2);  Pmin = -abs(dpdx*lx/2);
Pgrad = linspace(Pmax,Pmin,nx)'*ones(1,ny);
cMb = cMb_const*ones(nx,nyc);cMb(:,(nyc-ny)/2+1:(nyc-ny)/2+ny) = 0;
M = M*ones(nx,nyc)*(Dcap/(cHb50_0*Vavg));M(:,(nyc-ny)/2+1:(nyc-ny)/2+ny) = 0;

% boundary flow conditions
uN = x*0+0;       vN = avg(x)*0;
uS = x*0+0;       vS = avg(x)*0;
uW = avg(y)*0+1; vW = y*0+0;
uE = avg(y)*0+1; vE = y*0+0;

%--------------------------------------------------------------------------
% INITIALIZE OPERATORS
fprintf('initialization')
% Pressure
Lp = kron(speye(ny),K1(nx,hx,10))+kron(K1(ny,hy,1),speye(nx));
perp = symamd(Lp); Rp = chol(Lp(perp,perp)); Rpt = Rp';
% U-Velocity
A = (1/Re)*(kron(speye(ny),K1(nx-1,hx,2))+kron(K1(ny,hy,3),speye(nx-1)));
Lu =  speye((nx-1)*ny)+dt*A;
peru = symamd(Lu); Ru = chol(Lu(peru,peru)); Rut = Ru';
% V-Velocity
A = (1/Re)*(kron(speye(ny-1),K1(nx,hx,3))+kron(K1(ny-1,hy,2),speye(nx)));
Lv =  speye(nx*(ny-1))+dt*A;
perv = symamd(Lv); Rv = chol(Lv(perv,perv)); Rvt = Rv';
% O2 Concentration
A =
(Dox/(Vavg*Dcap))*(kron(speye(nyc),K1(nx,hx,1))+kron(K1(nyc,hy,1),speye(nx)))
;
Lc =  speye((nx)*nyc)+dt*A;
perc = symamd(Lc); Rc = chol(Lc(perc,perc)); Rct = Rc';
% Hemoglobin Saturation
A =
(DHb/(Vavg*Dcap))*(kron(speye(nyc),K1(nx,hx,1))+kron(K1(nyc,hy,1),speye(nx)))
;
Lshb =  speye((nx)*nyc)+dt*A;
pershb = symamd(Lshb); Rshb = chol(Lshb(pershb,pershb)); Rshbt = Rshb';
% Myoglobin Saturation
A =
(DMb/(Vavg*Dcap))*(kron(speye(nyc),K1(nx,hx,1))+kron(K1(nyc,hy,1),speye(nx)))
;
Lsmb =  speye((nx)*nyc)+dt*A;
persmb = symamd(Lsmb); Rsmb = chol(Lsmb(persmb,persmb)); Rsmbt = Rsmb';

%--------------------------------------------------------------------------
% ITERATE TO CALCULATE MICROCIRCULATION VALUES (phi,U,V,P,C)
fprintf(', time loop\n--20%%--40%%--60%%--80%%-100%%\n')
for k = 1:nt
   % CALCULATE RBC GEOMETRY USING LEVEL-SET EQUATION
   % boundary velocities
   Ubc = dt/Re*([2*uS(2:end-1)' zeros(nx-1,ny-2) 2*uN(2:end-
1)']/hx^2+[uW;zeros(nx-3,ny);uE]/hy^2);
```

```
   Vbc = dt/Re*([vS' zeros(nx,ny-3) vN']/hx^2+[2*vW(2:end-1);zeros(nx-2,ny-
1);2*vE(2:end-1)]/hy^2);
   % velocities(Ua,Va) and derivatives(Ud,Vd) at grid points
   Ue = [uW;U;uE]; Ue = [2*uS'-Ue(:,1) Ue 2*uN'-Ue(:,end)]; %#ok<AGROW>
   Ve = [vS' V vN']; Ve = [2*vW-Ve(1,:);Ve;2*vE-Ve(end,:)]; %#ok<AGROW>
   Ua = avg(Ue')'; Ud = diff(Ue,1,2)/2;
   Va = avg(Ve);   Vd = diff(Ve,1,1)/2;

   % transfer to fine grid
   phif = interp2(X,Y,phi,Xf,Yf);
   Uaf = interp2(X,Y,Ua,Xf,Yf); Vaf = interp2(X,Y,Va,Xf,Yf);
   for i = 1:f,
      phixf = (phif([2:end 1],:)-phif([end 1:end-1],:))/(2*hxf);
      phiyf = (phif(:,3:end)-phif(:,1:end-2))/(2*hyf); phiyf = phiyf(:,[1
1:end end]);
      F = (Uaf.*phixf+Vaf.*phiyf)./sqrt(phixf.^2+phiyf.^2+eps);
      F = (F([end 1:end-1],:)+F([2:end 1],:)+F(:,[1 1:end-1])+F(:,[2:end
end]))/4;

      % level-set update & reinitialization steps
      phif = phif-dtf*FabsgradP(phif,0.5*(hxf+hyf),F);
      for ir = 1:nr
         phif = phif-
dtf*FabsgradP(phif,0.5*(hxf+hyf),phif./sqrt(phif.^2+(hxf+hyf)^2),1);
      end
      if periodic_flag ~= 0,
          % periodicity
          phif(1,:) = phif(end,:);
      end

      % adjust for RBC volume loss/gain
      volf_f = length(find(phif<0));
      while(1-volf_f/volf_0)<-10*hxf*hyf
         phif = phif + hxf*hyf;
         volf_f = length(find(phif<0));
         num_shift1 = num_shift1-1;
      end
      while(1-volf_f/volf_0)>10*hxf*hyf
         phif = phif - hxf*hyf;
         phif = phif + hx*hy*[ones(nx*f+1,1) zeros(nx*f+1,ny*f-1)
ones(nx*f+1,1)];
         volf_f = length(find(phif<0));
         num_shift0 = num_shift0+1;
      end
   end
   % transfer to back to coarse grid
   phi = interp2(Xf,Yf,phif,X,Y);

   % CALCULATE VELOCITIES AND PRESSURE USING NAVIER-STOKES EQUATION
   % treat nonlinear terms
   gamma = min(1.2*dt*max(max(abs(U)))/hx,max(max(abs(V)))/hy),1);
   UVx = diff(Ua.*Va-gamma*abs(Ua).*Vd,1,1)/hx;
   UVy = diff((Ua.*Va-gamma*Ud.*abs(Va)),1,2)/hy;
```

```
   % calculate velocities(Ua,Va) and derivatives(Ud,Vd) at cell center
   Ua = avg(Ue(:,2:end-1));   Ud = diff(Ue(:,2:end-1),1,1)/2;
   Va = avg(Ve(2:end-1,:)')'; Vd = diff(Ve(2:end-1,:),1,2)/2;
   U2x = diff(Ua.^2-gamma*abs(Ua).*Ud,1,1)/hx;
   V2y = diff((Va.^2-gamma*abs(Va).*Vd),1,2)/hy;
   U = U-dt*(UVy(2:end-1,:)+U2x+dpdx*ones(nx-1,ny));
   V = V-dt*(UVx(:,2:end-1)+V2y);

   % implicit viscosity
   rhs = reshape(U+Ubc,[],1);
   u(peru) = Ru\(Rut\rhs(peru)); %#ok<AGROW>
   U = reshape(u,nx-1,ny);
   rhs = reshape(V+Vbc,[],1);
   v(perv) = Rv\(Rvt\rhs(perv)); %#ok<AGROW>
   V = reshape(v,nx,ny-1);

   % pressure correction
   phia = avg(avg(phi')');
   phia = [phia(end,:);phia;phia(1,:)]; %#ok<AGROW>
   curv = curvature(phia,hx,hy);
   Cplas = C(:,(nyc-ny)/2+1:(nyc-ny)/2+ny); Cplas =
[Cplas(end,:);Cplas;Cplas(1,:)]; %#ok<AGROW>
   st_mem = (k_mem*(Cplas/(cO2a_0/cHb50_0)).^(-index)).*curv;    % stress on
RBC membrane

   thetax = abs(phia(2:end-1,:))./(abs(phia(2:end-1,:))+abs(phia(3:end,:)));
   thetay = abs(phia(2:end-1,1:end))./(abs(phia(2:end-
1,1:end))+abs(phia(2:end-1,[2:end,end])));

   JL = zeros(nx,ny); JR = JL; JB = JL; JT = JL;     % Jump matrix
   for i = 1:nx,
      ii = i+1;
      for j = 2:ny-1,
         if sign(phia(ii-1,j)) > sign(phia(ii,j)),
            JL(i,j) = JL(i,j) + (thetax(i,j)*st_mem(ii-1,j)+(1-
thetax(i,j))*st_mem(ii,j))/hx^2;
         elseif sign(phia(ii-1,j)) < sign(phia(ii,j)),
            JL(i,j) = JL(i,j) - (thetax(i,j)*st_mem(ii-1,j)+(1-
thetax(i,j))*st_mem(ii,j))/hx^2;
         end
         if sign(phia(ii+1,j)) > sign(phia(ii,j)),
            JR(i,j) = JR(i,j) + (thetax(i,j)*st_mem(ii+1,j)+(1-
thetax(i,j))*st_mem(ii,j))/hx^2;
         elseif sign(phia(ii+1,j)) < sign(phia(ii,j)),
            JR(i,j) = JR(i,j) - (thetax(i,j)*st_mem(ii+1,j)+(1-
thetax(i,j))*st_mem(ii,j))/hx^2;
         end
         if sign(phia(ii,j-1)) > sign(phia(ii,j)),
            JB(i,j) = JB(i,j) + (thetay(i,j)*st_mem(ii,j-1)+(1-
thetay(i,j))*st_mem(ii,j))/hy^2;
         elseif sign(phia(ii,j-1)) < sign(phia(ii,j)),
            JB(i,j) = JB(i,j) - (thetay(i,j)*st_mem(ii,j-1)+(1-
thetay(i,j))*st_mem(ii,j))/hy^2;
         end
```

```
         if sign(phia(ii,j+1)) > sign(phia(ii,j)),
            JT(i,j) = JT(i,j) + (thetay(i,j)*st_mem(ii,j+1)+(1-
thetay(i,j))*st_mem(ii,j))/hy^2;
         elseif sign(phia(ii,j+1)) < sign(phia(ii,j)),
            JT(i,j) = JT(i,j) - (thetay(i,j)*st_mem(ii,j+1)+(1-
thetay(i,j))*st_mem(ii,j))/hy^2;
         end
      end
   end
   phia = phia(2:end-1,:);

   J = JL+JR+JB+JT;
   rhs = (1/dt)*reshape(diff([uW;U;uE],1,1)/hx+diff([vS' V vN'],1,2)/hy +
J,[],1);
   p(perp) = Rp\(Rpt\rhs(perp)); %#ok<AGROW>
   P = reshape(p,nx,ny); P = P+Pgrad;
   U = U-dt*diff(P-Pgrad-JL*hx^2-JB*hy^2,1,1)/hx;
   V = V-dt*diff((P-Pgrad-JL*hx^2-JB*hy^2),1,2)/hy;
   Ue = [uS' avg([uW;U;uE]')' uN'];   Ve = [vW;avg([vS' V vN']);vE];

   % CALCULATE O2 CONCENTRATION USING THE OXYGEN DIFFUSION EQUATION
   % calculate velocities at cell center; Hb concentration only inside RBC
   Ua = avg(avg(Ue')');   Va = avg(avg(Ve')');
   Ua = [zeros(nx,(nyc-ny)/2) Ua zeros(nx,(nyc-ny)/2)]; %#ok<AGROW>
   Va = [zeros(nx,(nyc-ny)/2) Va zeros(nx,(nyc-ny)/2)]; %#ok<AGROW>
   cHb = cHb_const*ones(nx,ny);cHb(phia>0) = 0;
   cHb = [zeros(nx,(nyc-ny)/2) cHb zeros(nx,(nyc-ny)/2)]; %#ok<AGROW>

   % calculate hemoglobin saturation
   if periodic_flag ~= 0
       SHbx = (SHb([2:end 1],:)-SHb([end 1:end-1],:))/(2*hx);
   else
       SHbx = [(SHb(2,:)-SHb(1,:))/hx; (SHb(3:end,:)-SHb(1:end-2,:))/(2*hx);
(SHb(end,:)-SHb(end-1,:))/hx];
   end
   SHby = [zeros(nx,1) (SHb(:,3:end)-SHb(:,1:end-2))/(2*hy) zeros(nx,1);];
   rhs = -kinvHb*(SHb-(1-SHb).*(C*(cHb50_0/cHb50)).^n)*(Dcap/Vavg) - Ua.*SHbx
- Va.*SHby;
   SHb = (SHb([end 1:end-1],:)+SHb([2:end 1],:)+SHb(:,[1 1:end-
1])+SHb(:,[2:end end]))/4 + dt*rhs;
   rhs = reshape(SHb,[],1);
   shb(pershb) = Rshb\(Rshbt\rhs(pershb)); %#ok<AGROW>
   SHb = reshape(shb,nx,nyc);

   % calculate myoglobin saturation
   if periodic_flag ~= 0
       SMbx = (SMb([2:end 1],:)-SMb([end 1:end-1],:))/(2*hx);
   else
       SMbx = [(SMb(2,:)-SMb(1,:))/hx; (SMb(3:end,:)-SMb(1:end-2,:))/(2*hx);
(SMb(end,:)-SMb(end-1,:))/hx];
   end
   SMby = [zeros(nx,1) (SMb(:,3:end)-SMb(:,1:end-2))/(2*hy) zeros(nx,1);];
   SMby(:,(nyc-ny)/2) = (SMb(:,(nyc-ny)/2)-SMb(:,(nyc-ny)/2-1))/(hy);
```

```
   SMby(:,(nyc-ny)/2+ny+1) = (SMb(:,(nyc-ny)/2+ny+2)-SMb(:,(nyc-
ny)/2+ny+1))/hy;
   SMby(:,(nyc-ny)/2+1:(nyc-ny)/2+ny) = 0;
   rhs = -kinvMb*(SMb-(1-SMb).*C*(cHb50_0/cMb50))*(Dcap/Vavg) - Ua.*SMbx -
Va.*SMby;
   SMb = (SMb([end 1:end-1],:)+SMb([2:end 1],:)+SMb(:,[1 1:end-
1])+SMb(:,[2:end end]))/4 + dt*rhs;
   rhs = reshape(SMb,[],1);
   smb(persmb) = Rsmb\(Rsmbt\rhs(persmb)); %#ok<AGROW>
   SMb = reshape(smb,nx,nyc);

   % calculate O2 concentration
   if periodic_flag ~= 0
       Cx = (C([2:end 1],:)-C([end 1:end-1],:))/(2*hx);
   else
       Cx = [(C(2,:)-C(1,:))/hx; (C(3:end,:)-C(1:end-2,:))/(2*hx); (C(end,:)-
C(end-1,:))/hx];
   end
   Cy = [zeros(nx,1) (C(:,3:end)-C(:,1:end-2))/(2*hy) zeros(nx,1);];

   % rate of hemoglobin O2 production, myoglobin O2 absorption
   RHb = kinvHb*cHb.*(SHb-(1-
SHb).*(C*(cHb50_0/cHb50)).^n)*(Dcap/(cHb50_0*Vavg));
   RMb = kinvMb*cMb.*(SMb-(1-SMb).*C*(cHb50_0/cMb50))*(Dcap/(cHb50_0*Vavg));
   R = RHb+RMb+M;

   rhs = R - Ua.*Cx - Va.*Cy;
   C = (C([end 1:end-1],:)+C([2:end 1],:)+C(:,[1 1:end-1])+C(:,[2:end
end]))/4 + dt*rhs;
   rhs = reshape(C,[],1);
   c(perc) = Rc\(Rct\rhs(perc)); %#ok<AGROW>
   c(c<0) = 0; %#ok<AGROW>
   C = reshape(c,nx,nyc);

% --------------------------------------------------------------------
   % VISUALIZATION
   if floor(25*k/nt)>floor(25*(k-1)/nt),
      fprintf('.')
   end
   if k==1||floor(nsteps*k/nt)>floor(nsteps*(k-1)/nt)
      t_sec = round(k*dt);
      eval(['save Data\MicroData_',num2str(t_sec),'.mat x y yc Ue Ve C P phi
st_mem']);
      figure(1), contourf(x,y,-phi',[0 0],'k-');hold on;
         contour(x,y,Ue',20);colorbar;caxis([0 3]);hold off;
         title(sprintf('U at t=%0.2f',t_sec));xlabel('x');ylabel('y');
%
saveas(figure(1),['Data\U_',num2str(t_sec)],'fig');saveas(figure(1),['Data\U_
',num2str(t_sec)],'png');
      figure(2), contourf(x,y,-phi',[0 0],'k-');hold on;
         contour(x,y,Ve',20);colorbar;caxis([-0.05 0.05]);hold off;
         title(sprintf('V at t=%0.2f',t_sec));xlabel('x');ylabel('y');
```

```
%
saveas(figure(2),['Data\V_',num2str(t_sec)],'fig');saveas(figure(2),['Data\V_
',num2str(t_sec)],'png');
      figure(3), contourf(avg(x),avg(y),P',20,'w-');hold on;
         Len = sqrt(Ue.^2+Ve.^2+eps);
         quiver(x,y,(Ue./Len)',(Ve./Len)',.4,'k-');
         hold off, axis equal, axis(ax), colorbar;
         p = sort(reshape(P,1,[])); caxis(p([8 end-7]));
         title(sprintf('Re = %0.1g   t =
%0.2f',Re,t_sec));xlabel('x');ylabel('y');
%
saveas(figure(3),['Data\P_',num2str(t_sec)],'fig');saveas(figure(3),['Data\P_
',num2str(t_sec)],'png');
      figure(4), contourf(x,y,-phi',[0 0],'k-');hold on;
         [~,h]=contour(avg(x),avg(yc),C',0:0.25:4);colorbar;caxis([0 4]);axis
equal,axis(axc);hold off;
         set(h,'ShowText','on','TextStep',get(h,'LevelStep')*2);
         title(sprintf('O_2 Concentration and RBC geometry at
t=%0.2f',t_sec));xlabel('x');ylabel('y');
%
saveas(figure(4),['Data\C_',num2str(t_sec)],'fig');saveas(figure(4),['Data\C_
',num2str(t_sec)],'png');
      drawnow;
   end

   % boundary conditions
   uE = mean([U(1,:);U(end,:)]); uW = uE;
   vE = [(vN(1)+vN(end))/2 mean([V(1,:);V(end,:)]) (vS(1)+vS(end))/2]; vW =
vE;
   if periodic_flag ~= 0
       C(1,:) = C(end,:);
   else
       C(1,:) = (cO2a/cHb50_0); C(end,:) = (cO2v/cHb50_0);
   end
end
fprintf(['\nRBC Volume Retained = ',num2str(100*volf_f/volf_0),'%% \n']);
fprintf(['\nlevel-set shifted down ',num2str(-num_shift1),' times and shifted
up ',num2str(num_shift0),' times by ',...
   num2str(hxf*hyf),' units in ',num2str(tf),' seconds\n']);
%=========================================================================

function B = avg(A,k)
if nargin<2,
   k = 1;
end
if size(A,1)==1,
   A = A';
end
if k<2,
   B = (A(2:end,:)+A(1:end-1,:))/2;
else
    B = avg(A,k-1);
end
if size(A,2)==1,
   B = B';
```

```
end

function A = K1(n,h,a11)
% a11: Neumann=1, Dirichlet=2, Dirichlet mid=3, Periodic = 10;
if a11 == 10,
    A = (spdiags(ones(n,1)*[-1 2 -1],-1:1,n,n) + spdiags(ones(n,1)*[1 1],[-
n+1 n-1],n,n))'/h^2;
else
    A = spdiags([-1 a11 0;ones(n-2,1)*[-1 2 -1];0 a11 -1],-1:1,n,n)'/h^2;
end

function F = curvature(P,hx,hy)
% computes curvature by central differences
Pxx = diff(P([1 1:end end],:),2,1)/hx^2;
Pyy = diff(P(:,[1 1:end end]),2,2)/hy^2;
Px = (P([2:end 1],:)-P([end 1:end-1],:))/(2*hx); %periodic along x;
Py = (P(:,3:end)-P(:,1:end-2))/(2*hy); Py = Py(:,[1 1:end end]);
Pxy = (Px(:,3:end)-Px(:,1:end-2))/(hx+hy); Pxy = Pxy(:,[1 1:end end]);
F = (Pxx.*Py.^2-2*Px.*Py.*Pxy+Pyy.*Px.^2)./(Px.^2+Py.^2).^1.5;
F = min(max(F,-1/(0.5*(hx+hy))),1/(0.5*(hx+hy)));

function dP = FabsgradP(P,h,F,c)
% level-set update function
if nargin<4,
   c = 0;
   if nargin<3,
      F = 1;
   end
end
DxP = diff(P,1,1)/h; DxmP = DxP([1 1:end],:); DxpP = DxP([1:end end],:);
DyP = diff(P,1,2)/h; DymP = DyP(:,[1 1:end]); DypP = DyP(:,[1:end end]);
Np = sqrt(max(DxmP,0).^2+min(DxpP,0).^2+max(DymP,0).^2+min(DypP,0).^2);
Nm = sqrt(min(DxmP,0).^2+max(DxpP,0).^2+min(DymP,0).^2+max(DypP,0).^2);
dP = max(F,0).*(Np-c)+min(F,0).*(Nm-c);

function SHb = Hb_Sat(PO2_pa,pHb50_pa,n)
PO2 = PO2_pa/133.322368; pHb50 = pHb50_pa/133.322368;    % Pa --> torr
SHb = (PO2.^n)./(pHb50^n+PO2.^n);
```

References

[1] **Platt, O. S., Brambilla, D. J., Rosse, W. F., Milner, P. F., Castro, O., Steinberg, M. H., Klug, P. P.** (1994). *Mortality In Sickle Cell Disease -- Life Expectancy and Risk Factors for Early Death.* New England Journal of Medicine. 330(23): 1639-1644.

[2] **Eppolito, Amanda.** (2005). *The Physiology of Sickle Cell Anemia.* Davidson College. http://www.bio.davidson.edu/people/midorcas/animalphysiology/websites/2005/Eppolito/intro.htm.

[3] **Friedman, Milton J.** (1978). *Erythrocytic mechanism of sickle cell resistance to malaria.* Proc. Nati. Acad. Sci. USA, 75(4): 1994-1997.

[4] **Secomb, T. W., Hsu, R., and Pries, A. R.** (2006). *Tribology of capillary blood flow.* Proc. IMechE, Part J: Engineering Tribology, 220: 767-774.

[5] **Dou, Q., Ferrone, F. A.** (1993). *Simulated Formation of Polymer Domains in Sickle Hemoglobin.* Biophysical J., 65: 2068-2077.

[6] **Cokic, V. P., Smith, R. D., Beleslin-Cokic, B. B., Njoroge, J. M., Miller, J. L., Gladwin, M. T., and Schechter, A. N.** (2003). *Hydroxyurea induces fetal hemoglobin by the nitric oxide–dependent activation of soluble guanylyl cyclase.* J. Clin. Invest. 111(2): 231-239.

[7] **Information Center for Sickle Cell and Thalassemic Disorders.** (2002). http://sickle.bwh.harvard.edu/hbsynthesis.html.

[8] **Le Floch-Yin, Francois T.** (2010). *Design of a Numerical Model for Simulation of Blood Microcirculation and Sickle Cell Disease.* (Ph.D. thesis – Dept. of Aeronautics and Astronautics). Massachusetts Institute of Technology, MA.

[9] **Berne, R. M., Levy, M. N., Koeppen, B. M., Stanton, B. A.** (2004). *PHYSIOLOGY: Fifth Edition.* Elsevier, Inc. Mosby; St. Louis, MO. Chap. 18-20.

[10] **Mark, Roger G.** (2004). *Introduction: The Functional Anatomy of the Cardiovascular System.* HST542J: Quantative Physiology: Organ Transport Systems. Harvard-MIT Division of Health Sciences and Technology.

[11] **Franklin Institute.** http://www.fi.edu/learn/heart/blood/blood.html

[12] **Vadapalli, A., Goldman, D., and Popel, A. S.** (2002). *Calculations of Oxygen Transport by Red Blood Cells and Hemoglobin Solutions in Capillaries.* Art. Cells, Blood Subs., and Immob. Biotech., 30(3): 157-188.

[13] **Seibold, B.** (2008). *A compact and fast Matlab code solving the incompressible Navier-Stokes equations on rectangular domains:*

mit18086_navierstokes.m. Applied Mathematics, Massachusetts Institute of Technology. (http://www-math.mit.edu/cse/).

[14] Osher, S., Sethian, J. A. (1988). *Fronts propagating with curvature-dependent speed: algorithms based on Hamilton-Jacobi formulations.* Journal of Computational Physics. Vol. 79: 12-49.

[15] Crank, J.; Nicolson, P. (1947). *A practical method for numerical evaluation of solutions of partial differential equations of the heat conduction type. Proc. Camb. Phil. Soc.* 43 (1): 50–67.

[16] Rand, R. P., Burton, A. C. (1964). *Mechanical Properties of the Red Cell Membrane: I. Membrane Stiffness and Intracellular Pressure.* Biophysical J., 4(2): 115-135.

[17] Berger, S. A., and King, W. S. (1980). *The Flow of Sickle Cell Blood in the Capillaries.* Biophysical J., 29(1): 119-148.

[18] Usami, S., Chien, S., Bertles, J. F. (1975). *Deformability of Sickle Cells as Studied by Microsieving.* J. Lab. Clin. Med., 86: 247-279.

[19] Winslow, R. M. (1976). *Blood Oxygen Equilibrium Studies in Sickle Cell Anemia.* In Proceedings of the Symposium on Molecular and Cellular Aspects of Sickle Cell Disease. J. I. Hercules et al., editors. National Heart, Lung, and Blood Institute, Bethesda, Md. (DHEW Publ. No. (NIH) 76-1007). 235.